1977

The Design and Analysis of a Rare Earth Iron Magnetostrictive Underwater Sound Transducer

Steven Wayne Meeks
University of Central Florida

THE DESIGN AND ANALYSIS OF A RARE EARTH IRON MAGNETOSTRICTIVE UNDERWATER SOUND TRANSDUCER

BY

STEVEN WAYNE MEEKS
B.S., Florida Technological University, 1974

RESEARCH REPORT

Submitted in partial fulfillment of the requirements
for the degree of Master of Science in the Graduate
Studies Program of the College of Engineering
of Florida Technological University

Orlando, Florida
January 1977

ABSTRACT

The design and analysis of a low-frequency, resonant, tonpilz type, rare earth iron underwater sound transducer using rods of $Tb_{.27}Dy_{.73}Fe_{1.95}$ are described. An equivalent circuit is presented which predicts the performance of the transducer in the presence of eddy currents and demagnetization. The effect of eddy currents on the impedance of a rod is discussed. The predicted performance of a laminated transducer is compared with that of an unlaminated transducer. The performance of the rare earth iron transducer is compared with the performance of the same transducer with identical ceramic active elements. Data on transmitting current response, transmitting voltage response, free field voltage sensitivity, coupling coefficient, efficiency, and linearity are presented. Advantages, disadvantages, and possible uses of rare earth iron material are discussed.

ACKNOWLEDGMENTS

I wish to extend my deepest appreciation to my mother and father for providing the inspiration and help necessary to continue my education. Thanks are due to the Naval Research Laboratory's Underwater Sound Reference Division (USRD) for supplying the equipment and laboratory space for this research project. Appreciation is extended to USRD employees Mark Young, Dick Hugus, and Ted Henriquez of the Standards Branch for several helpful discussions, to John Heins and the men of the Machine Shop for their competent and timely fabrication of the transducer parts, to Elmo Thomas of the Materials Section for his competent technical assistance, and to the men of the Lake Facility for their assistance. I wish to extend a special thanks to Dr. Robert Timme for many long enlightening discussions, for helpful suggestions, and for reviewing this manuscript.

TABLE OF CONTENTS

LIST OF TABLES

LIST OF FIGURES

CHAPTER I

INTRODUCTION

Background and History of the Rare Earth Iron Alloys

This research report begins with a brief historical review of transduction materials given by Timme [1].

> Before the 1950's, the choices of energy conversion materials available to designers of underwater sound transducers were limited to magnetostrictive metals such as nickel and its alloys and natural or man-grown piezoelectric crystals such as quartz, ammonium dihydrogen phosphate, and a few others. The magnetostrictive metals were superior in many ways, but even they were limited to maximum strains of a few tens of parts per million. With the discovery in the 1950's of the piezoelectric qualities of the polarized ferroelectric ceramics barium titanate and lead zirconate titanate, use of the magnetostrictive metals declined. Thus, in recent years, piezoelectric ceramic materials have been used as the acoustic element in most sonar devices. The ceramics have had many advantages, but recent developments in magnetostrictive materials prompt investigation of their applications as acoustic elements.

Magnetostriction or Joule magnetostriction is the ability of a ferromagnetic material to strain (i.e., change in length) under the application of a magnetic field. The converse effect (Villari effect) is the production of a flux density by the application of stress to a ferromagnetic material.

In 1963 and 1964 the rare earth elements terbium (Tb) and dysprosium (Dy) were discovered to possess extremely large magnetostrictions, as much as 1%. These magnetostrains were not immediately useful for application to transducers (energy conversion

devices) because they occurred only at cryogenic temperatures. Then in 1971 Clark and Belson [2] of the Naval Surface Weapons Center and Koon, Schindler, and Carter [3] of the Naval Research Laboratory discovered, independently and almost simultaneously, that the magnetostrains exhibited by binary alloys of certain rare earth elements and iron at room temperature are 10 to 100 times that of nickel, a commonly used magnetostrictive metal. Although the binary alloys such as terbium iron ($TbFe_2$) and samarium iron ($SmFe_2$) exhibit extremely large magnetostrains they require large magnetic fields (on the order of 1.6 MA/m or 20,000 Oe) to generate these strains [4]. This is due to a large magnetic anisotropy, which means it is very difficult to rotate the direction of magnetization. Thus a transducing device using the binary alloys is met with the practical problem of efficiently generating large magnetic fields. Additional investigations by Williams and Koon [5] and by Clark [6] have shown that the anisotropy of a ternary alloy of terbium holmium iron or terbium dysprosium iron is much lower than that of the binary alloy and even though the magnetostrain is somewhat reduced, it is still 20 times larger than nickel. Koon et al. [7], Timme and Koon [8], and Timme [1] have investigated the magnetomechanical properties of the terbium holmium iron system. Savage et al. [9], Clark and Savage [10], and Savage and Ferranco [11] have measured the same properties of the terbium dysprosium iron system.

Investigations have recently begun of quaternary alloys of terbium holmium dysprosium iron. Koon and Williams [12] have found that a rare earth composition of 20% terbium, 58% holmium, and 22%

dysprosium has its lowest order magneto-crystalline anisotropy constants near zero and similar to that of nickel, while the magnetostrain is still very large. It is possible that the quaternarys will turn out to be the most useful compositions, but the data are too preliminary to tell.

The best rare earth iron composition presently available is the ternary alloy of 27% terbium-73% dysprosium iron ($Tb_{.27}Dy_{.73}Fe_{1.95}$). This particular composition was chosen because it has low anisotropy, large magnetostriction, and a large magnetomechanical coupling coefficient. The coupling coefficient is a figure of merit of a transducing material and is a measure of the energy conversion capability of the material.

As an introduction to this alloy consider table 1. Shown here are the coupling constant, electromechanical energy density, and typical operating efficiency for nickel, PZT-4 (a commonly used piezoelectric ceramic), and $Tb_{.3}Dy_{.7}Fe_2$. The coupling constant of PZT-4 and terbium dysprosium iron is nearly the same and about twice that of nickel. The electromechanical energy density which relates the amount of electrical or magnetic energy that can be transformed to elastic energy under the proper conditions is much larger for terbium dysprosium iron than for the ceramic which in turn is larger than for nickel. The typical efficiency of a sonar transducer using nickel or PZT-4 is also given but cannot be compared to terbium dysprosium iron at this time. This table implies that terbium dysprosium iron might have great promise because it equals or exceeds certain characteristics of the ceramic which is a widely

used transducer material that has nearly replaced nickel.

TABLE 1

COMPARISON OF SEVERAL TRANSDUCER MATERIALS

Material	Maximum Coupling Constant	Electromechanical Energy Density (J/m^3)	Typical Efficiency (%)
Nickel	0.3	27	15
PZT-4	0.7	630	70
$Tb_{.3}Dy_{.7}Fe_2$	0.6	6800	?

In order to further introduce this alloy consider figure 1. Shown here is a comparison of the strains of terbium dysprosium iron and nickel versus flux density. The strain of the rare earth is about 20 times that of nickel at a flux density of 1.2 tesla (which corresponds to a field of 2000 Oe) and is still far from saturation at this flux density. The nickel sample saturates at about .5 tesla to a maximum negative strain of 40 parts per million. The strain of PZT-4 is also shown for comparison. There is no definite relationship between the units of the electric field and the magnetic flux density on the abscissa except that from a practical point of view, the problems encountered in handling an electric field of 0.5 MV/m and a magnetic field of 80 kA/m (which corresponds to a flux density of .95 tesla or a field of 1000 Oe) are nearly the same in degrees of difficulty. The dashed portion of the PZT-4 strain curve above 0.5 MV/m indicates the onset of depolarization in the ceramic.

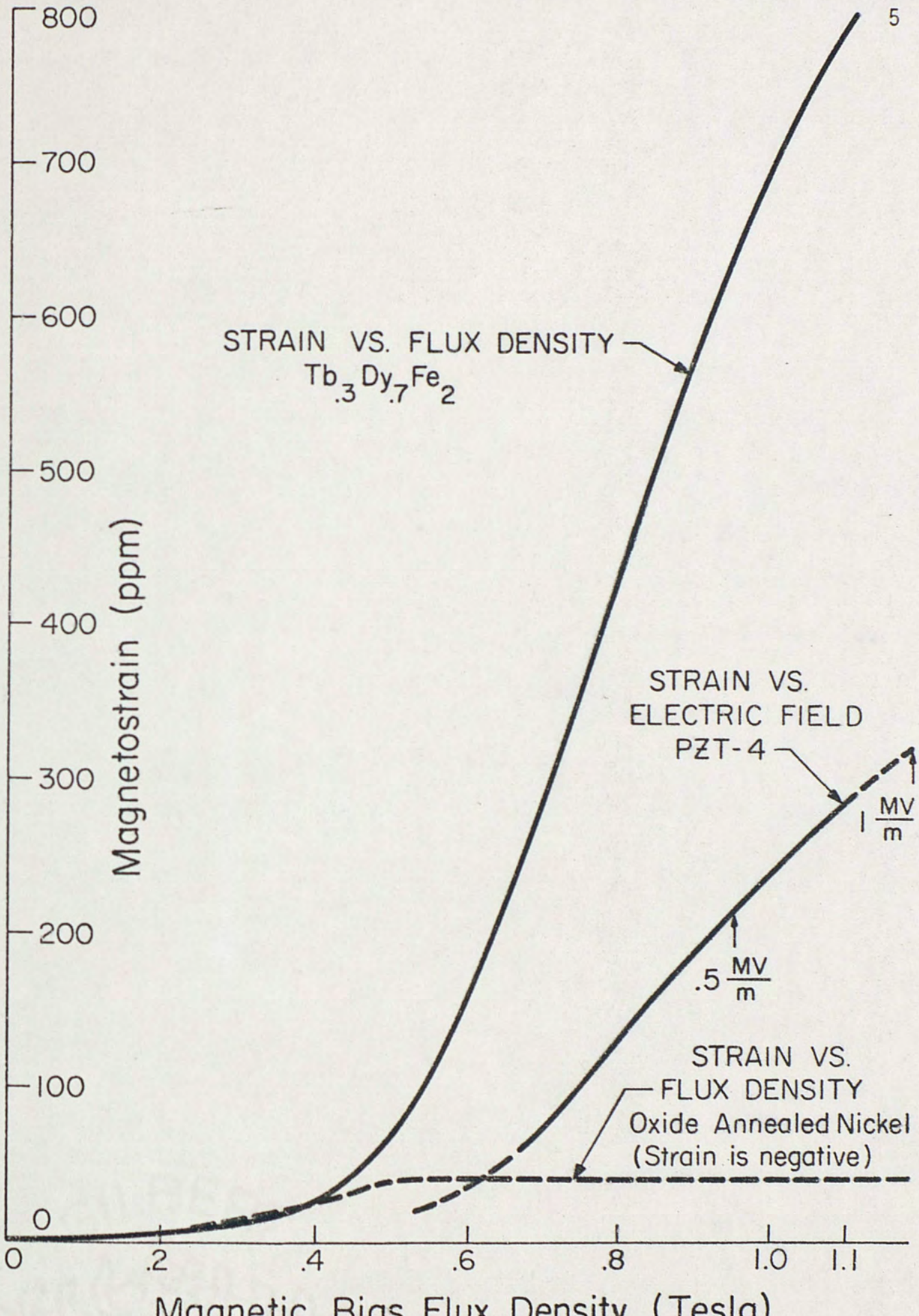

Fig. 1. Comparison of the strain of three transduction materials

Therefore, from figure 1 one sees that the rare earth iron alloy has considerably greater strain (to which the sound pressure is proportional) than either the nickel or ceramic material.

Figure 1 also indicates the linearity of the terbium dysprosium iron alloy. The strain of both the nickel and the terbium dysprosium iron alloy increase approximately as the square of flux density up to about .5 tesla (5000 G). Above .5 tesla nickel saturates but the rare earth alloy approaches a linear increase until it reaches about 1.1 tesla (11,000 G). Therefore a dynamic flux density about a fixed bias field, in the linear region, should yield a linear output. A linear output, using terbium holmium iron, has been observed by Timme [1] until the alternating field magnitude approached 80% of the bias field magnitude.

Previous Rare Earth Iron Transducers

The design of rare earth transducers has been less than optimum because the designs were initiated before the rare earth alloys were completely investigated. Not including the present work, four experimental rare earth iron transducers have been developed. All four designs utilize terbium dysprosium iron as their active elements.

Smith and Logan [13] have developed a multi-resonant, "folded horn", underwater sound transducer designed to operate in the 3-15 kHz range. Their major conclusions were that reasonable output pressure levels could be obtained utilizing the rare earth iron material. The rare earth transducer exhibited a lower

resonance frequency than the same transducer with a ceramic active element. There was insufficient data to decide whether the rare earth iron material could be competitive with the conventional ceramic material.

Akervold, Hutchins, Johnson, and Koepke [14] have developed a double-ended longitudinal vibrator. Again moderate sound pressures were generated over the 1-15 kHz region. Their study is incomplete at present, and they have not compared the rare earth device with the performance of the same transducer with identical ceramic active elements.

Butler and Ciosek [15] have developed two rare earth transducers. The first one was a small low-power longitudinal vibrator. They reached essentially the same conclusions as Smith and Logan as to the transducer's performance. The second transducer was a square ring transducer constructed of four rare earth iron rods arranged in a square. They found that the four rods in a square conformed to the resonance condition for a thin ring. The efficiency of their rare earth iron transducers is lower than the ceramic version's efficiency. They attributed this to electrical losses. Butler and Ciosek give a lossless equivalent circuit for the longitudinal vibrator but show no results from it.

Objectives

The objectives of this research report are as follows:

1. To design and test a rare earth iron underwater sound transducer.

2. To develop an equivalent circuit which predicts the performance of the rare earth transducer in the presence of eddy currents and demagnetization.

3. To compare the performance of the rare earth iron transducer with the results of the same transducer where the rare earth iron rods have been replaced by identically dimensioned piezoelectric ceramic rods.

CHAPTER II

THE DESIGN AND CONSTRUCTION OF A RARE EARTH IRON TRANSDUCER

This chapter will describe the design and construction of a low-frequency, resonant, tonpilz type (longitudinal vibrator) rare earth iron transducer. This design was expected to be less than optimum because of the nonlaminated construction. The design objective was to obtain a low-frequency, moderate-power, broad frequency range device. The transducer should also be adaptable for use with identically dimensioned piezoelectric ceramic rods for comparison of the two active materials. This chapter is organized into three sections:

1) a discussion of the magnetic material properties of the ternary alloy $Tb_{.27}Dy_{.73}Fe_{1.95}$,
2) the preparation of the rare earth iron rods, and
3) the design of the rare earth iron transducer.

Discussion of the Magnetic Material Properties of $Tb_{.27}Dy_{.73}Fe_{1.95}$

The active elements of the present transducer are ternary alloy rods of $Tb_{.27}Dy_{.73}Fe_{1.95}$. A short (1.24-cm diameter by 2.3-cm long) sample rod was cut from one of the unused active elements and placed in a magnetic yoke described by Timme [1] in order to measure its magnetic properties. This section will present the results of

these measurements.

The importance of the magnetic material properties of a magnetostrictive material can be realized by looking at equations (1) and (2), which are the equations of state, using tensor notation, for a thin rod with no lateral stresses (that is, the stress is only along the axis of the rod). The symbols in these equations are consistent with the "IEEE Standard on Magnetostrictive Materials" [16].

$$S_3 = s_{33}^{B} T_3 + \frac{d_{33}}{\mu_{33}^{T}} B_3 \tag{1}$$

$$H_3 = -\frac{d_{33}}{\mu_{33}^{T}} T_3 + \frac{1}{\mu_{33}^{T}} B_3 \tag{2}$$

Equations (1) and (2) relate the applied stress, T_3, and flux density, B_3, to the resulting strain, S_3, and magnetic field, H_3, through the elastic and magnetic constants. The subscript 3 on H_3 and B_3 indicates the direction of the field or flux density and is the axial direction. The stress, T_3, and strain, S_3, are in general second-rank tensors. In the case of a thin rod the stress, T_3, is the quotient of the force, F_3, in the three direction divided by the cross-sectional area of the rod. The strain, S_3, occurs only in the axial direction for the thin rod.

The dynamic or incremental permeability at constant stress (the "free" permeability) is μ_{33}^{T}. The permeability is in general a second-rank tensor. In the special case of a thin rod only the element μ_{33}^{T} need be considered. The superscript T in μ_{33}^{T} indicates

that this is the permeability at constant stress. The first 3 in the subscript of μ_{33}^{T} indicates that the coil is wrapped along the three direction (axial direction). The second subscript indicates that the piezomagnetically induced strain, or the applied stress, is in the three direction.

The elastic compliance coefficient at constant flux density is s_{33}^{B}. In general the elastic compliance coefficient is a fourth-rank tensor but the case of a thin rod simplifies to the single element s_{33}^{B}. The superscript B indicates that this is the compliance coefficient measured at constant flux density. The subscripts in s_{33}^{B} indicate that strain and stress, respectively, are in the three direction. The reciprocal of s_{33}^{B} is the Young's modulus.

The magnetostrictive strain constant is d_{33}. In general the magnetostrictive strain constant is represented by a third-rank tensor. The special case of a thin rod simplifies the tensor to the single element d_{33}. The subscripts of d_{33} have the same meaning as those of the permeability μ_{33}^{T}.

Another constant, which has been discussed previously, is the coupling coefficient, k_{33}, which can be determined in terms of the above-mentioned constants. The subscripts of k_{33} have the same meaning as those of μ_{33}^{T}. The relationship between d_{33}, μ_{33}^{T}, s_{33}^{B}, and k_{33} is given by equation (3).

$$\frac{k_{33}^2}{1 - k_{33}^2} = \frac{d_{33}}{\mu_{33}^{T} s_{33}^{B}} \tag{3}$$

The units used throughout this paper are the International

System of Units (abbreviated "SI") which includes the rationalized mks unit system. The units of the previously discussed parameters are as follows:

T_3 = stress = newtons per (meter)^2 = $\frac{N}{m^2}$

S_3 = strain = parts per million (numeric) = ppm

H_3 = magnetic field = amperes per meter = $\frac{A}{m}$

B_3 = magnetic flux density = tesla = T

F_3 = force = newtons = N

μ_{33}^{T} = incremental permeability at constant stress
= Henries per meter = $\frac{H}{m}$

s_{33}^{B} = elastic compliance coefficient at constant flux density = (meters)^2 per newton = $\frac{m^2}{N}$

d_{33} = magnetostrictive strain constant
= meters per ampere = $\frac{m}{A}$

k_{33} = magnetomechanical coupling coefficient = numeric.

The static and incremental relative permeabilities of terbium dysprosium iron are shown in figure 2. The static permeability is reasonably large ranging from 100 at low fields to 10 at high fields. The incremental or dynamic permeability is small ranging from 9 at low fields to 2 at high fields. The low incremental permeability has both a desirable and an undesirable effect. The desirable effect is that a low permeability (as will be shown later) reduces eddy current loss. The undesirable effect is that there is

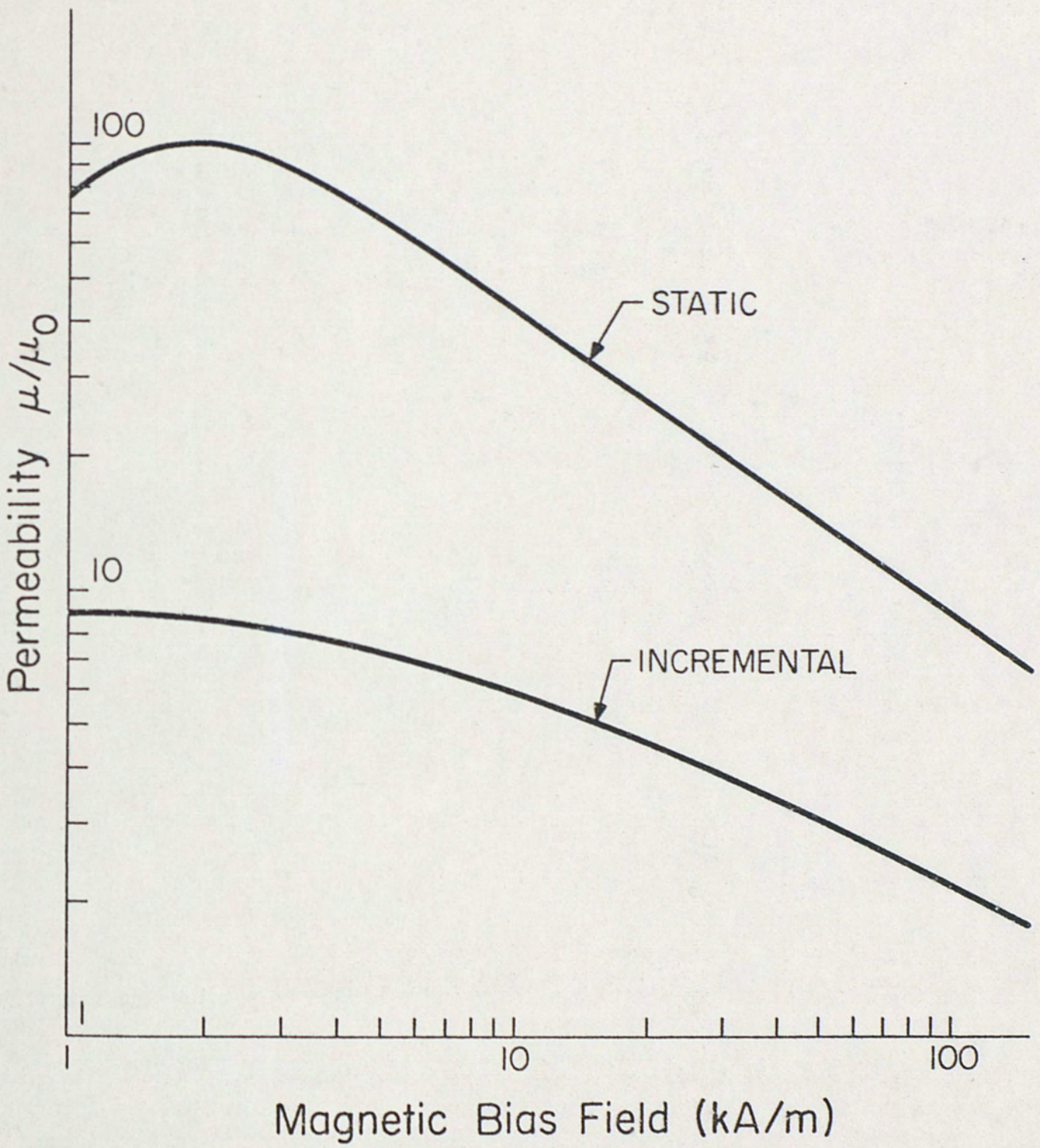

Fig. 2. Relative permeability, $\frac{\mu}{\mu_o}$, versus bias field for $Tb_{.27}Dy_{.73}Fe_{1.95}$

greater magnetic fringing or leakage flux with a low incremental permeability.

Figure 3 shows $\frac{1}{s_{33}^B}$ or Young's modulus versus bias field. Terbium dysprosium iron exhibits a very large change of Young's modulus with applied field [17] (this is known as the "ΔE effect"). The large change in Young's modulus, and hence the sound speed, makes terbium dysprosium iron a good candidate for a variable acoustic delay line. The Young's modulus, which is directly proportional to the stiffness, of terbium dysprosium iron is about one half that of the commonly used ceramic PZT-4. The lower stiffness is generally considered an advantage but it is offset somewhat by the tendency of Young's modulus to increase with mechanical bias stress [18].

The magnetostrictive strain constant d_{33} is shown in figure 4. The strain constant rises rapidly with applied field reaching a peak at 12 $\frac{kA}{m}$ (150 Oe) and gradually decreasing past this point. The strain constant d_{33} is defined as

$$d_{33} \equiv \frac{\partial S_3}{\partial H_3} \tag{4}$$

and as such it relates the amount of strain per applied field.

Shown in figure 5 is the magnetomechanical coupling coefficient versus bias field. The coupling coefficient rises rapidly to a peak at about 20 $\frac{kA}{m}$ (250 Oe) and slowly decreases. A large value of k_{33} is maintained over a wide range of bias fields; this is advantageous since in an application the material is held at a fixed bias and the alternating field magnitude is varied over a large

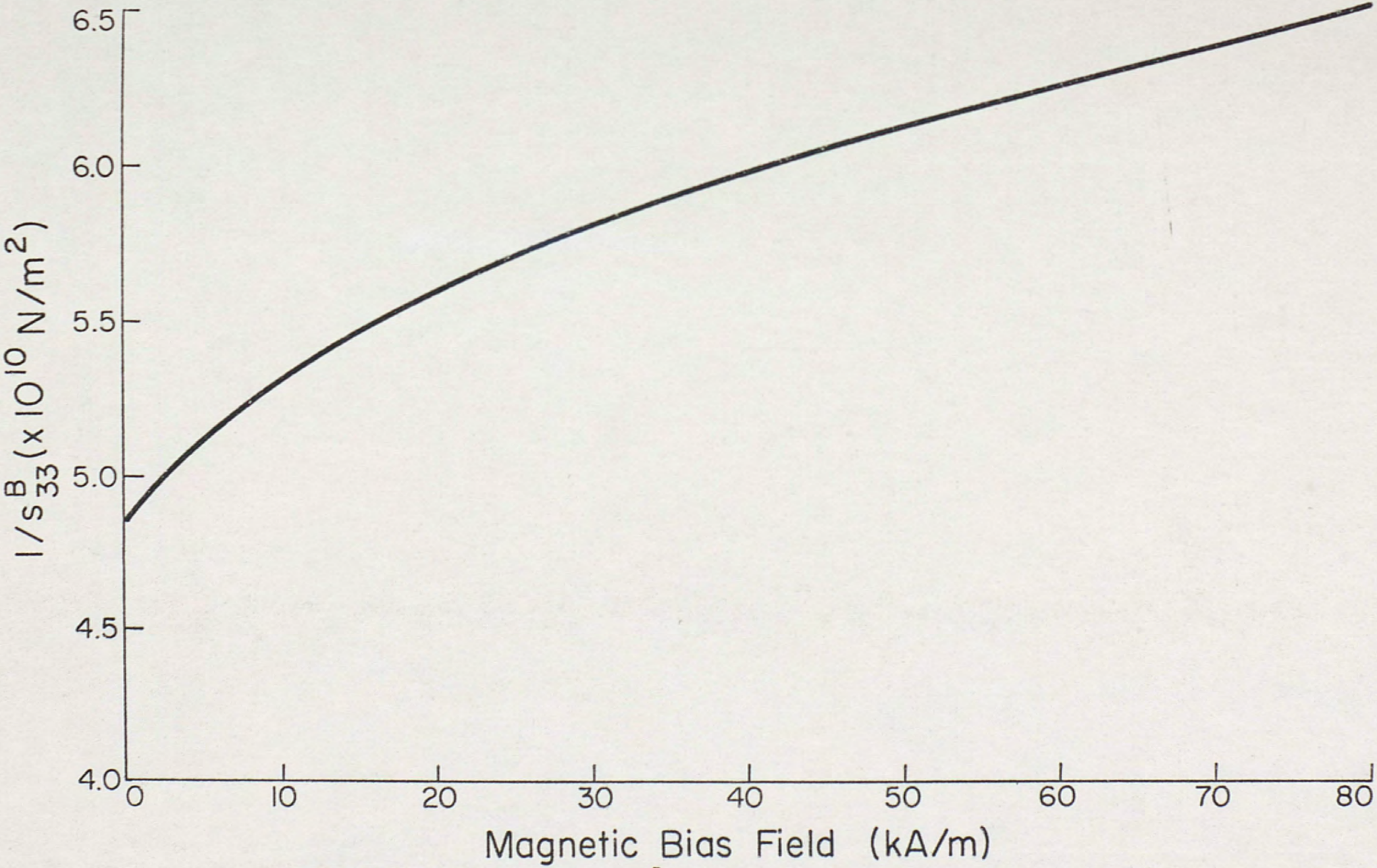

Fig. 3. Young's modulus, $1/s^B_{33}$, versus bias field for $Tb_{.27}Dy_{.73}Fe_{1.95}$

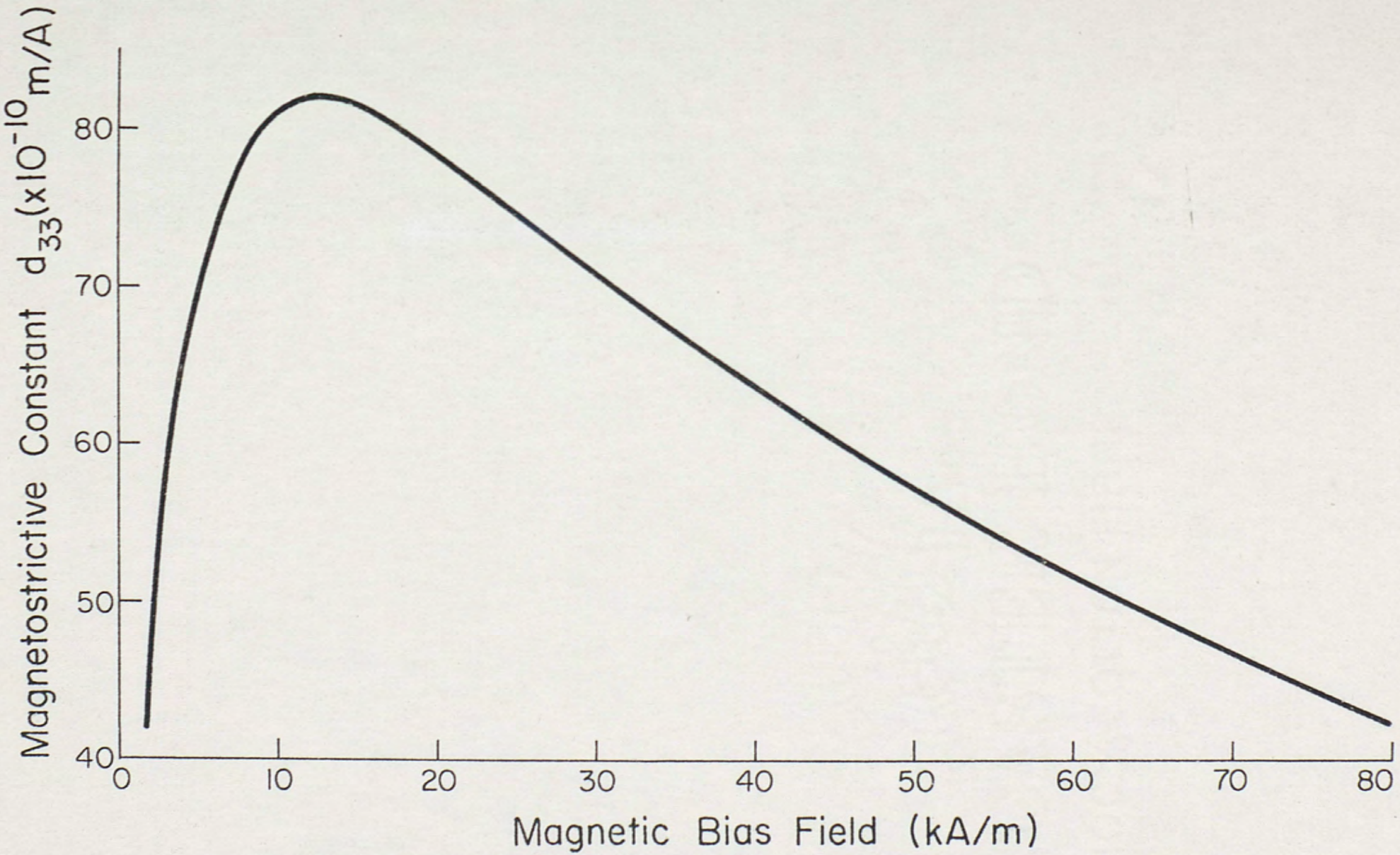

Fig. 4. Magnetostrictive constant, d_{33}, versus bias field for $Tb_{.27}Dy_{.73}Fe_{1.95}$

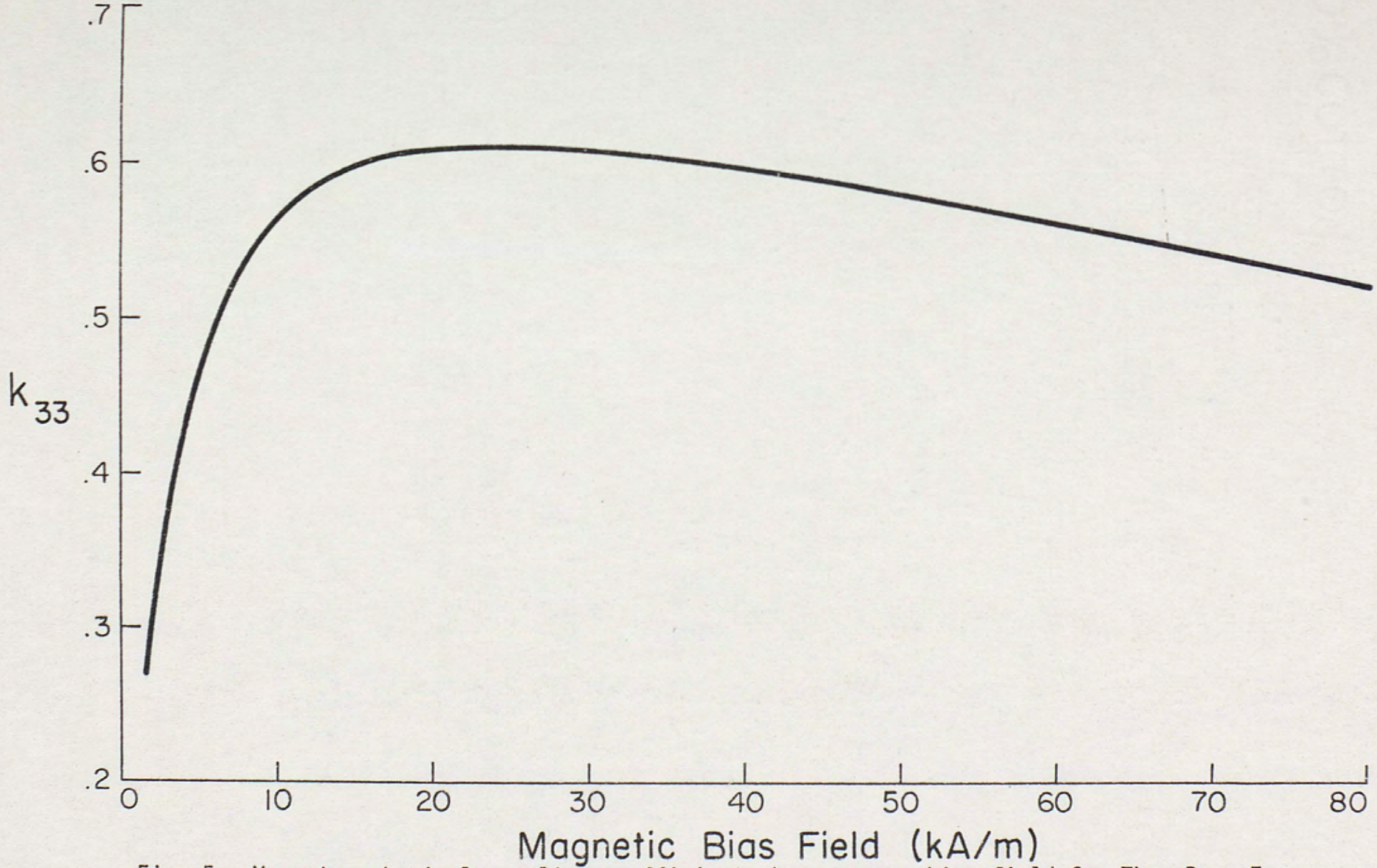

Fig. 5. Magnetomechanical coupling coefficient, k_{33}, versus bias field for $Tb_{.27}Dy_{.73}Fe_{1.95}$

range about the bias.

Preparation of the Rare Earth Iron Rods

Five rods of $Tb_{.27}Dy_{.73}Fe_{1.95}$ each 1.24-cm in diameter by 6.4-cm in length were prepared by Gschneidner [19] at Iowa State University by arc melting the proper proportions of the starting materials and casting ingots in an argon atmosphere. The five resulting rods were x-rayed for cracks or faults by Clark [20]. One rod was found to have a void near one end, and another had a crack running through its length. The remaining three rods were fixed in a small cutting jig and cut to size using a precision saw (Macrotome II, Metals Research LTD., Cambridge, England) and a diamond impregnated blade. The final cut length was 5.06 cm for each rod.

The rare earth iron material has a brittle nature, much like the conventional ceramic material. This requires the rods to be mechanically bias stressed (i.e., compression prestressed) to prevent them from going into tension where they could fracture under high dynamic drive. Thus the ends of the rods were required to be very nearly parallel to prevent shear stresses as the rods were mechanically bias stressed. This was accomplished by the use of a polishing apparatus which was designed and described by Timme [21]. The apparatus consisted of an aluminum body supported by three precision, carbide-tipped micrometer heads spaced equally on a 5.08-cm radius. The rare earth rod to be polished was held in place by nylon screws in a mount in the center of the apparatus. Rough polishing was

accomplished by circular motion on a 120-grit silicon carbide paper. The grit of the paper was successively decreased until a final polish was obtained by a 600-grit diamond impregnated lap. The parallelism of the two surfaces was checked by use of a precision autocollimator (Nikon Model 6D). The Nikon autocollimator is well suited for measuring small-diameter, poor light reflectors because it utilizes dark field illumination. Once the angle of nonparallelism was determined the micrometers on the polishing apparatus were adjusted so that the rod would be polished at a new angle. All three rods were polished with their ends plane and parallel to within 6 minutes of arc and to within the same length to ± .01 mm.

Design of the Rare Earth Iron Transducer

This section will describe in detail each of the parts which make up the rare earth iron transducer. This transducer is constructed of three basic parts:

1. the front mass,
2. the active elements (rare earth iron rods), and
3. the back mass.

The front mass is the vibrating mass which produces the sound pressure. The active elements (rare earth iron rods) produce the strain which drives the front mass. The back mass is made much more massive than the front mass thus assuring that the majority of the displacement appears at the front mass.

Figure 6 shows a view of the assembled transducer. The

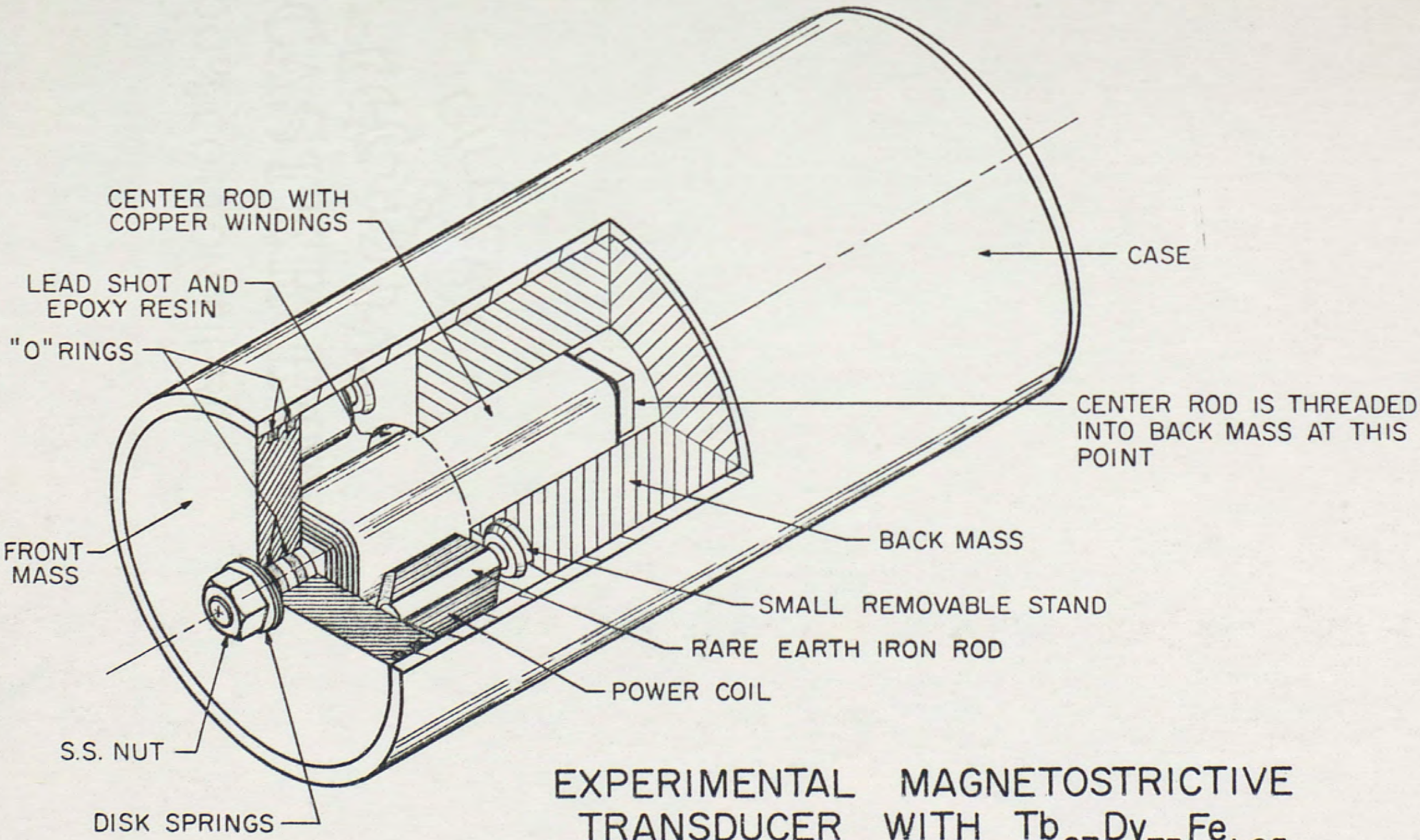

EXPERIMENTAL MAGNETOSTRICTIVE TRANSDUCER WITH $Tb_{.27}Dy_{.73}Fe_{1.95}$

Fig. 6.

square rod running along the center axis is 21.6-cm long and is constructed of Armco magnetic iron. This center rod serves two purposes. The first is to provide a mechanical bias stress. Located at the top of the rod is a 1.27-cm (½-in.) stainless-steel nut which compresses a large washer (not shown) over two disk springs. The disk springs provide compression and at the same time make the stress rod much more compliant than the rare earth iron rods. Below the disk springs are two "O-rings" which seal the rod. Wrapped around the rod along its length are 13 layers of epoxy impregnated number 24 AWG high-temperature copper wire yielding a turn density of 200 turns per centimeter of longitudinal length. Thus the second purpose of the center rod is to provide a bias magnetic field to the rare earth iron rods. The magnetic flux produced by the solenoid travels along the center rod through the front mass down through the rare earth rods and returns through the backmass. The center rod is threaded with a 1.59-cm (5/8-in.) diameter thread which secures the rod into the backmass. The 5-cm diameter hole into which the rod is placed in the backmass is filled with lead shot and epoxy resin to damp spurious resonances.

Spaced at 120° intervals on a 9.2-cm diameter circle surrounding the center rod are the rare earth iron rods and the coils which supply the alternating magnetic field. These coils are also constructed of 13 layers of epoxy impregnated number 24 AWG high-temperature copper wire. They are each 3.1-cm in diameter by 5.3-cm long with 1180 turns of wire yielding a turn density of 225 turns

per centimeter of length. Between the inside diameter of the coil and the rare earth iron rod is a 1.6-mm space left for the flow of cooling fluid. The coils, as well as the rare earth iron rods, are each epoxied to a small removable stand located in the backmass. The epoxy cement which attaches the small stand and the rare earth iron rods was allowed to set while the rods were under a small mechanical bias stress so that any slack in the system would be taken up by the epoxy. The rare earth iron rods are not epoxied to the front mass but are held in place only by the compression exerted by the disk springs. The coils wrapped about the rare earth iron rods are used to supply an additional bias magnetic field as well as the alternating field. Shown in figure 7 is the bias flux density, B_B, versus current generated by the center rod and by the coil about one of the rare earth iron rods. The flux density was measured by using an integrating flux meter (Magnemetrics Model MF-1) to measure the flux through a small sense coil wrapped about one of the rare earth iron rods. Notice that only about .3 tesla can be obtained on each of the rods with the center coil. This is due to a saturation of the magnetic path at the front of the center rod where it decreases in diameter so that it will pass through the hole in the front mass. The remainder of the required bias field is supplied by the coils wrapped about the rare earth iron rods. This transducer was tested at two bias flux densities, .4 and .6 tesla.

Consider the field produced by the coils wrapped about the

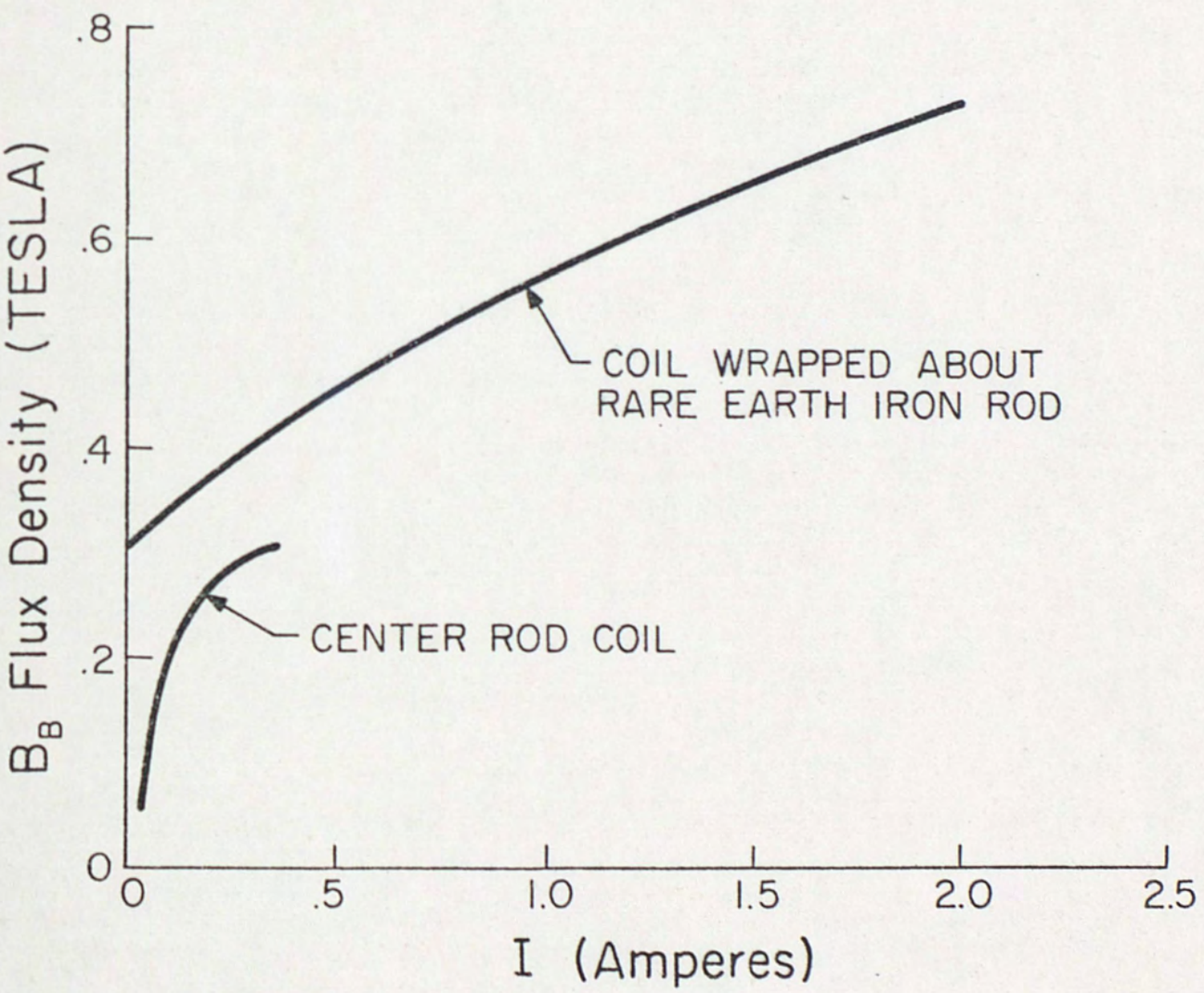

Fig. 7. Flux density versus current

rare earth iron rods. The expression for the field produced by a short fat (many layers of wire) coil is given by Bozorth [22] as

$$H_o(x) = \frac{NI}{2\ell}\left[\frac{\ell + x}{2\,(a - b)}\,\ell og_e\left[\frac{a + s_2}{b + s_1}\right] + \frac{\ell - x}{2\,(a - b)}\,\ell og_e\left[\frac{a + r_2}{b + r_1}\right]\right] \tag{5}$$

where I is the current in amperes,

$H_o(x)$ is the field produced in $\frac{\text{amperes}}{\text{meter}}$ at point x,

N is the number of turns of wire,

x is the distance from the middle of the coil in meters to a point on the longitudinal axis of the coil,

2ℓ is the length of the solenoid in meters,

a is the radius of the outer windings in meters, and

b is the radius of the inner windings in meters.

Also,

$$r_1^2 = b^2 + (\ell - x)^2, \tag{6}$$

$$r_2^2 = a^2 + (\ell - x)^2, \tag{7}$$

$$s_1^2 = b^2 + (\ell + x)^2, \text{ and} \tag{8}$$

$$s_2^2 = a^2 + (\ell + x)^2. \tag{9}$$

In order to simplify the expression for the field, choose the field

at the center of the coil on axis, that is, let x = 0. Then $r_1 = s_1$ and $r_2 = s_2$, and

$$H_o(0) = \frac{NI}{2\ell}\left[\frac{\ell}{a - b}\log_e\left(\frac{a + s_2}{b + s_1}\right)\right]. \tag{10}$$

When the rare earth iron rod is introduced into the coil, the field H_o is reduced by the poles induced on the ends of the magnetic rare earth iron rod. This demagnetizing effect can be accounted for by reducing H_o by $N'M$ where N' is a demagnetization factor and $M = (B - \mu_o H)/\mu_o$ is the magnetization of the rod. Therefore,

$$H(0) = H_o(0) - N'M \tag{11}$$

or by substituting for M and manipulating

$$H(0) = \frac{H_o(0)}{1 + N'_{SI}\left(\frac{\mu}{\mu_o} - 1\right)} \tag{12}$$

where N'_{SI} signifies the demagnetizing factor in the SI unit system. Values of $N'_{EMU}/4\pi$(cgs electromagnetic units) are given by Bozorth [22] versus length-to-diameter ratio for several permeabilities. It can be shown that

$$\frac{N'_{EMU}}{4\pi} = N'_{SI} \tag{13}$$

thus the values given by Bozorth are the ones which appear in equation (12). The values of the demagnetizing factor given by Bozorth

are for a rod with no low reluctance flux return path. It is believed that this is the case here since above .3 tesla the flux return path is saturated by the center coil flux leaving no low reluctance return path. The expression for the field in the presence of demagnetization becomes

$$H(0) = \frac{NI}{2\ell}\left[\frac{\ell}{a - b}\,\ell og_e\left(\frac{a + s_2}{b + s_1}\right)\right]\left[\frac{1}{1 + N_{SI}'\left(\frac{\mu}{\mu_o} - 1\right)}\right] \qquad (14)$$

where $2\ell = 5.25 \times 10^{-2}$ m,

$N = 1179$ turns,

$a = 1.553 \times 10^{-2}$ m,

$b = .732 \times 10^{-2}$ m,

$s_1 = 2.725 \times 10^{-2}$ m, and

$s_2 = 3.05 \times 10^{-2}$ m.

Substituting these values into equation (14) yields equation (15) for the direct current bias magnetic field, $H_B(0)$

$$H_B(0) = \frac{2.058 \times 10^4\ I}{1 + N_{SI}'\left(\mu_r^{STATIC} - 1\right)} \qquad (15)$$

where $\mu_r^{STATIC} = \frac{\mu^{STATIC}}{\mu_o}$ indicates the relative static permeability. The static permeability shown in figure 2 can be fit to the curve

$$\mu_r^{STATIC} = 2.168 \times 10^4\ H_B^{-.676},\ 4\ \frac{kA}{m} \leq H_B \leq 160\ \frac{kA}{m} \qquad (16)$$

where H_B is the magnetic bias field (the abcissa) of figure 2.

Substituting equation (16) in equation (15) and using $N_{SI}' = .048$ and $H_B \simeq H_B(0)$ results in equations (17) and (18) after suitable manipulation.

$$I = \frac{H_B(0) + 1093\ H_B(0)^{.324}}{2.162 \times 10^4} \tag{17}$$

$$B = (.0272)\ H_B(0)^{.324}. \tag{18}$$

These expressions are plotted in figure 8. Also shown is the measured flux density taken from figure 7. The conclusion is that equation (14) gives a good approximation to the actual field produced in the rod by the coil surrounding it.

The circular mass at the front of the transducer is the active or vibrating mass. It is also referred to as the front mass and is constructed of Armco magnetic iron. Its mass is 1.896 kg and it is 2-cm thick and 12.7-cm in diameter. The size of the front mass was determined by the desire for a low resonance frequency with a reasonable sound pressure output. The front mass is sealed by two "O-rings" running along its outer circumference and two "O-rings" around the center rod.

The backmass of this transducer has been made approximately ten times the mass of the front piston. This has been done to insure that the majority of the radiation comes from the front mass. The backmass is also constructed of Armco magnetic iron. The electrical feed-throughs are in the backmass and consist of 3 holes drilled along its length with 3 bulkhead connectors (not shown) at the rear

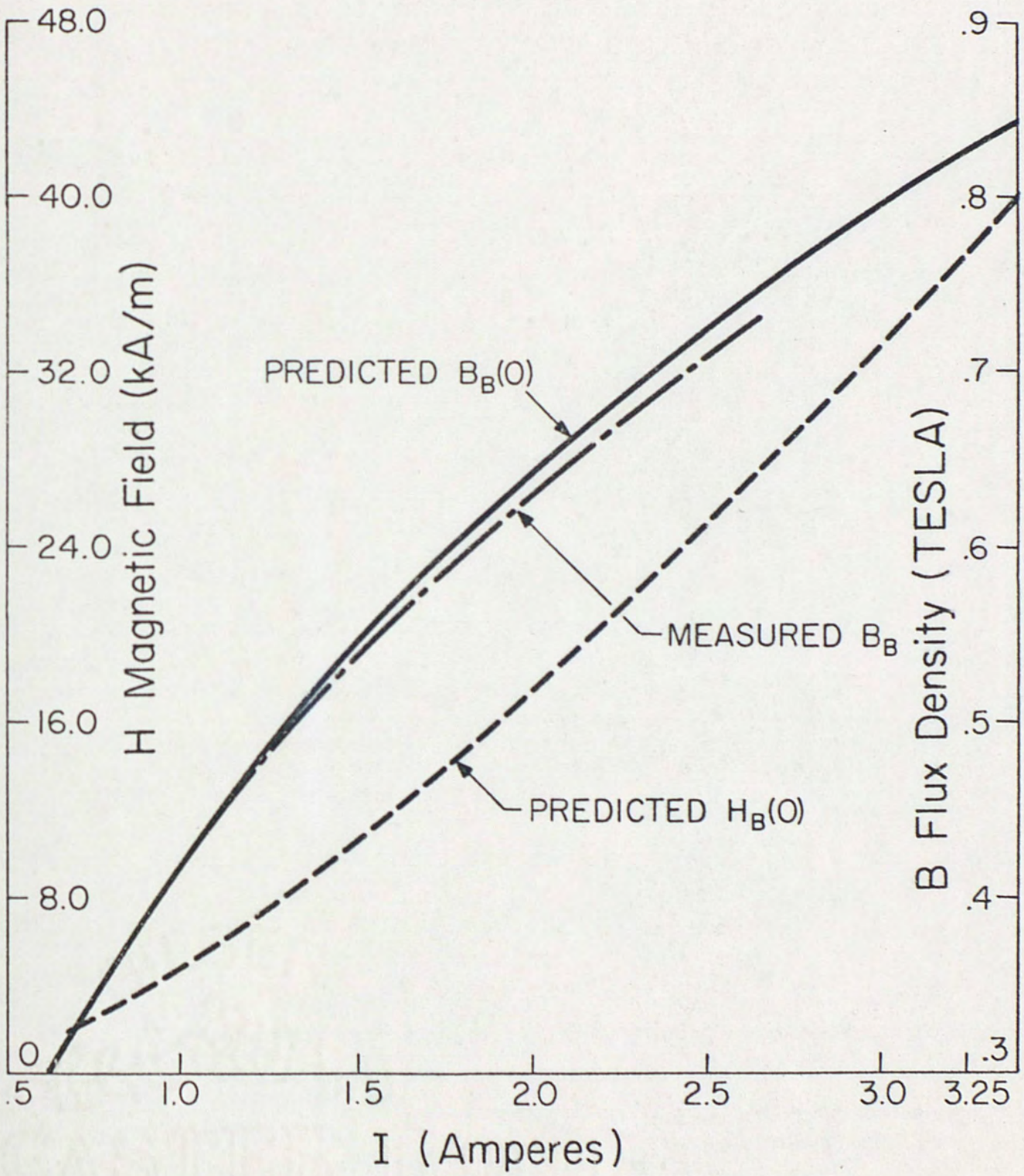

Fig. 8. Magnetic field and flux density versus current

of the device. The backmass is also sealed with two "O-rings" running about its circumference.

The case which fits over the entire transducer is constructed of anodized aluminum. It is 15.2-cm in diameter and 33-cm long. Not shown in figure 6 is a submersible pump and radiator assembly which provides forced cooling of the rods and coils. The pump and radiator fit on the outside of the case and supply a low viscosity transducer fluid (polyalkylene glycol) through two holes in the case. This limited the temperature rise of the solenoids surrounding the rare earth iron rods to 25°C at an input power of 140 watts.

The required bias stress was placed on the rare earth iron rods by a Baldwin Universal Testing Machine. This was accomplished by placing a 4.3-cm diameter, .64-cm thick, stainless-steel washer between the disk springs on the center rod and the nut which secures them. A large plate (21.6-cm diameter by 1.3-cm thick) with a centered hole to allow the center rod nut to pass through was then placed upon the washer. The Universal Testing Machine then exerted a stress upon the plate which was transferred via the disk springs to the rare earth iron rods. Once the required stress was obtained the nut was tightened down to hold the springs in compression. This system worked very well exerting a stress of up to 18.5 MPa (2700 lb./in.^{2}) on each of the rods without any problems. The stress used when testing the transducer was 12.4 MPa (1800 lb./in.^{2}). The mass of the completely assembled transducer was approximately 30 kg.

CHAPTER III

THEORY - THE EQUIVALENT CIRCUIT OF A MAGNETOSTRICTIVE TRANSDUCER IN THE PRESENCE OF EDDY CURRENTS

The objective of this chapter is to derive the equivalent circuit of the transducer described in Chapter II and use the equivalent circuit to predict the performance of a laminated transducer. This chapter will be organized into four parts: the derivation of the blocked or electrical impedance will be presented first; next will be the motional or mechanical impedance of the transducer; then the acoustical impedance; and finally a discussion of the complete equivalent circuit.

Eddy Currents in a Rod

When an alternating current is applied to a solenoid, a circumferential electric field is generated by the time changing flux. If a conducting rod is placed in the solenoid the electric field generates circumferential currents in the rod. These currents are in a direction so as to generate a magnetic field which opposes the applied magnetic field. These circulating currents are known as eddy currents. In a rod the magnitude of the eddy currents increases in direct proportion to the radial distance from the center of the rod. Thus near the center of the rod the opposing magnetic field

generated by the eddy currents is the largest, since all the eddy currents encircle this axis. This effectively shields the center of the rod from the applied magnetic field leading to the well known skin effect. Since the rod in the solenoid has a finite resistivity the eddy currents also generate an ohmic loss. In this section the electrical or blocked impedance of a rod in the presence of eddy currents will be derived for various frequency ranges.

The penetration of flux into a solid conducting wire or rod is governed by the differential equation given by Bozorth [22]:

$$\frac{1}{r}\frac{\partial}{\partial r}\left(r\frac{\partial \overline{H}}{\partial r}\right) = \frac{\mu}{\rho}\frac{\partial \overline{H}}{\partial t} \tag{19}$$

whose solution, considering magnitude only, to a sinusoidally penetrating field is

$$H(r,t) = H_s \sin(\omega t)\left[\frac{\mathrm{ber}^2\left(\frac{2\theta r}{d}\right) + \mathrm{bei}^2\left(\frac{2\theta r}{d}\right)}{\mathrm{ber}^2\theta + \mathrm{bei}^2\theta}\right] \tag{20}$$

where r is the radial distance from the cylinder axis to the point in question,

d is the diameter of the rod, and

$H_s \sin(\omega t)$ is the magnetic field intensity at the surface of the rod.

The parameter θ is given by

$$\theta = \pi d\left(\frac{\mu f}{2\pi\rho}\right)^{\frac{1}{2}} \tag{21}$$

where μ, ρ, and f are the rod's incremental permeability,

resistivity, and frequency, respectively, in SI units. In the solution of equation (19) it is assumed that the permeability is constant, independent of field strength. Figure 2 on page 13 shows that this is a good assumption for terbium dysprosium iron (note that the abcissa of figure 2 is a logarithmic axis). The ber and bei functions in equation (20) are combinations of Bessel functions of the first and second kinds and have been tabulated [23].

Define a characteristic frequency, f_c, by setting $\theta = 1$. Solving for f_c yields

$$f_c = \frac{2\rho}{\pi d^2 \mu} . \tag{22}$$

In order to examine the physical significance of f_c solve equation (20) for $\frac{H(0,t)}{H_s}$ (i.e., let $r = 0$, which is the center of the rod) when $\theta = 1$, which corresponds to $f = f_c$. This yields $\frac{H(0,t)}{H_s} = .97$. Thus the magnetic field at the center of the rod is 97% of its value at the surface. Therefore f_c corresponds to the frequency, for a given diameter, permeability, and resistivity, below which the penetration of flux into the rod is essentially uniform.

A magnetostrictive material has two identifiable incremental permeabilities, the free and the clamped permeabilities. The free permeability (designated by μ_{33}^T) is the permeability which would be measured when the magnetostrictive rod is held under a constant (or zero) stress, hence the term "free permeability". The clamped permeability is designated by μ_{33}^S and is the permeability which would be measured when the magnetostrictive rod is held at a constant strain,

thus the term "clamped permeability". The clamped permeability is the permeability which determines the electrical inductance. It is also known as the "blocked permeability". The free and the clamped permeabilities are related via the coupling coefficient; the relationship is

$$\mu_{33}^{S} = \mu_{33}^{T}\left[1 - k_{33}^{2}\right]. \tag{23}$$

In order to determine which permeability appears in the expression for the characteristic frequency (equation 22) consider the following argument. Imagine a magnetic field penetrating a magnetostrictive rod. In practice it is virtually impossible to clamp the motion of the rod as it is excited by the magnetic field. Thus the magnetic field sees the free or total permeability. That is, the magnetic field sees the measured permeability, which is in fact the free incremental permeability μ_{33}^{T}. Thus for a magnetostrictive material equation (22) contains μ_{33}^{T} rather than μ. Because of the arguments presented above, it would appear that the use of the clamped permeability by other authors [24], [25] is in error. In the case of conventional magnetostrictive materials like nickel the error in f_c is quite small since the clamped and free permeabilities differ by only about 7% because the coupling coefficient is small. The difference is quite large with the rare earth iron materials ($\simeq$36%) since $k_{33} \simeq 0.6$.

Eddy current losses can be accounted for by multiplying the permeability by a complex eddy-current factor χ. The eddy-

current factor depends upon geometry as well as the ratio of frequency to f_c. Thus the impedance of the rods (the core impedance) becomes

$$Z_c = j\omega L_o \chi = j\omega L_o \chi_o e^{-j\zeta} \tag{24}$$

where L_o is the blocked or purely electrical inductance,

$\chi_o = \left[\chi_R^2 + \chi_I^2\right]^{\frac{1}{2}}$, and

$\zeta = \tan^{-1}\left(\frac{\chi_I}{\chi_R}\right)$.

Equation (24) can be rewritten in terms of its real and imaginary parts as shown in equations (25) and (26)

$$Z_c = j\omega L_o \left(\chi_R - j\chi_I\right) \tag{25}$$

$$= \omega L_o \chi_I + j\omega \left(L_o \chi_R\right) \tag{26}$$

where χ_R and χ_I are the real and imaginary parts of the eddy-current factor for a rod which are given by Bozorth [22] and shown in equations (27) and (28) in terms of f/f_c.

$$\chi_R = \frac{\mu'}{\mu} = 2\left(\frac{f_c}{f}\right)^{\frac{1}{2}} \left[\frac{\operatorname{ber}\left(\frac{f}{f_c}\right)^{\frac{1}{2}} \operatorname{bei}'\left(\frac{f}{f_c}\right)^{\frac{1}{2}} - \operatorname{bei}\left(\frac{f}{f_c}\right)^{\frac{1}{2}} \operatorname{ber}'\left(\frac{f}{f_c}\right)^{\frac{1}{2}}}{\operatorname{ber}^2\left(\frac{f}{f_c}\right)^{\frac{1}{2}} + \operatorname{bei}^2\left(\frac{f}{f_c}\right)^{\frac{1}{2}}}\right] \tag{27}$$

$$\chi_I = \frac{\Delta R}{2\pi f L} = 2\left(\frac{f_c}{f}\right)^{\frac{1}{2}} \left[\frac{\operatorname{ber}\left(\frac{f}{f_c}\right)^{\frac{1}{2}} \operatorname{ber}'\left(\frac{f}{f_c}\right)^{\frac{1}{2}} + \operatorname{bei}\left(\frac{f}{f_c}\right)^{\frac{1}{2}} \operatorname{bei}'\left(\frac{f}{f_c}\right)^{\frac{1}{2}}}{\operatorname{ber}^2\left(\frac{f}{f_c}\right)^{\frac{1}{2}} + \operatorname{bei}^2\left(\frac{f}{f_c}\right)^{\frac{1}{2}}}\right] \tag{28}$$

The permeability, μ', in equation (27) is the "apparent permeability". That is, it is the permeability which the magnetic field sees in the presence of eddy currents. The permeability, μ, in equation (27) is the limiting value of μ', approached at low frequencies. The ΔR in equation (28) is the difference between the measured alternating current resistive component of the impedance, R, and the direct current resistance, R_o. The difference ΔR is caused by eddy currents. The inductance, L, in equation (28) is the limiting value of the measured inductance, approached at low frequencies. Figure 9 shows plots of χ_R, χ_I, χ_o, and ζ. The use of equation (27) and figure 9 shows that the "apparent permeability", μ', is a decreasing function of frequency.

In equation (26) it is seen that in the presence of eddy currents the core impedance takes on a resistive component which is proportional to χ_I. The physical significance of the resistive component is that it represents the energy dissipating mechanism of the eddy currents. It is also seen that the core inductance becomes proportional to χ_R. This causes the core inductance to decrease with frequency. The total electrical or blocked impedance consists of the core impedance and the leakage impedance. The core impedance results from flux which passes through the rods and is affected by eddy currents. The leakage impedance consists of the copper resistance and the flux which passes through the air (the leakage inductance). The equivalent circuit of electrical impedance in the general case is shown in figure 10.

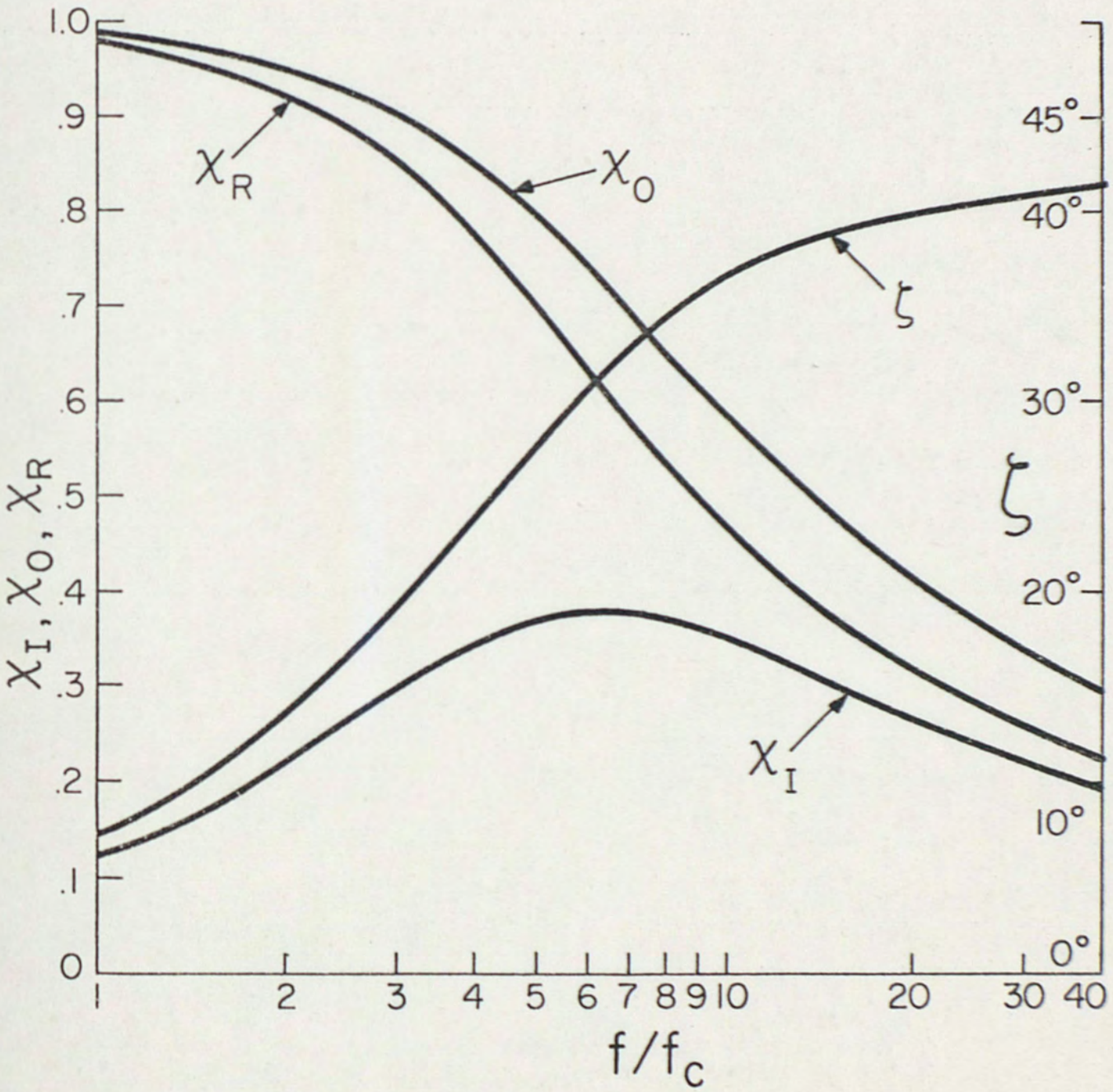

Fig. 9. Eddy current components for a rod

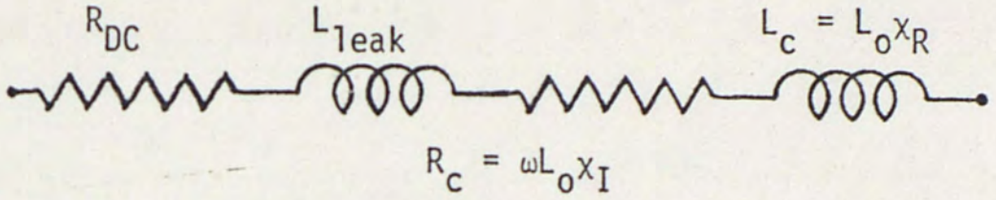

Fig. 10. General equivalent circuit of a rod in the presence of eddy currents

Unfortunately the equivalent circuit of figure 10 is not strictly applicable to the present transducer. This is because the present transducer has eddy current losses in the unlaminated front and back masses which are difficult to account for theoretically. The way in which the blocked impedance was determined was to experimentally measure the total reactance and resistance at 0.4 tesla. Then from these curves the blocked impedance could be approximately determined by drawing a straight line from a point far above resonance (where the motional impedance is small) to one far below resonance. This technique is described in detail in reference [24]. The resulting curves are shown in figures 11 and 12.

The general equivalent circuit shown in figure 10 is inconvenient because both R_c and L_c depend upon frequency. In order to derive a lumped (where none of the components vary with frequency) equivalent circuit consider the expressions given by Bozorth [22] for χ_I and χ_R for $\theta << 1$ shown below.

$$\chi_R = 1 - \frac{\theta^4}{48} + \frac{19\ \theta^8}{30{,}720} + \cdots \tag{29}$$

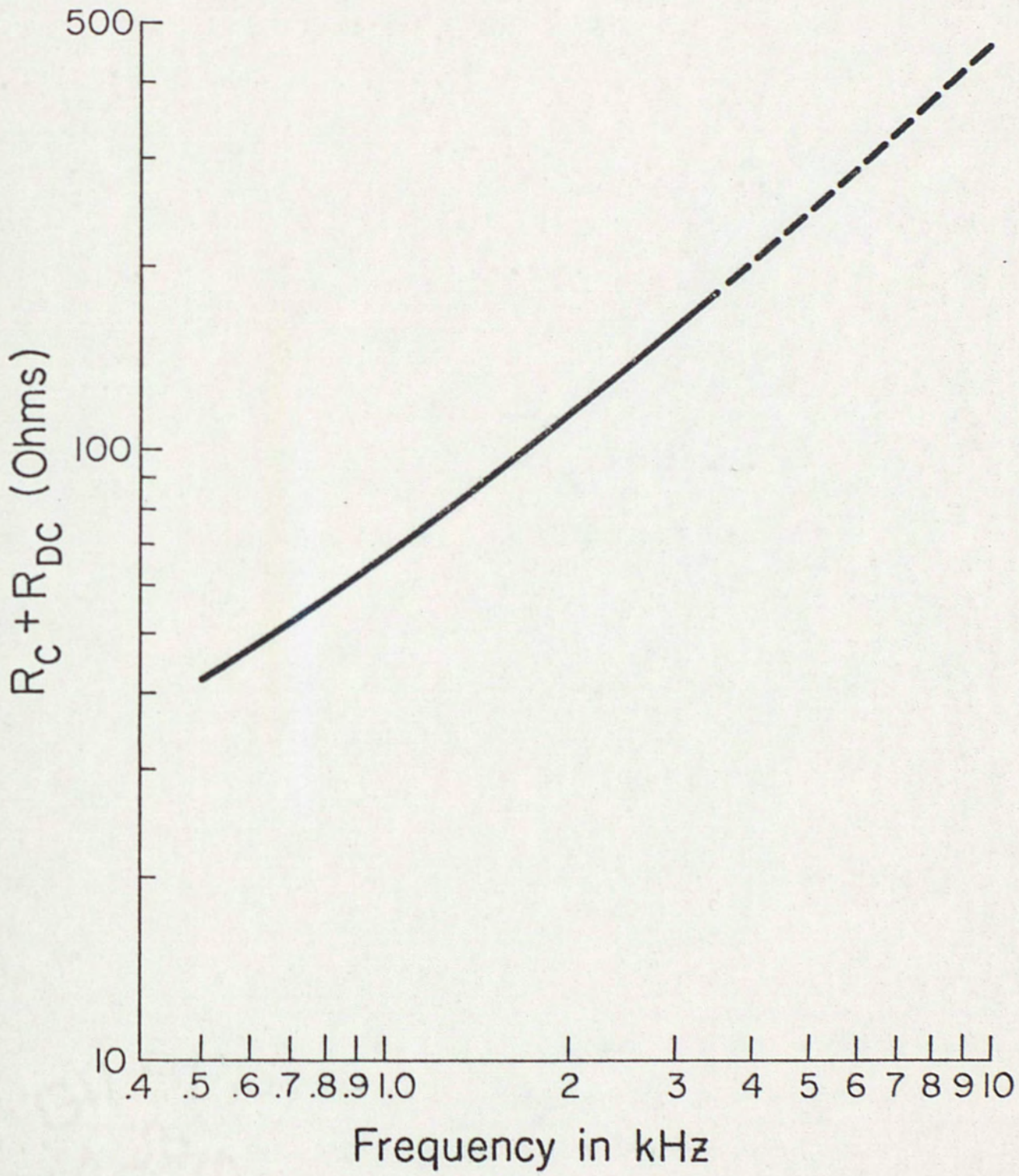

Fig. 11. Approximate blocked resistance at 0.4 tesla

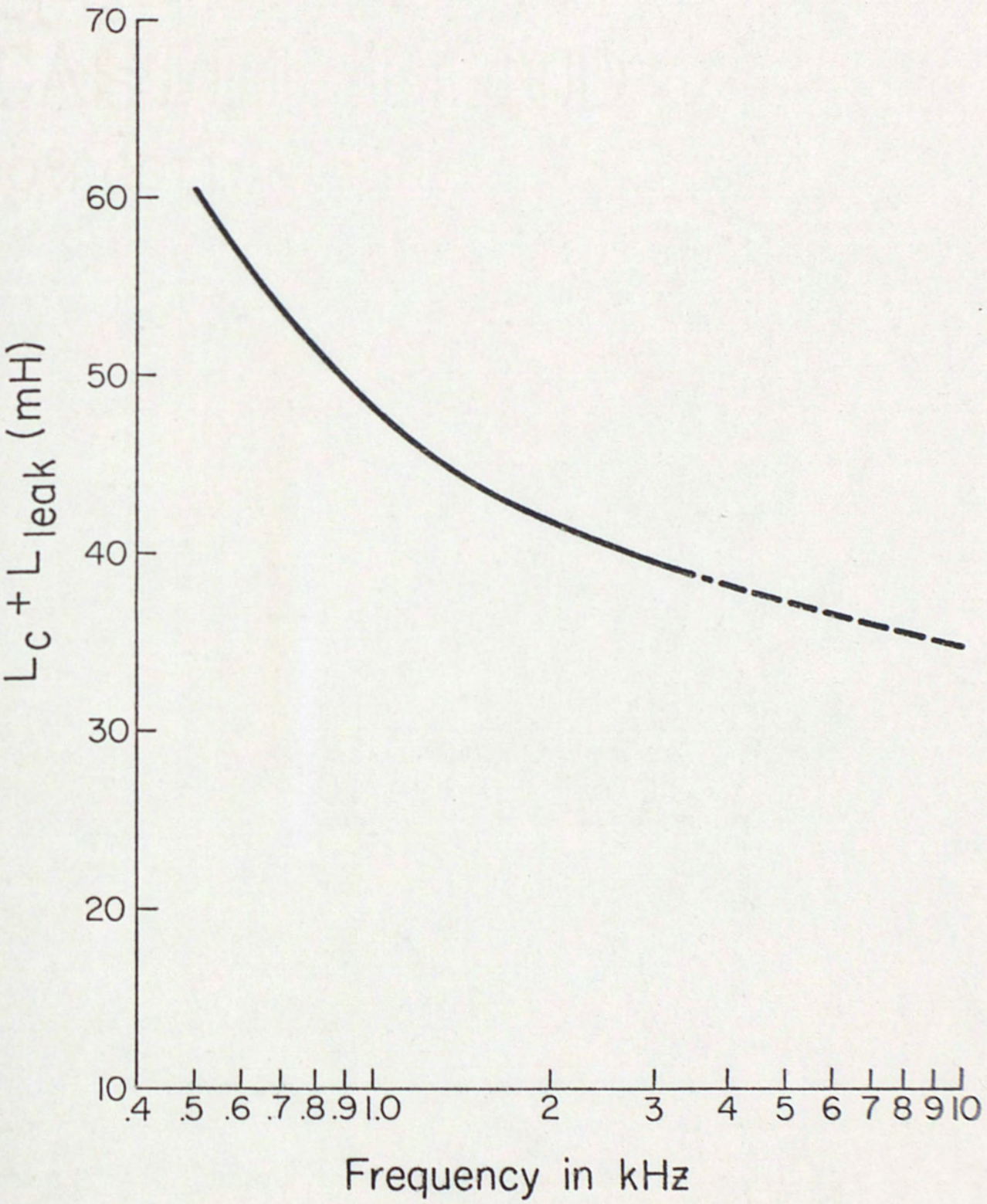

Fig. 12. Approximate blocked inductance at 0.4 tesla

$$\chi_I = \frac{\theta^2}{8} - \frac{11\ \theta^6}{3{,}072} + \frac{473\ \theta^{10}}{4{,}343{,}680} + \cdots \tag{30}$$

Take the first term of χ_R and χ_I and substitute into equation (26). By noting that $\theta = \left(\frac{f}{f_c}\right)^{1/2}$ the result is obtained that

$$Z_c \simeq \frac{\omega L_o f}{8 f_c} + j\omega L_o \tag{31}$$

$$= \frac{\pi L_o f^2}{4 f_c} + j\omega L_o \text{ for } f/f_c < 1. \tag{32}$$

The equivalent circuit is shown in figure 13.

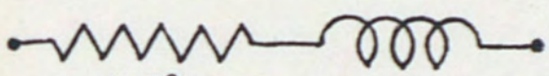

$$R_{cs} = \frac{\pi L_o f^2}{4 f_c} \qquad L_{cs} = L_o$$

Fig. 13. Series equivalent circuit of a rod in the presence of eddy currents for $f < f_c$

This circuit is still somewhat inconvenient since the series core resistance R_{cs} depends upon frequency squared. If the above circuit is converted to its equivalent parallel circuit, the parallel core resistance and inductance R_{cp} and L_{cp}, respectively, are given by equations (33) and (34) below

$$R_{cp} = 16\pi f_c L_o \left[1 + \frac{f^2}{64 f_c^2}\right] \tag{33}$$

$$L_{cp} = L_o \left[1 + \frac{f^2}{64 f_c^2}\right] . \tag{34}$$

When $f < f_c$ the term $\frac{f^2}{64f_c^2}$ can be neglected with an error of less than 2%. Thus the lumped equivalent circuit shown in figure 14 is obtained. Similar equivalent circuits have been obtained by other authors for a thin flat sheet [24] and a ring armature [26]. The case of a thin flat sheet yields $6\pi f_c L_o$ for the resistance where

$$f_c = \frac{2\rho}{\pi t^2 \mu_{33}^T} \tag{35}$$

and t is the thickness of the flat sheet and SI units are used.

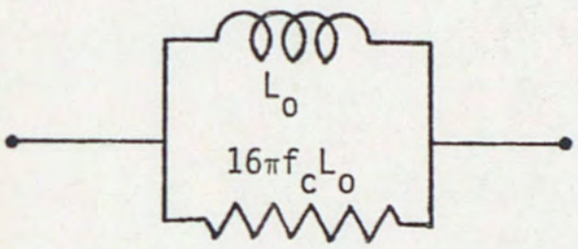

Fig. 14. Parallel equivalent circuit of a rod in the presence of eddy currents for $f < f_c$. Where f_c for a rod = $\frac{2\rho}{\pi d^2 \mu_{33}^T}$.

The complex impedance of the equivalent circuit shown in figure 14 is given by equation (36). Let the real and imaginary portions of equation (36) be equal to R_c and X_c, respectively.

$$Z_c = \frac{16\pi f_c \omega^2 L_o}{\omega^2 + \left[16\pi f_c\right]^2} + j\left[\frac{\left[16\pi f_c\right]^2 \omega L_o}{\omega^2 + \left[16\pi f_c\right]^2}\right] \tag{36}$$

Thus,

$$\frac{R_c}{\omega_c L_o}\Bigg|_{\substack{\text{Equivalent} \\ \text{Circuit}}} = \frac{8\left[\frac{f}{f_c}\right]^2}{\left[\frac{f}{f_c}\right]^2 + 64} \tag{37}$$

$$\left.\frac{X_c}{\omega_c L_o}\right|_{\substack{\text{Equivalent}\\ \text{Circuit}}} = \frac{64\left(\frac{f}{f_c}\right)}{\left(\frac{f}{f_c}\right)^2 + 64} \tag{38}$$

The exact expressions for $R_c/(\omega_c L_o)$ and $X_c/(\omega_c L_o)$ are given by the real and imaginary portions of equation (26) respectively normalized to $\omega_c L_o$ and shown in equations (39) and (40).

$$\left.\frac{R_c}{\omega_c L_o}\right|_{\text{Theoretical}} = \frac{f x_I}{f_c} \tag{39}$$

$$\left.\frac{X_c}{\omega_c L_o}\right|_{\text{Theoretical}} = \frac{f x_R}{f_c} \tag{40}$$

Figure 15 is a comparison of the loci of points predicted by equations (37) and (38) (the equivalent circuit of figure 14) and those predicted by equations (39) and (40) (the exact equivalent circuit). The loci of the impedance of the lumped equivalent circuit describes an arc of a circle which agrees within 1% with the exact equivalent circuit up to $f = f_c$. Above $f = f_c$ deviations begin (particularly in the resistance) but agreement is still fair at three times f_c and usable up to $f = 4f_c$. If the loci of the impedance of a lossless inductor were plotted on figure 15 it would appear as a straight line located on the ordinate with the frequency scale increasing upward.

An interesting alternate derivation of the equivalent circuit

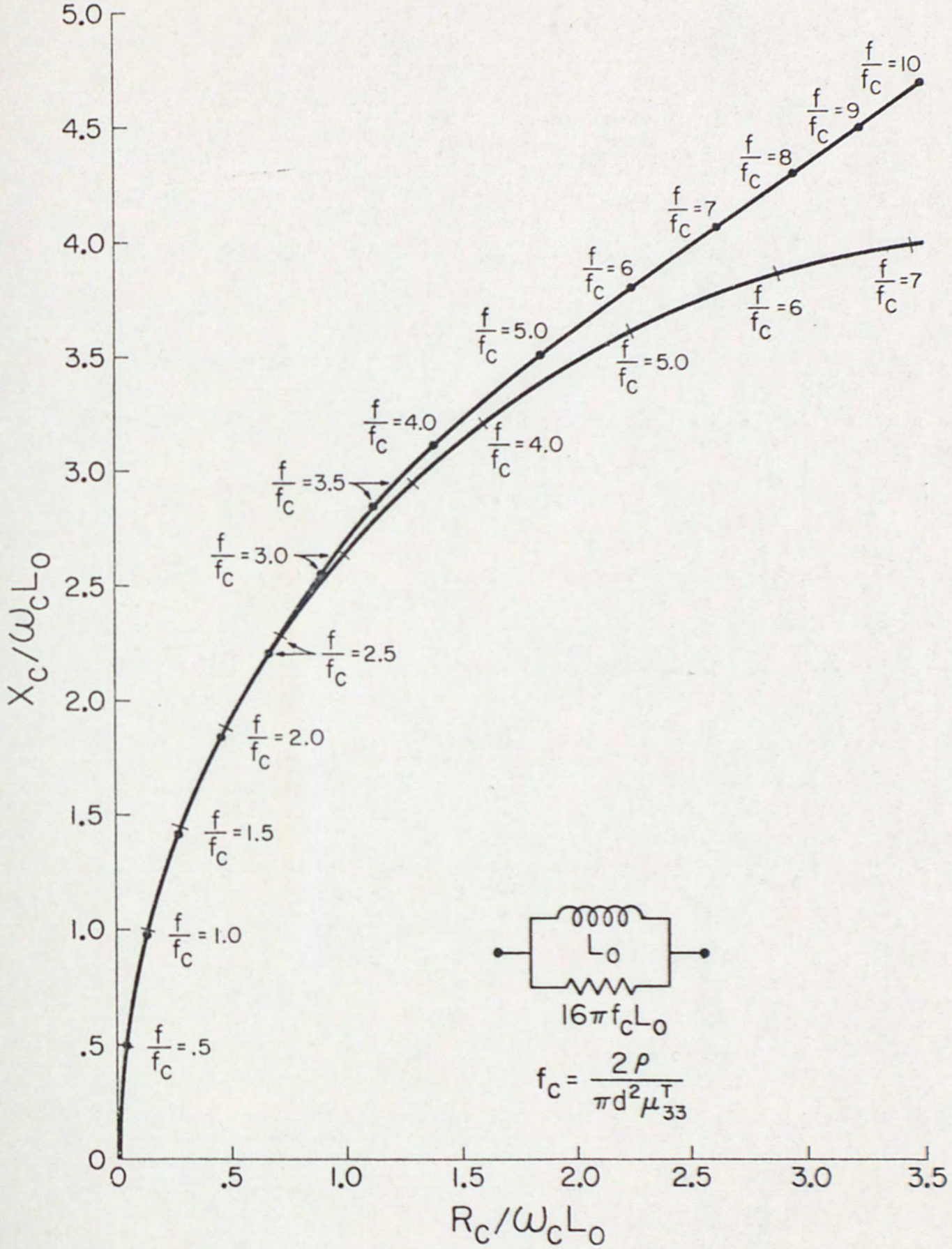

Fig. 15. The upper curve is a plot of the normalized theoretical components of the impedance of a core composed of a rod. The lower curve is a plot of the normalized components of the impedance of the equivalent circuit shown above.

of figure 14 can be obtained through use of Faraday's law. Consider figure 16 which shows a conducting rod in the presence of an alternating magnetic flux. Make the assumption that the flux density is increasing and uniform across the cross-sectional area of the rod. This assumption means that the rod is very long and that the frequency is below the characteristic frequency. Faraday's law relates the time changing magnetic flux to the electric field produced for a fixed region in space.

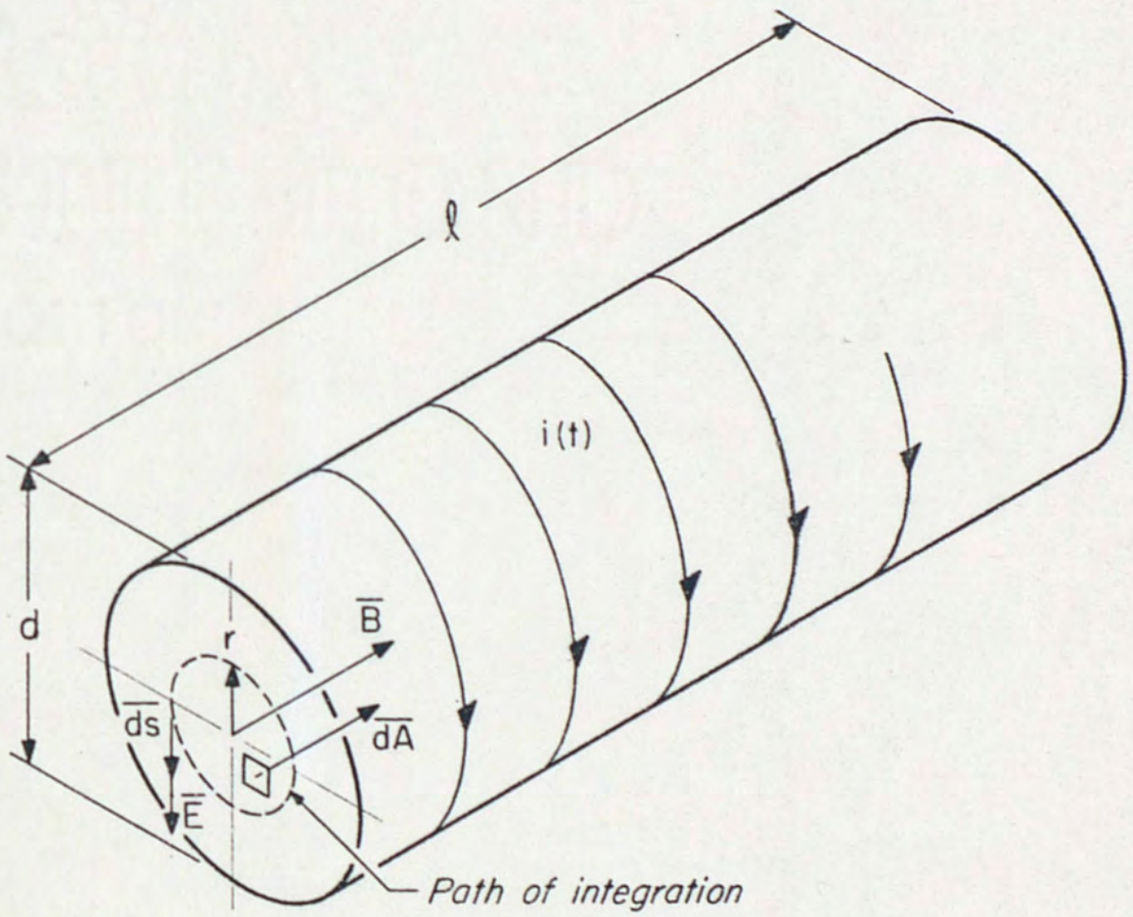

Fig. 16. Eddy currents in a conducting rod. The current i(t) is increasing with time.

$$-\oint \overline{E} \cdot \overline{ds} = \frac{d}{dt} \int_A \overline{B} \cdot \overline{dA} \qquad (41)$$

Now perform the line integral of the electric field about the circular path a distance r from the axis. The electric field magnitude is constant and tangential around this path due to the circular symmetry. The angle between $\overline{E}$ and $\overline{ds}$ is zero degrees. The flux density, $\overline{B}$, is also uniform across the rod and the angle between $\overline{B}$ and $\overline{dA}$ is zero degrees. Considering magnitude only

$$E \oint ds = \frac{d}{dt} B \int_A dA \tag{42}$$

$$E2\pi r = \frac{d}{dt} \pi r^2 B \tag{43}$$

$$= \pi r^2 \frac{dB}{dt} \tag{44}$$

which implies that

$$E = \frac{r}{2} \frac{dB}{dt} . \tag{45}$$

The circumferential surface current density at a radius r is given by

$$J = \frac{E}{\rho} = \frac{r}{2\rho} \frac{dB}{dt} . \tag{46}$$

The total instantaneous power lost is given by

$$p(t) = \oint_v \rho J^2 \, dv \tag{47}$$

$$= \int_{z=0}^{\ell} \int_{\theta=0}^{2\pi} \int_{r=0}^{\frac{d}{2}} \rho \frac{r^2}{4\rho^2} \left(\frac{dB}{dt}\right)^2 r \, dr \, d\theta \, dz \tag{48}$$

which yields

$$p(t) = \frac{\pi d^2 \ell}{4} \frac{d^2}{32\rho} \left(\frac{dB}{dt}\right)^2 \tag{49}$$

where $\frac{\pi d^2 \ell}{4}$ is the volume of the rod. Let A equal the area of the rod

then

$$p(t) = \frac{A\ell d^2}{32\rho}\left(\frac{dB}{dt}\right)^2. \tag{50}$$

The voltage induced in the coil is given by

$$e(t) = NA\frac{dB}{dt}. \tag{51}$$

Solving equation (51) for $\left(\frac{dB}{dt}\right)^2$ yields

$$\left(\frac{dB}{dt}\right)^2 = \frac{e^2(t)}{N^2A^2}. \tag{52}$$

Substituting equation (52) into equation (50) yields

$$p(t) = \frac{d^2e^2(t)\ell}{32\rho N^2A} = \frac{e^2(t)}{R} \tag{53}$$

which implies that

$$R = \frac{32\rho N^2A}{d^2\ell} \text{ ohms}. \tag{54}$$

Compare the resistance given in equation (54) with the $16\pi f_c L_o$ derived previously. Since a long rod was initially assumed with no mention of magnetostriction, L_o is given by

$$L_o = \frac{N^2A\mu}{\ell}. \tag{55}$$

Equation (55) and the expression for f_c (equation 22) yield for the resistance equation (56).

$$R = 16\pi\left(\frac{2\rho}{\pi d^2\mu}\right)\frac{N^2A\mu}{\ell} = \frac{32\rho N^2A}{d^2\ell}. \tag{56}$$

Thus both derivations yield the same result for a very long non-magnetostrictive rod. The derivation using Faraday's law is somewhat less satisfying than the first derivation since it does not indicate whether the resistance is a series or a parallel element.

Consider what happens when a long magnetostrictive rod is introduced into a solenoid. Here L_o is given by equations (57) and (58).

$$L_o = \frac{N^2 A \mu_{33}^S}{\ell} \tag{57}$$

$$= \frac{N^2 A \mu_{33}^T (1 - k_{33}^2)}{\ell} \tag{58}$$

The clamped permeability, μ_{33}^S, is used above since the purely electrical or blocked inductance is required. The resistance, $16\pi f_c L_o$, for a long magnetostrictive rod becomes

$$16\pi f_c L_o = \frac{32\rho N^2 A (1 - k_{33}^2)}{d^2 \ell} \quad . \tag{59}$$

The equivalent circuit of a long magnetostrictive rod for $f < f_c$ is shown in figure 17. Since L_o is the blocked or purely electrical inductance, R is by analogy the blocked or purely electrical resistance of the magnetostrictive rod. The equivalent circuit of a nonmagnetostrictive rod can be obtained by substituting equations (55) and (56) for L_o and R respectively in figure 17. The same circuit can also be obtained from figure 17 by letting the magnetomechanical coupling go to zero and replacing μ_{33}^T by μ.

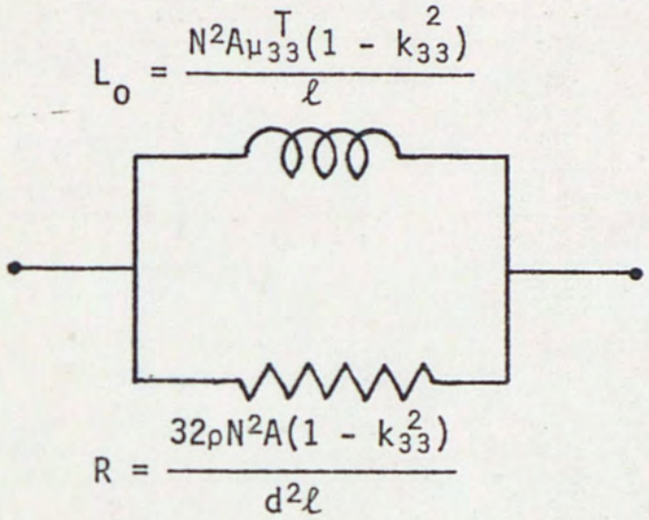

Fig. 17. Equivalent circuit of a long magnetostrictive rod for $f < f_c$

Consider the power loss due to eddy currents in two rods identical in every respect (i.e., identical geometry, permeability, and resistivity) except that one rod is magnetostrictive and the other is not. Assume that the same amount of current is passed through the equivalent circuit representing the electrical impedance of each rod. Figure 17 and equations (55) and (56) show that the current in the resistive branch is the same regardless of magnetostriction. But the resistance in the magnetostrictive case is lower by a factor of $1 - k_{33}^2$. Thus the power loss due to eddy currents is lower, in a magnetostrictive material, by the factor $1 - k_{33}^2$. This shows an additional benefit to the large coupling coefficient of terbium dysprosium iron.

In the actual analysis of the transducer's performance, two equivalent circuits for the blocked impedance were used. The first was for the unlaminated transducer and was a series combination of a resistance and inductance. The values for the resistance and inductance were taken from figures 11 and 12. The second representation of the blocked impedance was generated to predict the performance of a laminated transducer. In the laminated version it was assumed that the cross section of each of the three rods was cut into quarters. The rods were then cemented together with each quarter being insulated from its neighbor. The equivalent circuit for the blocked impedance of three rods in series is shown in figure 18. Three quantities, L_o, f_c, and L_{leak}, need to be determined for a quartered rod. The characteristic frequency of a quartered rod can be determined by considering each quarter to be a rod with one half the diameter of the original rod. This comes about since each section of the rod has one quarter the area yielding an equivalent diameter of one half the original diameter of the solid rod.

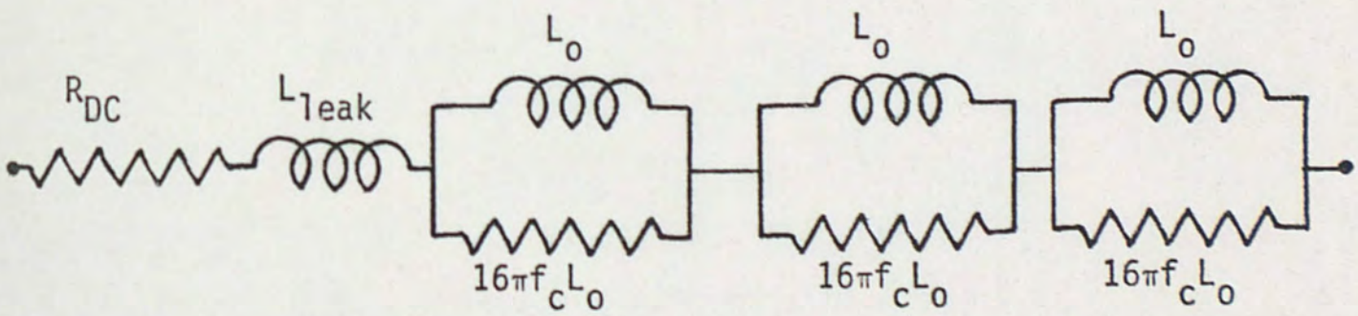

Fig. 18. Equivalent circuit of the electrical impedance of three rods in series for $f < f_c$

In equation (22) it is seen that the characteristic frequency increases by a factor of four when the diameter is cut in half. This means that in the quartered rod the flux density stays uniform up to a frequency four times higher than in the solid rod. The characteristic frequency (equation 22) is calculated in table 2 for the laminated and unlaminated configurations and two bias flux densities. The resistivity of terbium dysprosium iron is 60×10^{-8} ohm-meter at room temperature. The diameter of the original rods was 1.24×10^{-2} m.

TABLE 2

CHARACTERISTIC FREQUENCIES FOR SOLID AND QUARTERED RARE EARTH IRON RODS

Configuration	Bias Flux Density (Field)	Relative Incremental Permeability	f_c
Solid	0.4 tesla ($4.3 \frac{kA}{m}$)	7.5	260 Hz
Solid	0.6 tesla ($14.3 \frac{kA}{m}$)	5.4	370 Hz
Quartered	0.4 tesla ($4.3 \frac{kA}{m}$)	7.5	1060 Hz
Quartered	0.6 tesla ($14.3 \frac{kA}{m}$)	5.4	1470 Hz

The characteristic frequency (assuming $\rho = 8 \times 10^{-8}$ ohm-meter and relative incremental permeability = 30) of a nickel rod of the same size is about 9 Hz. This points out that eddy current losses are inherently lower in the rare earth iron material due to its lower

permeability and higher resistivity.

The blocked inductance L_o can be obtained via the relationship

$$L_o = \frac{d\ (N\Phi)}{d\ i_{rms}} \tag{60}$$

where Φ is the flux in webers and i_{rms} is the root mean square value of the sinusoidally varying current.

Also,

$$N\Phi = NBA = N\mu_{33}^{S}HA \tag{61}$$

where the magnetic field H is taken from equation (10) using the values for 2ℓ, N, a, b, s_1, s_2 given on page 26.

Thus,

$$H_{rms}(0) = 2.058 \times 10^4\ i_{rms} \tag{62}$$

hence,

$$\begin{aligned} L_o &= 2.058 \times 10^4\ \mu_{33}^{T}\ (1 - k_{33}^2)\ AN \\ &= .0186 \text{ henries at } 0.4 \text{ tesla.} \end{aligned} \tag{63}$$

The leakage inductance can be obtained by calculating the inductance of the air gap between the rare earth iron rod and the inner diameter of the coil about the rod. The use of equations (10) and (60) yields the leakage inductance for the three rods and coils shown in equation (64).

$$L_{leak} = 2.058 \times 10^{4}\ \mu_o\ A_{air}\ 3N \qquad (64)$$

$$= .0043\ H.$$

The symbol μ_o is the permeability of free space and A_{air} is the area of the air gap which equaled $4.64 \times 10^{-3}\ m^2$. A summary of the values required by the equivalent circuit in figure 18 is shown in table 3.

TABLE 3

VALUES REQUIRED BY EQUIVALENT CIRCUIT OF FIGURE 18

Component	Value
R_{DC}	23 ohms
L_{leak}	.0043 H
L_o	.0186 H at 0.4 T
$16\pi f_c L_o$	990 ohms at 0.4 T (quartered rod)

An equivalent circuit for a rod which is being operated far above its characteristic frequency (i.e., $\theta >> 1$) can be derived from equation (26) and the limiting forms of equations (27) and (28). This circuit is shown in figure 19. Notice that both the resistance and reactance are proportional to $\omega^{\frac{1}{2}}$.

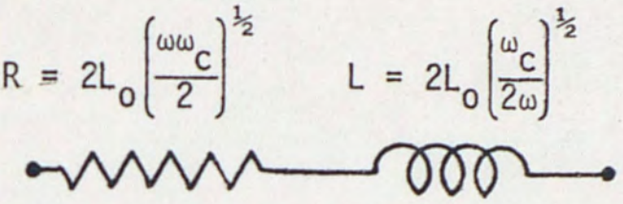

Fig. 19. Equivalent circuit of a rod when $f >> f_c$. The angular characteristic frequency is $\omega_c = (4\rho)/d^2\mu_{33}^T$.

In this chapter three equivalent circuits of a magnetostrictive rod in the presence of eddy currents have been derived. The first circuit was shown in figure 10 and is a general equivalent circuit for all frequency ranges. The next equivalent circuit was given in figure 14. The circuit of figure 14 yields almost exact agreement with the general equivalent circuit up to $f = f_c$ and usable results up to $f = 4f_c$. The third equivalent circuit was presented in figure 19 and is valid when $f >> f_c$.

The Mechanical (Motional) Impedance of the Magnetostrictive Transducer

This section will present the mechanical impedance of both the magnetostrictive rods and the remainder of the transducer. The equivalent circuit of a magnetostrictive transducer can be represented in three ways:

1) the mobility analogy,

2) by shifting force and velocity by 90°, or

3) F. V. Hunt's space operator.

In the mobility analogy force is analogous to current and velocity is analogous to voltage. The core impedance in the mobility analogy appears in series with the electromechanical transformer. In the latter two representations, the core impedance appears in parallel with the electromechanical transformers. F. V. Hunt [27] gives an enlightening discussion of all three representations. The mobility analogy is chosen for the present analysis because it is the most widely accepted and simplest to use.

The equivalent circuit of a lossless magnetostrictive rod in the mobility analogy is given by Katz [28] and is shown in figure 20. This circuit will be modified to account for the effects of eddy currents and demagnetization. F_1 and F_2 are the forces on the two respective ends of the rod. V_1 and V_2 are the velocities of these two ends.

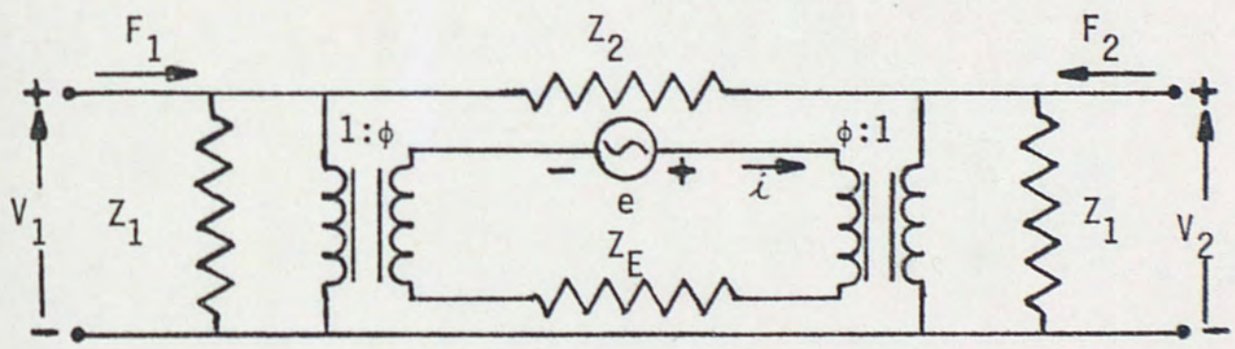

Fig. 20. Equivalent circuit of a magnetostrictive rod in the mobility analogy

Z_E is the purely electrical or blocked impedance of the rod in the presence of eddy currents and was discussed in detail in the previous section. A sinusoidal current and voltage, i and e respectively, are applied to the coil surrounding the rod. The turns ratio, ϕ, of the electromechanical transformer relates the electrical units on the one side of the transformer to the mechanical units on the other side. The units of ϕ are newtons per ampere. Z_1 and Z_2 are motional impedance terms which are given by Katz [28] and shown in equations (65) and (66)

$$Z_1 = \frac{1}{j\tan\left(\frac{\beta\ell}{2}\right) Z_o} \tag{65}$$

$$Z_2 = \frac{j\sin(\beta\ell)}{Z_o} \tag{66}$$

where $Z_o = A\left(\frac{\rho}{s_{33}^B}\right)^{1/2}$,

$\beta = \omega\left(\rho s_{33}^B\right)^{1/2}$,

ℓ = length of rod,

A = cross-sectional area of the rod, and

ρ = density of the rod.

Equations (65) and (66) can be approximated by

$$Z_1 \simeq \frac{1}{j\omega\left(\frac{\rho\ell A}{2}\right)} = \frac{1}{j\omega\,\frac{m}{2}} \tag{67}$$

$$Z_2 \simeq j\omega\left(\frac{s_{33}^B \ell}{A}\right) = j\omega C \tag{68}$$

where m is the static mass of the rod and C is its compliance. Equations (67) and (68) were arrived at by using the small angle approximations that tanx ≃ x and sinx ≃ x. At the resonance frequency of the transducer (2500 Hz) the approximation to the tangent term leads to an error of only 1%. The approximation to the sine term yields an error of 2%. Even at 5 kHz the approximations to the tangent and sine terms lead to errors of only 4 and 7.5%, respectively.

The equivalent circuit shown in figure 20 can be simplified to the present case by realizing that one end of the rod is clamped (i.e., velocity = 0) by the large backmass of the transducer. The result of the velocity of one end of the rod being zero is that one of the output terminals of figure 20 is short-circuited. This results in the impedance Z_2 becoming parallel to Z_1. The result of these approximations and simplifications is shown in figure 21 for three rods mechanically in parallel. The Z_E shown in figure 21 is the electrical impedance of the three rods in the presence of eddy currents.

The derivation of the electromechanical turns ratio ϕ begins with the magnetostrictive equation of state given in equation (1). The factor of three multiplying ϕ in figure 21 results from the fact that three rods produce three times the force for the same amount of current. If S_3 is set equal to zero in equation (1), equation (69) is obtained.

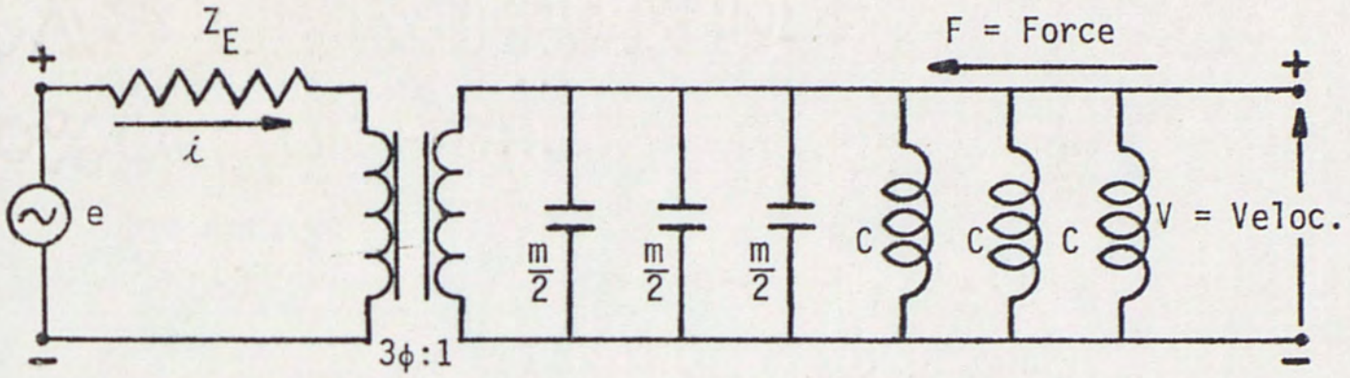

Fig. 21. Simplified equivalent circuit of three magnetostrictive rods mechanically in parallel with one end clamped

$$T_3 = - \frac{d_{33} B_3}{\mu_{33}^T s_{33}^B} \tag{69}$$

The flux density in the clamped($S_3 = 0$) rod is given by equation (70).

$$B_3 = \mu_{33}^S \times H_3. \tag{70}$$

The effect of the eddy currents is accounted for by assuming a complex permeability as in equation (24). That is, μ_{33}^S is multiplied by the complex eddy current factor. If the result of equation (70) is substituted into equation (69), equation (71) is obtained.

$$T_3 = - \frac{d_{33} \mu_{33}^S \times H_3}{\mu_{33}^T s_{33}^B} . \tag{71}$$

The force, F_3, is given by equation (72) and equation (73) where A is the cross-sectional area of the rod.

$$F_3 = T_3 A \tag{72}$$

$$F_3 = - \frac{d_{33}\, \mu_{33}^{S}\, \chi\, H_3\, A}{\mu_{33}^{T}\, s_{33}^{B}} \tag{73}$$

The expression for the magnetic field, H_3, is taken from equation (14) page 26 and shown in equation (74).

$$H_3(0) = \frac{2.058 \times 10^4\, i}{1 + N_{SI}' \left[\frac{\mu_{33}^{T}}{\mu_o} \chi_R - 1 \right]} \tag{74}$$

In the expression for $H_3(0)$ above, the relative incremental permeability μ_{33}^{T}/μ_o is used since the dynamic field is of concern here. The real part of the eddy current factor, χ_R, is multiplied by the relative permeability in equation (74) to yield the "apparent permeability" as indicated by equation (27), page 34. Again, as in the bias field case, complete demagnetization is assumed since no low reluctance path for the alternating flux is provided. The demagnetizing factor for a rod, taken from Bozorth [22], versus relative permeability for a fixed length-to-diameter ratio is shown in figure 22. Equations (73) and (74) can be combined to yield the expression for the force shown in equation (75) (considering magnitude only).

$$F_3 = \frac{d_{33}\, \mu_{33}^{S}\, \chi\, A}{\mu_{33}^{T}\, s_{33}^{B}} \; \frac{2.058 \times 10^4\, i}{1 + N_{SI}' \left[\frac{\mu_{33}^{T}}{\mu_o} \chi_R - 1 \right]} \tag{75}$$

Equation (75) can be rewritten using the relationships

$$\mu_{33}^{S} = \mu_{33}^{T} \left[1 - k_{33}^{2} \right] ,$$

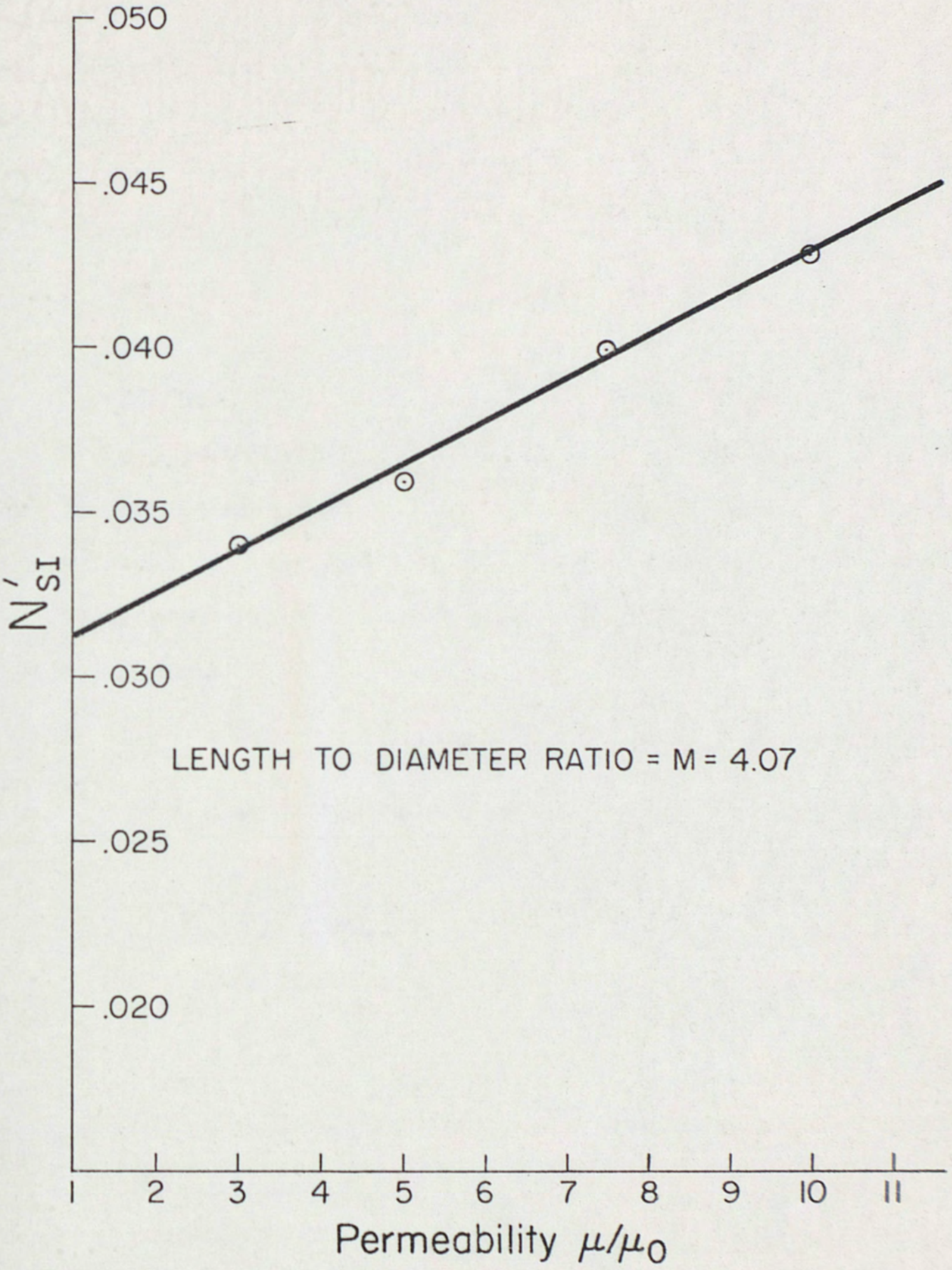

Fig. 22. Demagnetizing factor versus relative permeability for a fixed length-to-diameter ratio

$$\chi = \chi_o \, e^{-j\zeta}, \text{ and}$$

$$\phi = \frac{F_3}{i} \quad .$$

Therefore, the turns ratio ϕ is given by equation (76).

$$\phi = \frac{F_3}{i} = \frac{d_{33} \left[1 - k_{33}^2\right] A \, \chi_o e^{-j\zeta}}{s_{33}^B} \; \frac{2.058 \times 10^4}{1 + N_{SI}' \left[\frac{\mu_{33}^T}{\mu_o} \chi_R - 1\right]} \tag{76}$$

The values for d_{33}, k_{33}, and s_{33}^B were taken from figures 3, 4, and 5. The magnitude of d_{33}, k_{33}, and s_{33}^B have been corrected for the 12.4-MPa mechanical bias stress [18]. The 12.4-MPa bias stress causes $1/s_{33}^B$ to increase by 55%, d_{33} to decrease by 8%, and k_{33} to increase by 11.5%. The values used are shown in table 4 for two bias flux densities.

TABLE 4

VALUES OF d_{33}, k_{33}, AND $1/s_{33}^B$ CORRECTED FOR 12.4 MPa BIAS STRESS

Flux Density (Field)	d_{33}	k_{33}	$1/s_{33}^B$
0.4 T ($4.3 \frac{kA}{m}$)	$6.13 \times 10^{-9} \frac{m}{A}$	.569	$7.88 \times 10^{10} \frac{N}{m^2}$
0.6 T ($14.3 \frac{kA}{m}$)	$7.49 \times 10^{-9} \frac{m}{A}$	.666	$8.45 \times 10^{10} \frac{N}{m^2}$

If the values in table 4 are substituted into equation (76), equations (77) and (78) result for 0.4 tesla and 0.6 tesla, respectively.

$$\phi = \frac{809\ \chi_o e^{-j\zeta}}{1 + N_{SI}' \left[\frac{\mu_{33}^T}{\mu_o} \chi_R - 1 \right]} \tag{77}$$

$$\phi = \frac{873\ \chi_o e^{-j\zeta}}{1 + N_{SI}' \left[\frac{\mu_{33}^T}{\mu_o} \chi_R - 1 \right]} \tag{78}$$

The area of the rare earth iron rod used in equation (76) is 1.20 $\times 10^{-4}$ m^2. Notice that both equations (77) and (78) contain the magnitude and phase of the eddy current factor. By reference to figure 9, page 36, it is seen that χ_o and therefore the force produced by the magnetostrictive rods are decreasing functions of frequency. In tables 5 and 6 are found 3ϕ and the quantities which are necessary to determine ϕ and 3ϕ at discrete frequency points.

TABLE 5

ELECTROMECHANICAL TURNS RATIO 3ϕ IN NEWTONS PER AMPERE AT 0.4 T (4.3 $\frac{kA}{m}$) FOR DISCRETE FREQUENCY POINTS

Frequency	$\frac{f}{f_c}$	χ_o	ζ	χ_R	$\frac{T}{\mu_{33}}{\mu_o}\chi_R$	N_{SI}'	3ϕ	$\measuredangle$3ϕ
500 Hz	1.89	.950	12.7°	.923	6.9	.0392	1872	12.7°
800	3.03	.899	19.2	.845	6.3	.0383	1813	19.2
1100	4.17	.838	24.5	.760	5.7	.0375	1728	24.5
1400	5.30	.777	28.6	.677	5.1	.0368	1638	28.6
1700	6.44	.708	31.5	.602	4.5	.0358	1526	31.5
2000	7.58	.661	33.9	.551	4.1	.0355	1444	33.9
2300	8.71	.622	35.4	.510	3.8	.0350	1374	35.4
2600	9.85	.590	36.5	.473	3.6	.0346	1313	36.5
2650	10.04	.586	36.6	.468	3.5	.0345	1309	36.6
2900	10.98	.560	37.3	.441	3.3	.0343	1259	37.3
3200	12.12	.536	37.9	.417	3.1	.0341	1213	37.9
3500	13.26	.510	38.4	.385	2.9	.0338	1163	38.4
3800	14.39	.489	38.8	.376	2.8	.0337	1118	38.8
4000	15.15	.478	39.0	.365	2.7	.0336	1097	39.0
4500	17.05	.449	39.4	.343	2.6	.0334	1034	39.4
5000	18.94	.427	39.8	.329	2.5	.0332	987	39.8
6000	22.73	.393	40.2	.299	2.2	.0329	917	40.2
7000	26.52	.362	40.7	.277	2.1	.0327	848	40.7
8000	30.30	.341	41.0	.260	2.0	.0326	801	41.0
10,000	37.88	.304	41.4	.229	1.7	.0323	721	41.4

TABLE 6

ELECTROMECHANICAL TURNS RATIO 3ϕ IN NEWTONS PER AMPERE AT 0.6 T (14.3 $\frac{kA}{m}$) FOR DISCRETE FREQUENCY POINTS

Frequency	$\frac{f}{f_c}$	χ_o	ζ	χ_R	$\frac{\mu_{33}^T}{\mu_o}\chi_R$	N_{SI}	3ϕ	$\measuredangle$3ϕ
500 Hz	1.36	.975	9.4°	.957	5.2	.0368	2212	9.4°
800	2.18	.940	14.7	.903	4.9	.0364	2156	14.7
1100	3.00	.900	19.0	.850	4.6	.0360	2087	19.0
1400	3.81	.858	23.0	.787	4.3	.0355	2011	23.0
1700	4.63	.812	26.4	.722	3.9	.0352	1930	26.4
2000	5.45	.772	29.0	.665	3.6	.0348	1854	29.0
2300	6.27	.725	31.3	.615	3.3	.0345	1759	31.3
2550	6.95	.690	32.8	.577	3.1	.0341	1686	32.8
2650	7.22	.680	33.2	.569	3.1	.0341	1662	33.2
2684	7.31	.676	33.4	.563	3.0	.0339	1658	33.4
2800	7.63	.660	34.0	.550	3.0	.0339	1619	34.0
2900	7.90	.650	34.4	.540	2.9	.0338	1600	34.4
3200	8.72	.622	35.4	.510	2.8	.0336	1536	35.4
3500	9.54	.599	36.3	.483	2.6	.0334	1489	36.3
3800	10.35	.577	36.8	.460	2.5	.0333	1439	36.8
4000	10.90	.562	37.2	.442	2.4	.0330	1407	37.2
4500	12.26	.532	38.0	.410	2.2	.0328	1341	38.0
5000	13.62	.500	38.6	.390	2.1	.0327	1264	38.6
6000	16.35	.457	39.3	.352	1.9	.0325	1163	39.3
7000	19.07	.427	39.9	.328	1.8	.0323	1090	39.9
8000	21.80	.400	40.2	.305	1.7	.0321	1025	40.2
10,000	27.25	.358	40.7	.275	1.5	.0319	923	40.7

In addition to the compliance of the three rods shown in figure 21, page 57, the mechanical system contains other mechanical compliances. These are the compliance of the small stands in the backmass upon which the rare earth iron rods are placed, the compliance of the center stress rod, and the compliance of the disk springs. A schematic representation of the various compliances of the mechanical system of the rare earth iron transducer is shown in figure 23. The word "REFE" used in figure 23 is an acronym for rare earth iron.

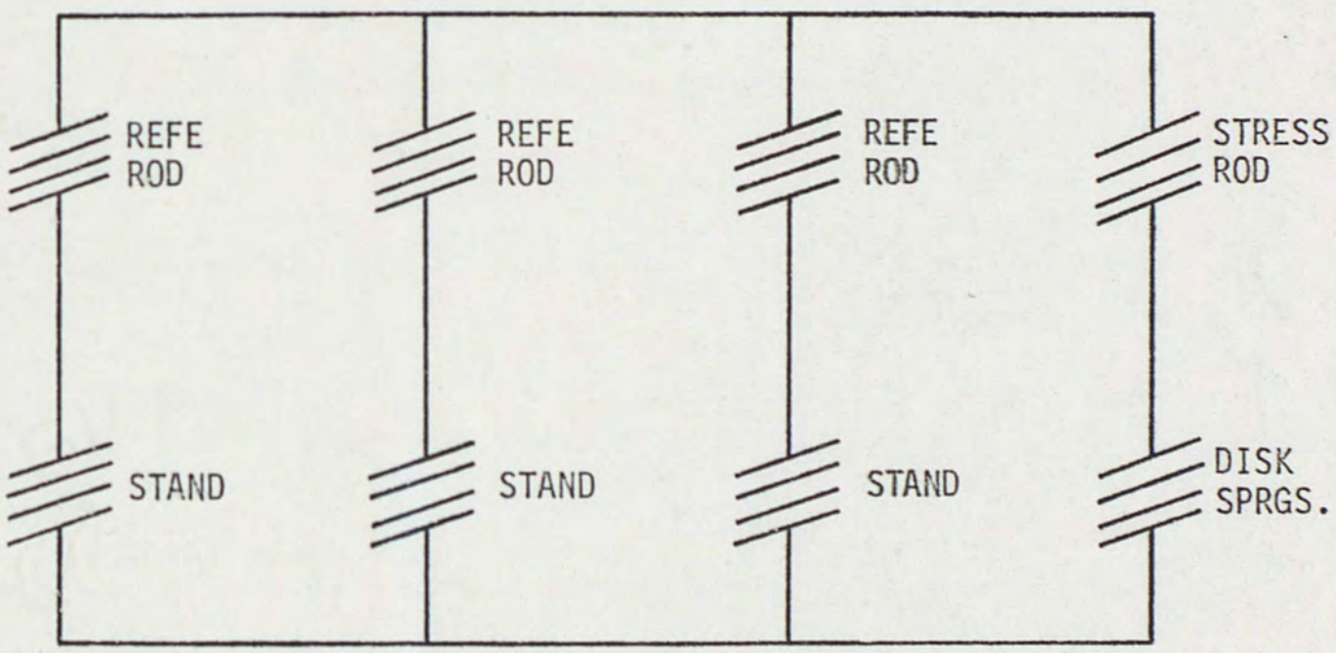

Fig. 23. Schematic representation of the various compliances of the mechanical system

In order to obtain the equivalent circuit of figure 23 in the mobility analogy, the symbols for the compliance are replaced by an inductance of the appropriate value. That is, the topology of the mechanical picture is preserved in the equivalent circuit. This is the main advantage of the mobility analogy. The resulting equivalent circuit

is shown in figure 24.

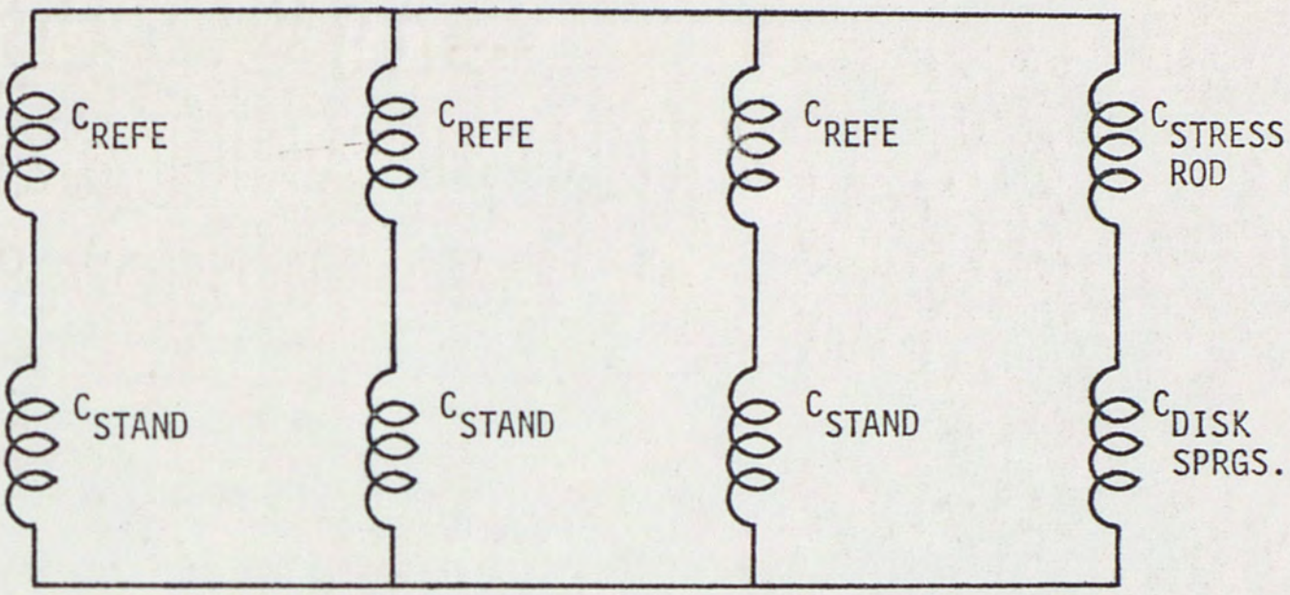

Fig. 24. Equivalent circuit of the mechanical compliance of the system

The compliance of the rare earth iron rods is given by equation (79).

$$C_{REFE} = \frac{s_{33}^{B} \ell}{A} \tag{79}$$

where ℓ is the length of the rare earth iron rod and A is its area. The values of the components of figure 24 are as follows (in mechanical units):

C_{REFE} at 0.4 T and 12.4 MPa = $5.34 \times 10^{-9} \frac{m}{N}$

C_{REFE} at 0.6 T and 12.4 MPa = $4.98 \times 10^{-9} \frac{m}{N}$

$C_{STAND} = 1.59 \times 10^{-10} \frac{m}{N}$

$C_{ROD} = 4.33 \times 10^{-9} \frac{m}{N}$

$C_{SPRINGS} = 9.38 \times 10^{-8} \frac{m}{N}$

The resultant compliance of the entire system is $1.80 \times 10^{-9} \frac{m}{N}$ at

0.4 T and 12.4 MPa and $1.68 \times 10^{-9} \frac{m}{N}$ at 0.6 T and 12.4 MPa. It should be noted that the compliance of the entire system differs by only about 1% from the compliances of the three rare earth iron rods in parallel. That is, at this point the compliance or stiffness of the entire system is controlled by the compliance of the rare earth iron rods. Also notice that the compliances of the stress rod and disk springs are about 50 times larger than the compliance of the three rare earth iron rods. Thus the motion of the active piston is not clamped by the bias stressing mechanism.

The dynamic mass of the active piston (front mass) was determined from the unloaded motional impedance loop and the known mechanical compliance. The dynamic mass of the system is given by equation (80). The resonance frequency ω_o is 2π times the in-air (unloaded) resonance frequency and C_{sys}

$$M_{sys} = \frac{1}{\omega_o^2 C_{sys}} \tag{80}$$

is the compliance of the total system given in the previous paragraph. By use of the compliance at 0.4 T and 12.4 MPa and the measured resonance frequency of 2505 Hz the mass of the system was determined to be 2.245 kg. The mass of the system consists of three parts: the mass of the active piston, half the mass of the rare earth iron rods, and the radiation mass of the air. The radiation mass of the air,which is the reactive portion of the acoustic radiation impedance, was calculated to be 0.6 g. Half the mass of the

rare earth iron rods is 84.2 g. The dynamic mass of the active piston was the unknown and was determined from equation (81). Equation (81) yields the dynamic mass of the piston to be 2.160 kg.

$$M_{sys} = M_{\substack{ACTIVE \\ PISTON}} + \frac{M_{REFES}}{2} + M_{RAD} \qquad (81)$$

The static mass was measured to be 1.896 kg or about 14% less than the dynamic mass. The dynamic mass of the piston appears as another capacitor in parallel with the capacitors of figure 21, page 57.

The mechanical resistance was also determined by use of the unloaded motional impedance loops and the known mass of the system. The mechanical resistance is given by equation (82). Where Q_{MECH} = 19.9 and is a measure of the sharpness of resonance. M_{sys} and ω_o have already been given. The result of equation (82) is R_{MECH} = 1770 kg/s (kilograms per second).

$$R_{MECH} = \frac{\omega_o M_{sys}}{Q_{MECH}} \qquad (82)$$

which has been corrected for the small radiation resistance of air. In the mobility analogy the inverse of the mechanical resistance is required which is $5.65 \times 10^{-4} \frac{s}{kg}$. The mechanical resistance appears as a resistor (inverse mechanical resistance) in parallel with the other elements in figure 21. The complete mechanical impedance of the transducer appears in figure 25.

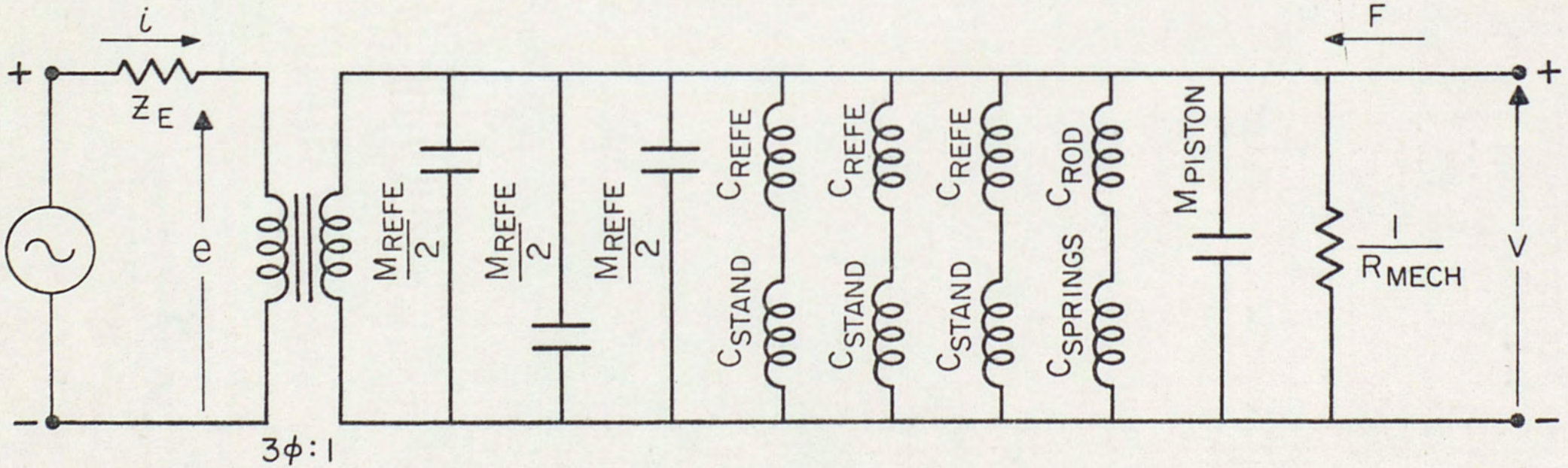

Fig. 25. The mechanical impedance of the transducer (mobility analogy)

Acoustic Impedance

This section will present the acoustic impedance of a piston in a tube and the acoustic impedance of the fluid contained behind the piston. The radiation impedance of a piston in a long tube (which is the load impedance in this case) is given by Beranek [29] and shown in figure 26.

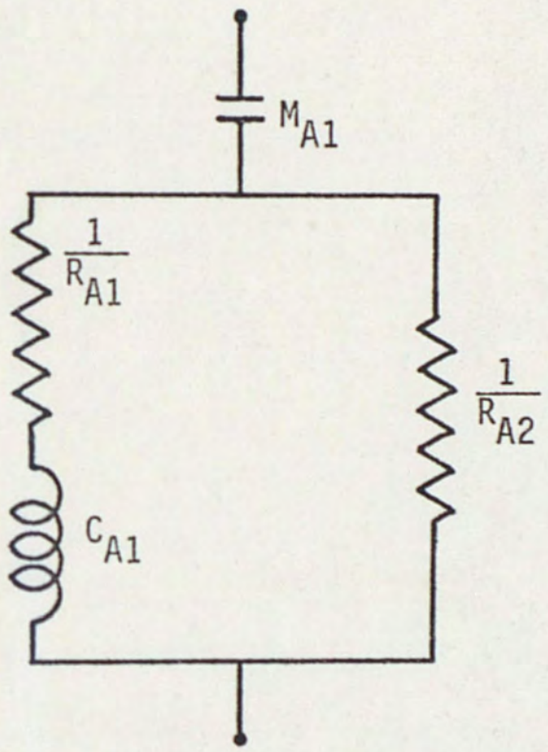

Fig. 26. Radiation impedance of a piston in a long tube (mobility analogy - acoustic units)

The symbols used in figure 26 have the following meanings:

$$M_{A1} = .1952 \frac{\rho_o}{a} \frac{kg}{m^4} \tag{83}$$

$$\frac{1}{R_{A1}} = \frac{6.23a^2}{\rho_o c_o} \frac{s}{kg\ m^4} \tag{84}$$

$$\frac{1}{R_{A2}} = \frac{\pi\ a^2}{\rho_o c_o} \frac{s}{kg\ m^4} \tag{85}$$

$$C_{A1} = \frac{5.44\ a^3}{\rho_o c_o^2} \quad \frac{m^5}{N} \tag{86}$$

where a = radius of the piston = .0635 m,

ρ_o = density of water = 997 kg/m^3 at 25°C, and

c_o = speed of sound in water = 1481 $\frac{m}{s}$ at 25°C.

The above indicated calculations yield:

M_{A1} = 3065 kg/m^4,

$\frac{1}{R_{A1}} = 1.701 \times 10^{-8} \quad \frac{s}{kg\ m^4}$,

$\frac{1}{R_{A2}} = 8.579 \times 10^{-9} \quad \frac{s}{kg\ m^4}$, and

$C_{A1} = 6.370 \times 10^{-13} \frac{m^5}{N}$.

Attached to the radiation impedance is a mechano-acoustic transformer. This transformer converts the acoustic units of the radiation impedance into mechanical units. The transformation ratio (turns ratio) is the area of the active piston. The transformer and the radiation impedance are shown in figure 27. The thru variable is the pressure P and the across variable is the volume velocity U which equals linear velocity times area.

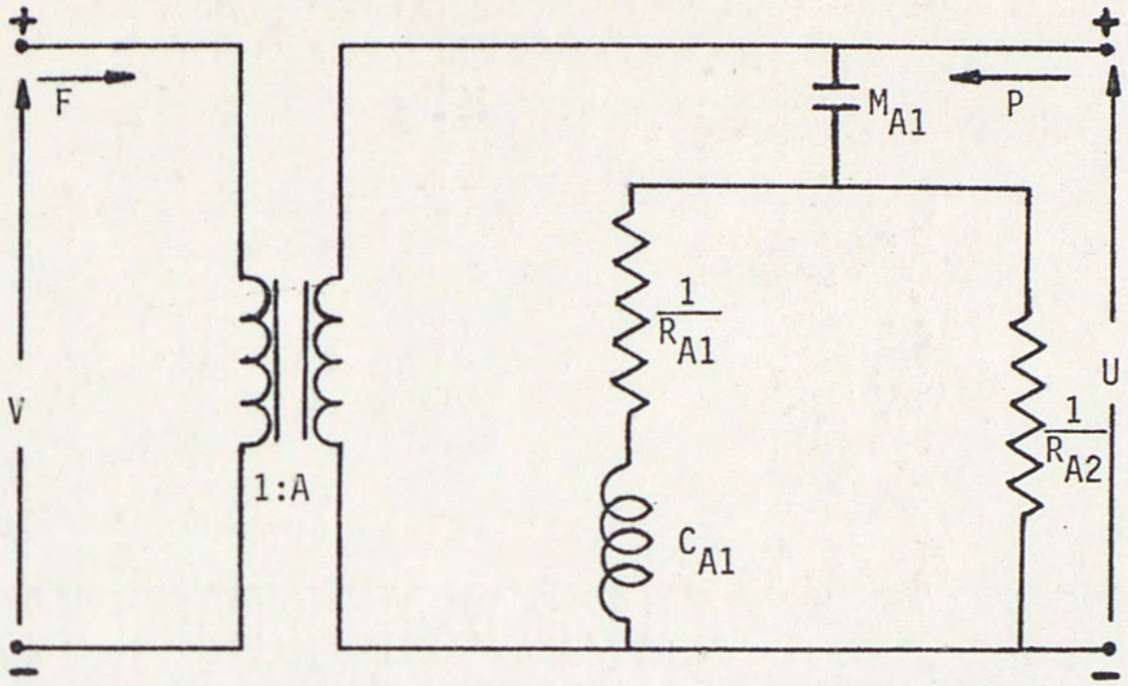

Fig. 27. Mechano-acoustic transformer and the radiation impedance(mobility analogy acoustic units)

One additional impedance is required to complete the equivalant circuit. This is the acoustic impedance of the contained cooling fluid. This is also given by Beranek [29] and is shown in equation (87)

$$Z_A = \left(\frac{-j\rho c}{\pi a^2}\right) \cot(k\ell) \tag{87}$$

where a = radius of tube,

ℓ = length of tube,

ρ = density of contained fluid, and

c = speed of sound in contained fluid.

Equation (87) gives the acoustic impedance of a length of tube rigidly closed at one end with a piston vibrating at the other end. Equation (87) can be approximated by the first two terms of its series expansion. This is shown as equation (88)

$$Z_A \simeq \frac{-j}{\omega\left(\frac{V_f}{\rho c^2}\right)} + j\omega\left(\frac{\ell\rho}{3\pi a^2}\right) \tag{88}$$

where V_f is the volume of the fluid in the tube. Equation (88) represents a series combination of an acoustic mass, $\left(\frac{\ell\rho}{3\pi a^2}\right)$, and an acoustic compliance, $\left(\frac{V_f}{\rho c^2}\right)$. But equation (88) is the classical analogy. In the mobility analogy the series combination becomes the parallel combination shown in figure 28. A resistor (an inverse acoustic resistance) has been added to account for viscous losses in the fluid.

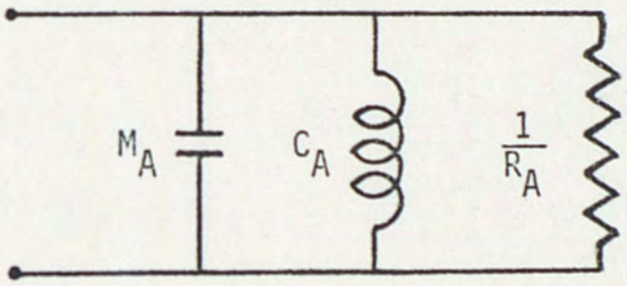

Fig. 28. Acoustic impedance (mobility analogy) of the contained fluid

The acoustic compliance C_A is given by equation (89) and the acoustic mass by equation (90)

$$C_A = \frac{V_f}{\rho c^2} \tag{89}$$

$$M_A = \frac{\ell\rho}{3\pi a^2} \tag{90}$$

The equivalent circuit given in figure 28 is valid within 5% for ℓ's up to about $\frac{\lambda}{7}$. A wavelength of $\frac{\lambda}{7}$ in the closed tube corresponds to a frequency of 3300 Hz. Thus the equivalent circuit of figure 28 can be expected to be usable up to about 5 kHz. The terminals of figure 28 are attached to the right terminal pair in figure 27 to complete the acoustic impedance of the transducer.

If the acoustic compliance indicated by equation (89) is calculated and used in the equivalent circuit, it is found to yield a resonance frequency which is too high. This is due to the fact that the assumption of a rigidly closed tube is not completely valid. The volume behind the vibrating piston has two holes in it (to allow cooling fluid to pass) which are connected to hoses leading to the radiator and pump assembly. The additional volume of fluid in the hoses and the compliance of the hoses increase the acoustic compliance.

The acoustic compliance was calculated via the motional impedance loops, assuming the acoustic mass to be relatively unaffected. The mechanical equivalent of the acoustic mass, $M_A A^2$, was calculated to be .240 kg. When this mass is added to the previously determined total mass of the system, the result is a mass of 2.485 kg. This corresponds to the mass of system when it is fluid-filled vibrating in air. By knowing the mass of the system, it is possible to calculate the compliance of the total system using equation (91).

$$C_{\substack{\text{SYSTEM}\\ \text{FLUID}\\ \text{FILLED}}} = \frac{1}{\omega_o^2 \, M_{\substack{\text{SYSTEM}\\ \text{FLUID}\\ \text{FILLED}}}} \qquad (91)$$

The resonance frequency, ω_o, was taken from the in-air fluid-filled motional impedance loop and was 2870 Hz. Now by knowing the compliance of the system when it is not fluid filled (see figure 24) and that this compliance appears as an inductor in parallel with the compliance of the fluid, it is possible to calculate the compliance of the fluid alone. Equation (92) was used to calculate a value of $3.97 \times 10^{-9} \frac{m}{N}$ for the compliance of the fluid. This is about 84% larger than the compliance derived from equation (89).

$$C_{\substack{\text{SYSTEM} \\ \text{FLUID} \\ \text{FILLED}}} = \left[\frac{1}{C_{\substack{\text{SYSTEM} \\ \text{UNFILLED}}}} + \frac{1}{C_{\text{FLUID}}} \right]^{-1} \tag{92}$$

There is no theoretical expression for the viscous losses which lead to the inverse acoustic resistance in figure 28. It must be determined from the fluid-filled and unfilled in-air motional impedance loops. The acoustic resistance can be determined from equation (93).

$$A^2 R_{\text{ACOUSTIC}} + R_{\text{MECH}} = \frac{\omega_o \, M_{\text{FLUID FILLED}}}{Q_{\text{FLUID FILLED}}} \tag{93}$$

The mass of the fluid-filled system is 2.485 kg. The resonance frequency of the system when it is fluid filled is 2870 Hz. The Q of the system when fluid filled is 4.5. Substituting these values into equation (93) yields equation (94) after correcting for the small radiation resistance of air

$$A^2R_{ACOUSTIC} + R_{MECH} = 9950 \frac{kg}{s} \quad (94)$$

but $R_{MECH} = 1770 \frac{kg}{s}$

thus,

$$A^2R_{ACOUSTIC} = 8180 \frac{kg}{s}. \quad (95)$$

The value given by equation (95) yields theoretical sound pressure levels which are about 1 dB lower than the measured sound pressure at resonance. Although this is good agreement when experimental error is considered, exact agreement at resonance (at 0.4 T) can be obtained by using a somewhat smaller acoustic resistance shown in equations (96) and (97).

$$A^2R_{ACOUSTIC} = 6250 \frac{kg}{s} \quad (96)$$

or

$$\frac{1}{R_{ACOUSTIC}} = 2.57 \times 10^{-8} \frac{s}{kg \times m^4} \quad (97)$$

Notice that the acoustic resistance is about 3.5 times larger than the mechanical resistance. Thus the viscous losses in the fluid control the height of the response at the resonance frequency.

Discussion of the Complete Equivalent Circuit

When the acoustic equivalent circuit discussed in the previous section is connected to the mechanical equivalent circuit shown in figure 25, the result is figure 29. The input to the equivalent circuit in figure 29 is an ideal sinusoidal current generator. R_b and L_b shown in figure 29 are the blocked resistance and inductance taken from figures 11 and 12. The mass of the rare earth iron

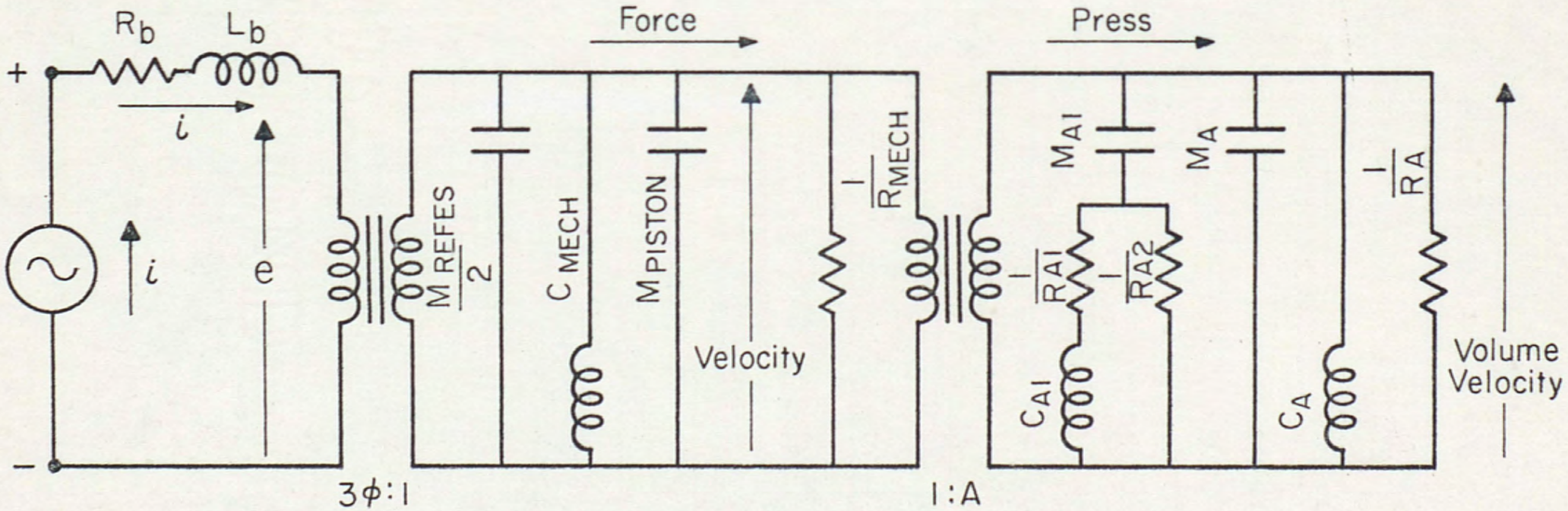

Fig. 29. Complete equivalent circuit (mobility analogy)

rods has been collected into one element in figure 29. Also, the mechanical compliance of the system has been gathered into a single element labled C_{MECH}. The circuit shown in figure 29 is inconvenient to use because of the phase angle (due to eddy currents) of the electromechanical transformer. If both of the transformers are removed by moving them to the right, the circuit will then be in electrical units. If this is carried out, the phase angle (which is a function of frequency) of the electromechanical transformer will appear in the impedances of figure 29. Thus the complex impedance of each of the components rotates as a function of frequency making the analysis of the circuit very difficult.

To make the analysis somewhat simpler, it was necessary to convert the circuit to mechanical units. This was done by moving the mechano-acoustic transformer to the right and the electromechanical transformer to the left. This results in the equivalent circuit shown in figure 30. The resistors in figure 30 represent inverse mechanical resistances with units of seconds per kilogram. The inductors represent mechanical compliances with units of meters per newton. The capacitors represent masses with units of kilograms. The through variable (current) is the force produced by the rods in newtons. The across variable (voltage) is the velocity of the rods in meters per second. Notice that in figure 30 the turns ratio, and hence the phase angle, appears in only two impedance components: the blocked mechanical resistance and the blocked mechanical inductance. In order to obtain the blocked mechanical resistance and

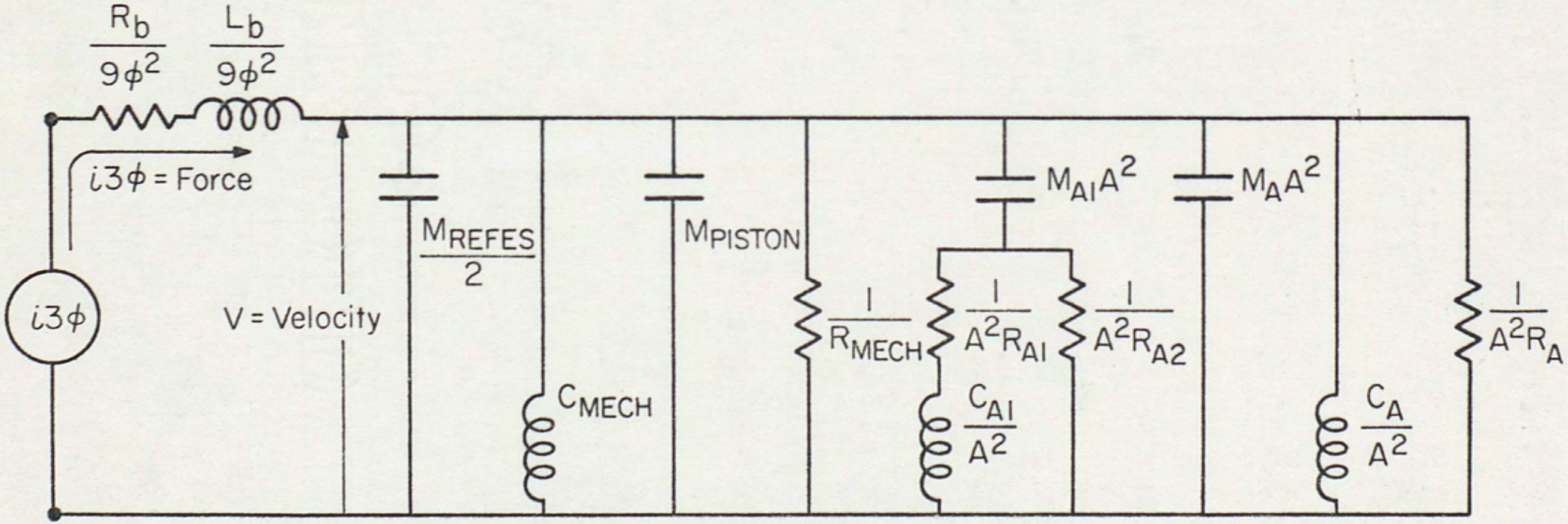

Fig. 30. Equivalent circuit with transformers removed (mobility analogy - mechanical units)

inductance, the turns ratio and phase angle are taken from tables 5 and 6 and the blocked resistance and inductance are taken from figures 11 and 12. The resulting impedances are vectorially added and separated into a real and imaginary portion.

In figure 30 the ideal sinusoidal current generator becomes a force generator of value $i3\phi$ newtons. Notice that since ϕ (see equations (77) and (78)) is directly proportional to χ_o, which is a decreasing function of frequency, then the force produced by the rods is also a decreasing function of frequency. Thus an ideal sinusoidal current generator becomes a monotonically decreasing force generator. The decrease in the force as a function of frequency is due to the flux generated by the eddy currents. The eddy current flux opposes the applied magnetic flux resulting in a lower net flux. The monotonic decrease of force with frequency may be explained by noting that the eddy currents increase with frequency and hence the opposing magnetic field increases resulting in a continual decrease in the net flux which produces the force from the REFE rods. In tables 5 and 6 it can be seen that at the resonance frequency (2650 Hz) at 0.4 tesla the force is reduced to 59% of its ideal value, at 0.6 tesla the force is 69% (at 2550 Hz) of its ideal value. Thus eddy current losses are large in this unlaminated transducer. If eddy current losses are to be kept small, the rods should be sufficiently laminated to keep $\frac{f}{f_c}$ below 2 over the operating frequency range [24].

The equivalent circuit of a laminated transducer can be

obtained by replacing the blocked mechanical impedance in figure 30 by the circuit in figure 18. Each of the elements in figure 18 must be divided by $(3\phi)^2$ so that they will be in mechanical units. If the rods are laminated, additional simplifying assumptions can be made. First since the characteristic frequency is rather high for a laminated rod (1058 Hz at 0.4 tesla), the assumption may be made that ϕ is independent of frequency. It is also assumed that there is no demagnetization. It should be noted that figure 18 does not account for eddy current losses in a flux return path. These losses could be accounted for by an additional resistor and inductor in parallel with L_o and $16\pi f_c L_o$. The assumptions of no demagnetization and that ϕ is independent of frequency change the expression for ϕ (equation 77). Equation (77) becomes simply ϕ = 809 newtons per ampere. It is further assumed that the phase angle of ϕ is negligible. These assumptions are reasonably valid up to about $\frac{f}{f_c} = 2.5$, which corresponds to 2650 Hz for the quartered rods at 0.4 tesla. Thus for the laminated transducer a completely lumped circuit can be obtained. That is, all of the elements can be represented as inductors, resistors, or capacitors--none of which change with frequency, including the force generator.

In order to analyze the mechanical equivalent circuit of figure 30, an alternating current circuit analysis program was used on a PDP-11/45 computer. The values of the resistors, inductors, capacitors, and the force generator are input into the computer

program in mechanical units. Thus the branch and node voltages output by the computer program must be interpreted as velocities. The branch currents must be interpreted as forces.

The ultimate goal of the equivalent circuit is to produce the acoustic power radiated by the mechanical radiation resistances. The power dissipated in a mechanical resistance R_{MECH} is given by equation (98), where V is the velocity and F is the force.

$$\text{RMS POWER} = V^2 R_{MECH} = \frac{F^2}{R_{MECH}} \tag{98}$$

Since figure 30 has two inverse radiation resistances, the acoustic power radiated, P_a, is given by equation (99)

$$P_a = V_1^2 A^2 R_{A1} + V_2^2 A^2 R_{A2} \tag{99}$$

where V_1 is the velocity across R_{A1} and V_2 is the velocity across R_{A2}. In this analysis the current is set at 1 ampere. That is, the force generated is simply 3ϕ. The voltage applied to the transducer is given by equation (100) where V is the velocity produced by the force generator.

$$\text{Driving Voltage} = V3\phi = \text{Velocity} \times \text{Turns Ratio} \tag{100}$$

The acoustic pressure at a distance r from the piston can be obtained from equation (101) [30]

$$p = \frac{1}{r}\left[\frac{P_a \rho_o c_o R_\theta}{4\pi}\right]^{1/2} \tag{101}$$

where P_a is given by equation (99) and ρ_o, c_o are the density and

speed of sound in water, respectively. R_θ is the directivity factor. The directivity factor is the ratio of the intensity I_o or the rms pressure squared, p_o^2, in a reference direction (usually the axis of the transducer) to the intensity $\overline{I}$ or $\overline{p^2}$ the rms pressure squared averaged over all space. Thus the directivity factor is a measure of the sharpness of the sound beam. The directivity factor when expressed in logarithmic form is known as the directivity index as shown in equation (102).

$$D.I. = 10 \log_{10} (R_\theta) = 10 \log_{10} \left[\frac{I_o}{\overline{I}}\right] \tag{102}$$

The directivity index of the rare earth iron transducer was measured from the directivity patterns and is shown in figure 31, where k is the wavenumber and a is the radius of the piston. Also shown for comparison is the directivity index for a piston in an infinitely long tube. The largest departure of the rare earth iron transducer's D.I. from the ideal D.I. is about 2 dB.

The acoustic power radiated is found via equation (99) at the discrete frequency points indicated in tables 5 and 6 and the directivity factor is found with the aid of figure 31. The distance r in equation (101) is set at 1 meter which is the standard reference distance. The acoustic pressure then obtained through equation (101) is referenced to either the driving current or voltage. If the pressure is normalized to the driving current, the resulting frequency plot is known as the transmitting current response. If the pressure is normalized to the driving voltage, it is known as the transmitting voltage response.

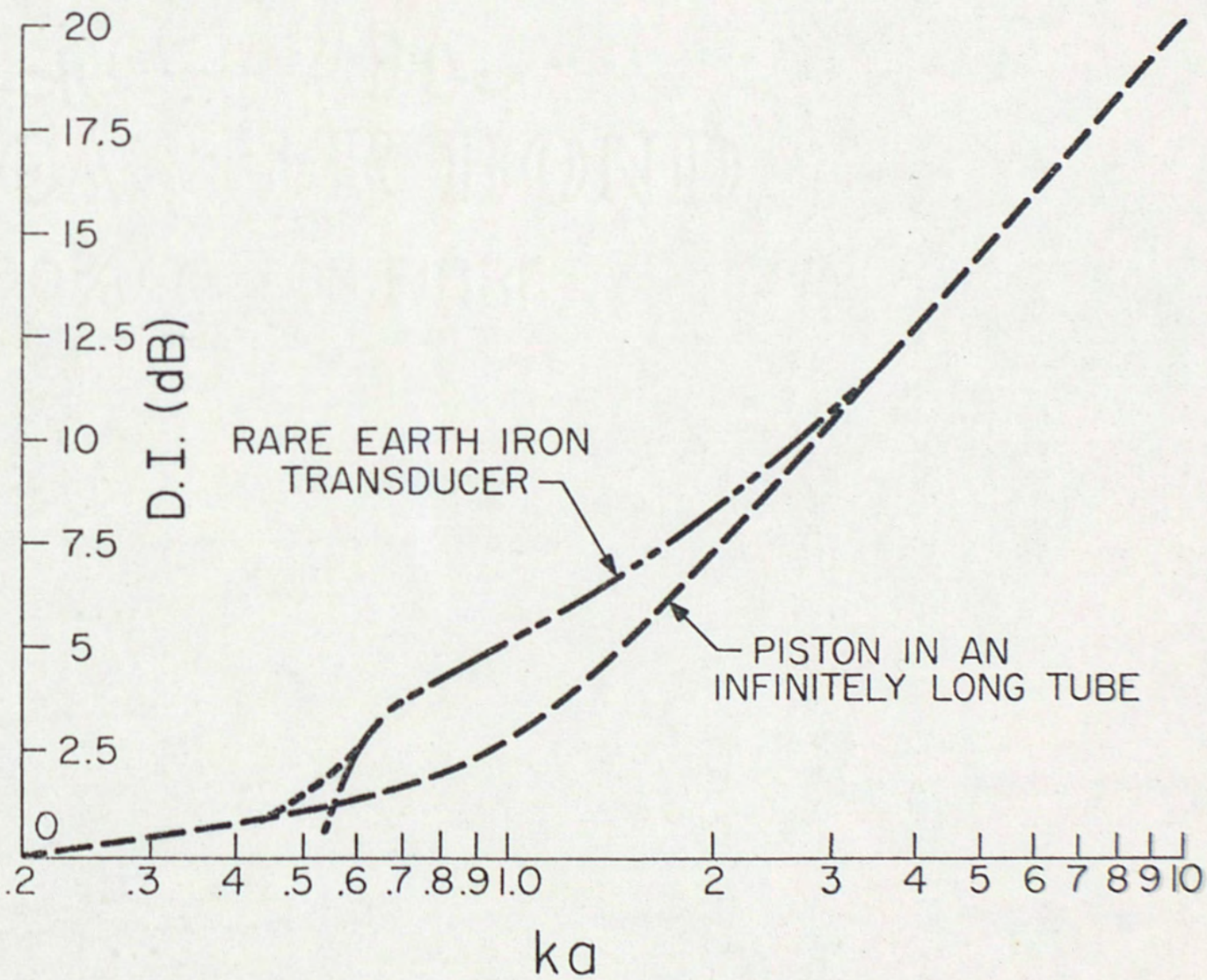

Fig. 31. Directivity index versus ka

CHAPTER IV

PRESENTATION AND DISCUSSION OF RESULTS

Circuits for Driving and Receiving with the Rare Earth Iron Transducer

The circuit which was used to drive the transducer is shown in figure 32.

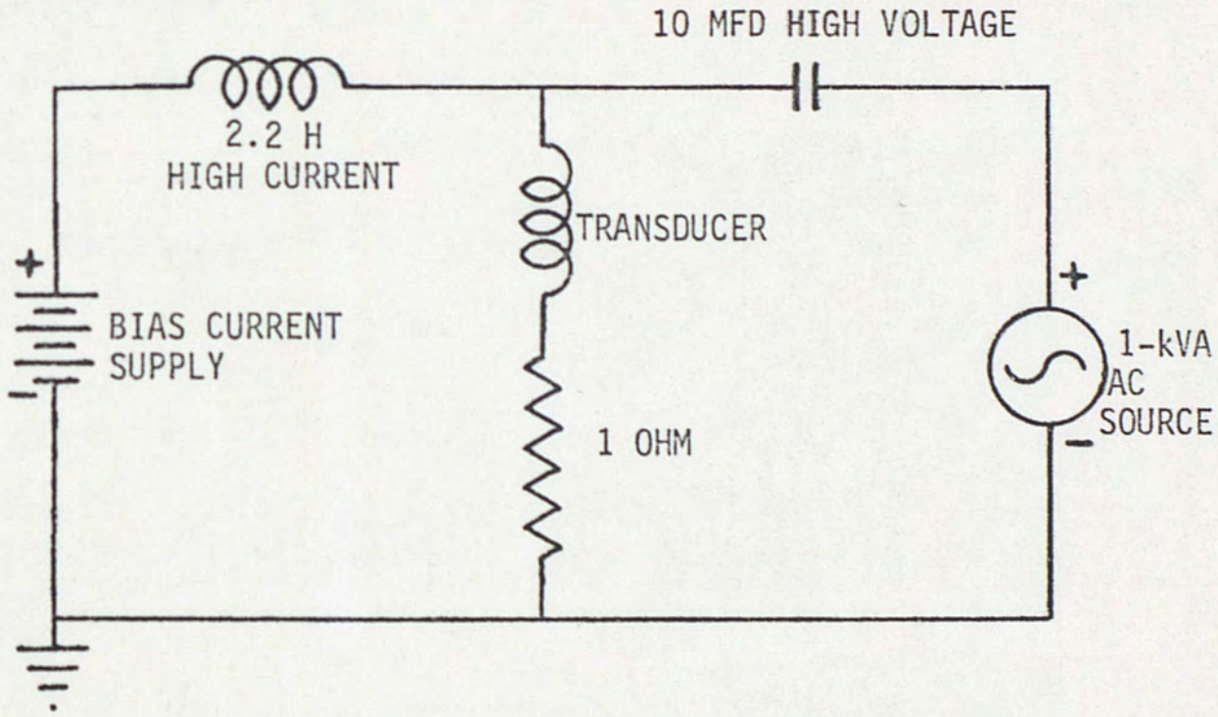

Fig. 32. Circuit for power drive

The 2.2 H inductor acts as a choke to the alternating current coming from the 1-kVA power source. This prevents the alternating current from feeding into the direct current source and forces the alternating current through the transducer. The direct current bias

current passes freely through the 2.2 H coil. The 10 MFD high-voltage capacitor blocks the direct current from the alternating current source and at the same time allows the alternating current to pass freely through. The purpose of the 1-ohm resistor below the transducer is to measure the alternating current and direct current passing through the transducer.

Figure 33 shows the electrical circuit for receiving with the transducer. That is, a sound pressure is incident upon the transducer and the resulting voltage is received in the below manner. Even when the transducer is receiving, it is necessary to provide a bias current as shown in figure 33.

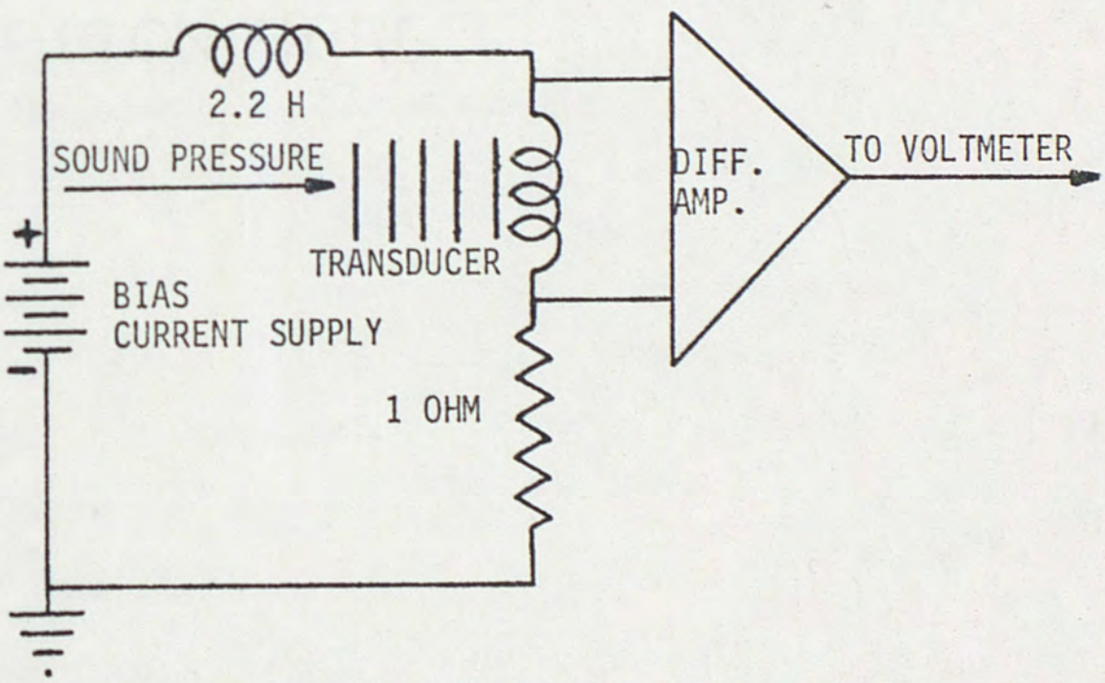

Fig. 33. Circuit for receiving

Transmitting Current Response at 0.4 Tesla

Figure 34 shows the transmitting current response versus frequency at 0.4 tesla (4.3 $\frac{kA}{m}$). The transmitting current response is

defined as the sound pressure output in micropascals (1 μPa = 10^{-6} $\frac{N}{m^2}$) per ampere of current at a distance of 1 meter. Shown in figure 34 is the measured response at 0.4 tesla compared with the response computed from the equivalent circuit of figure 30 using table 5. The computed response shows good agreement over the entire frequency range. The computed response without eddy currents or demagnetization is also shown in figure 34. This response was obtained by letting ϕ equal its ideal value of 809 newtons per ampere at 0.4 tesla which is independent of frequency. Notice that the blocked impedance need not be altered to obtain the ideal transmitting current response. This is because the blocked impedance is a series element, thus it consumes no current which would ordinarily pass through the radiation resistance. The ideal response is 5.5 dB or almost a factor of 2 above the computed response at resonance (2650 Hz). At 10 kHz the ideal response is 10 dB above the computed response. Notice that the ideal response above resonance is virtually flat while the same portion of the computed response has a negative slope. This negative slope is caused by the effect of the eddy currents in decreasing the magnitude of the force generator. If the effect of demagnetization alone is added to the ideal response, it is found that the resulting curve is 2 dB below (at all frequencies) the ideal response shown in figure 34. Thus eddy currents account for the major difference between the ideal and computed responses at the higher frequencies (resonance and above) while demagnetization

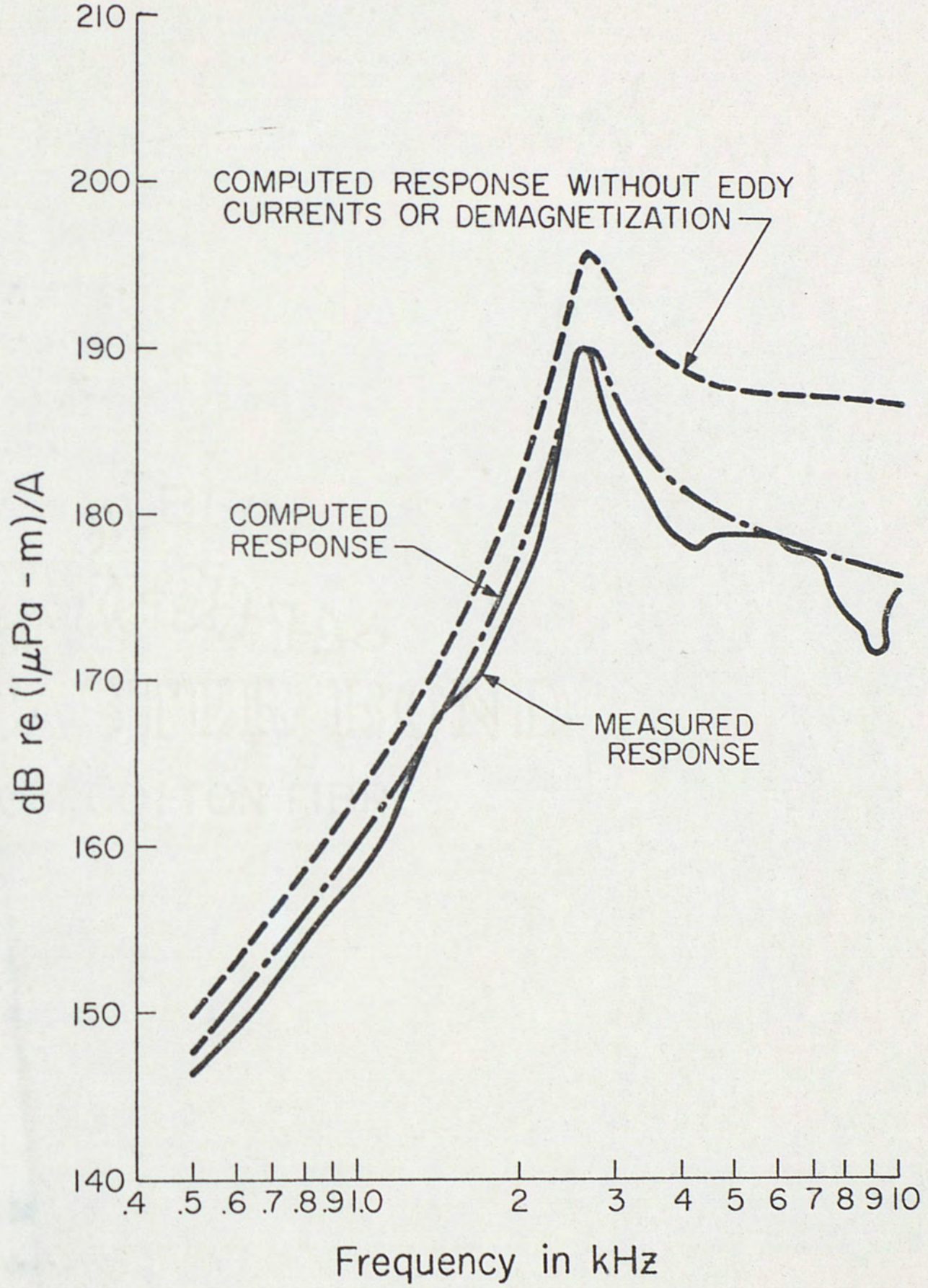

Fig. 34. Transmitting current response at 0.4 tesla (4.3 $\frac{kA}{m}$)

has a substantial effect at the lower frequencies. The "Q" (sharpness of resonance) of the transducer in water is 7.

Transmitting Current Response at 0.6 Tesla

Figure 35 shows the measured transmitting current response at 0.6 tesla (14.3 $\frac{kA}{m}$) compared with the response computed from the equivalent circuit of figure 30 and table 6. Here the agreement is not as good as in figure 34 but is still fair over the entire frequency range. Notice that the equivalent circuit predicts the resonance frequency to increase to about 2700 Hz due to the increase in stiffness of rare earth iron rods with bias field. The measured resonance frequency decreases about 100 Hz to 2550 Hz. This discrepancy, though small, is unexplained at this point. The major differences in the measured responses of figures 34 and 35 are that figure 35 has a decrease in resonance frequency, an increase of 1 dB in the response at resonance, and an increase of 1 dB in the response above resonance. Notice also that figures 34 and 35 show a 12-dB increase from 500 Hz to 1000 Hz or an ω^2 rise which is typical of a magnetostrictive device far below resonance. The "Q" of the transducer at 0.6 tesla is 10.

Transmitting Voltage Response at 0.4 Tesla

The transmitting voltage response versus frequency at 0.4 tesla is shown in figure 36. The transmitting voltage response is defined as the sound pressure output by the transducer at 1 meter normalized by the driving voltage. The transmitting voltage response

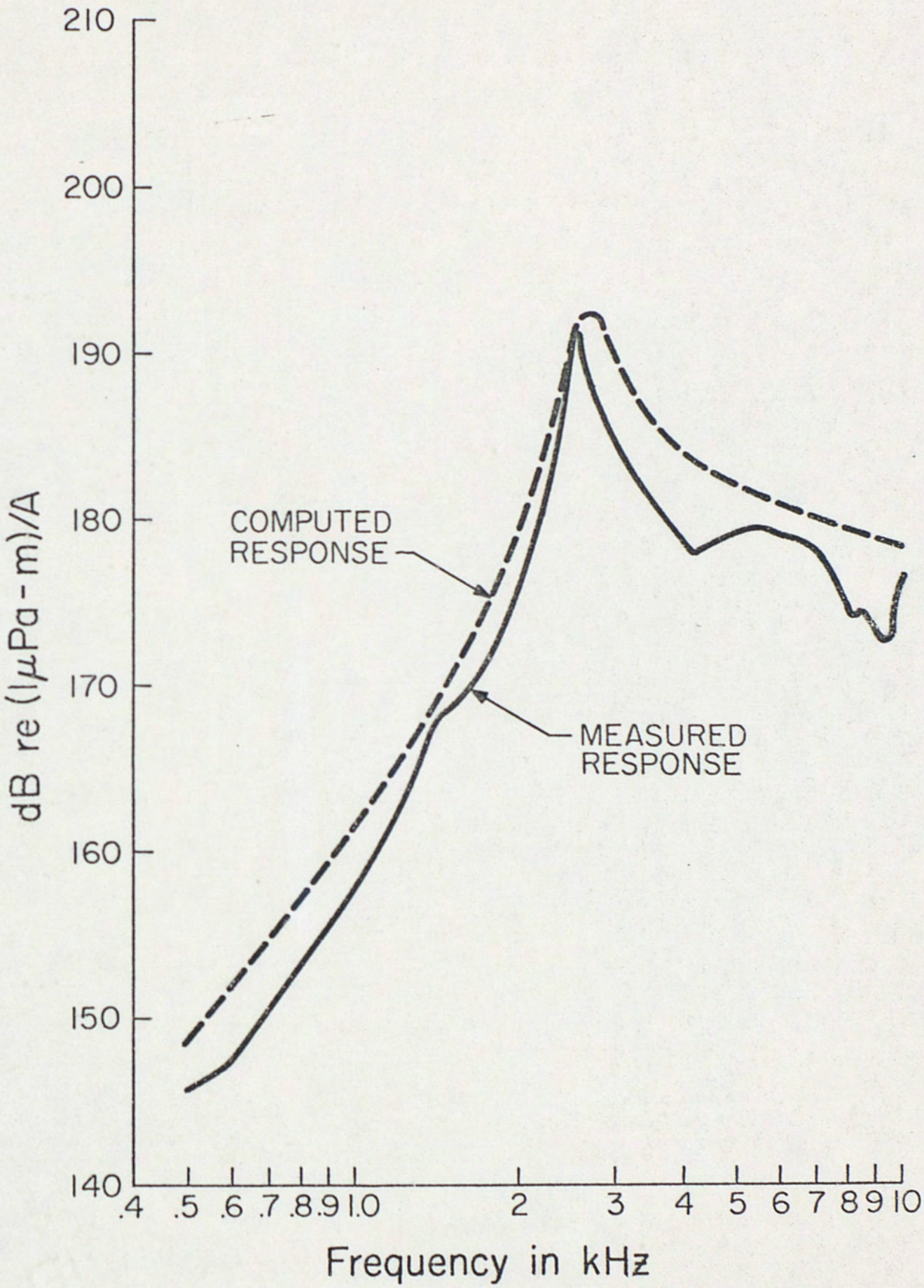

Fig. 35. Transmitting current response at 0.6 tesla (14.3 $\frac{kA}{m}$)

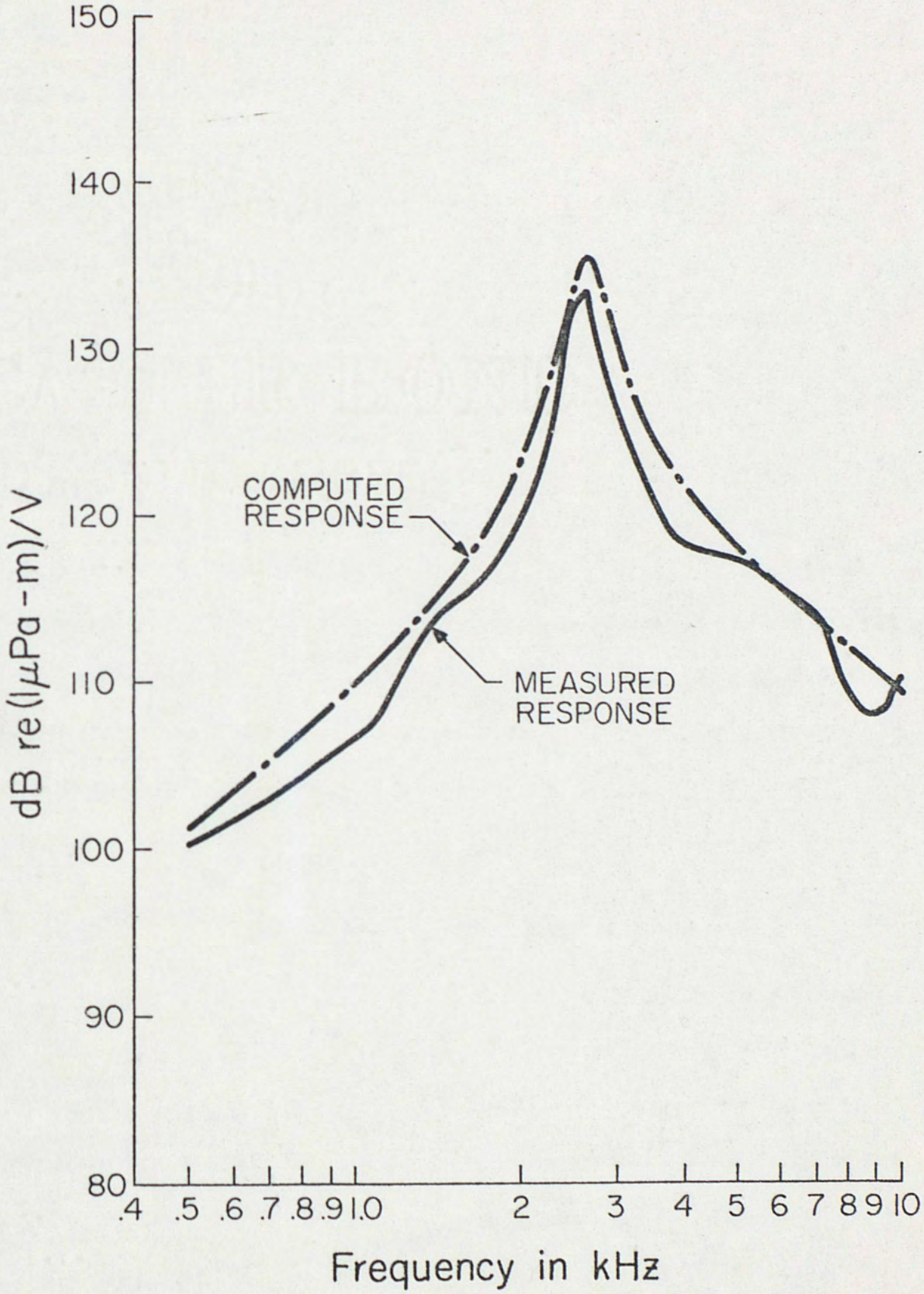

Fig. 36. Transmitting voltage response at 0.4 tesla ($4.3 \frac{kA}{m}$)

is expressed in decibels by taking twenty times the logarithm of the pressure per volt divided by (referenced to) 1 μPa per volt. The computed response was obtained from figure 30 using table 5 and the blocked impedance curves of figures 11 and 12. Again good agreement is obtained between measured and predicted values over the entire frequency range. Notice that the transmitting voltage response falls off more rapidly, as expected, above the resonance frequency (2650 Hz) than does the transmitting current response. The "Q" of the transducer in this frequency plot is 8.

Free Field Voltage Sensitivity at 0.6 Tesla

When the rare earth iron transducer is placed in a region containing a free field plane progressive wave a voltage is generated at the terminals of the transducer via the inverse magnetostrictive effect. The free field voltage sensitivity is a measure of the open circuit output voltage per unit incident pressure and is given by equation (103) in dB.

$$20 \log M = 20 \log \left(\frac{\text{open-circuit output voltage}}{\text{free-field plane-wave pressure}} \right) \qquad (103)$$

The sensitivity is referenced to (divided by) 1 volt per micropascal. Thus if a calibrated frequency plot of the sensitivity is obtained, it is possible to obtain the sound pressure in the water by merely measuring a voltage. The free field voltage sensitivity at 0.6 tesla is shown in figure 37. The computed sensitivity was obtained by using the computed transmitting current response of figure 35 and the free field reciprocity parameter. The reciprocity parameter is the

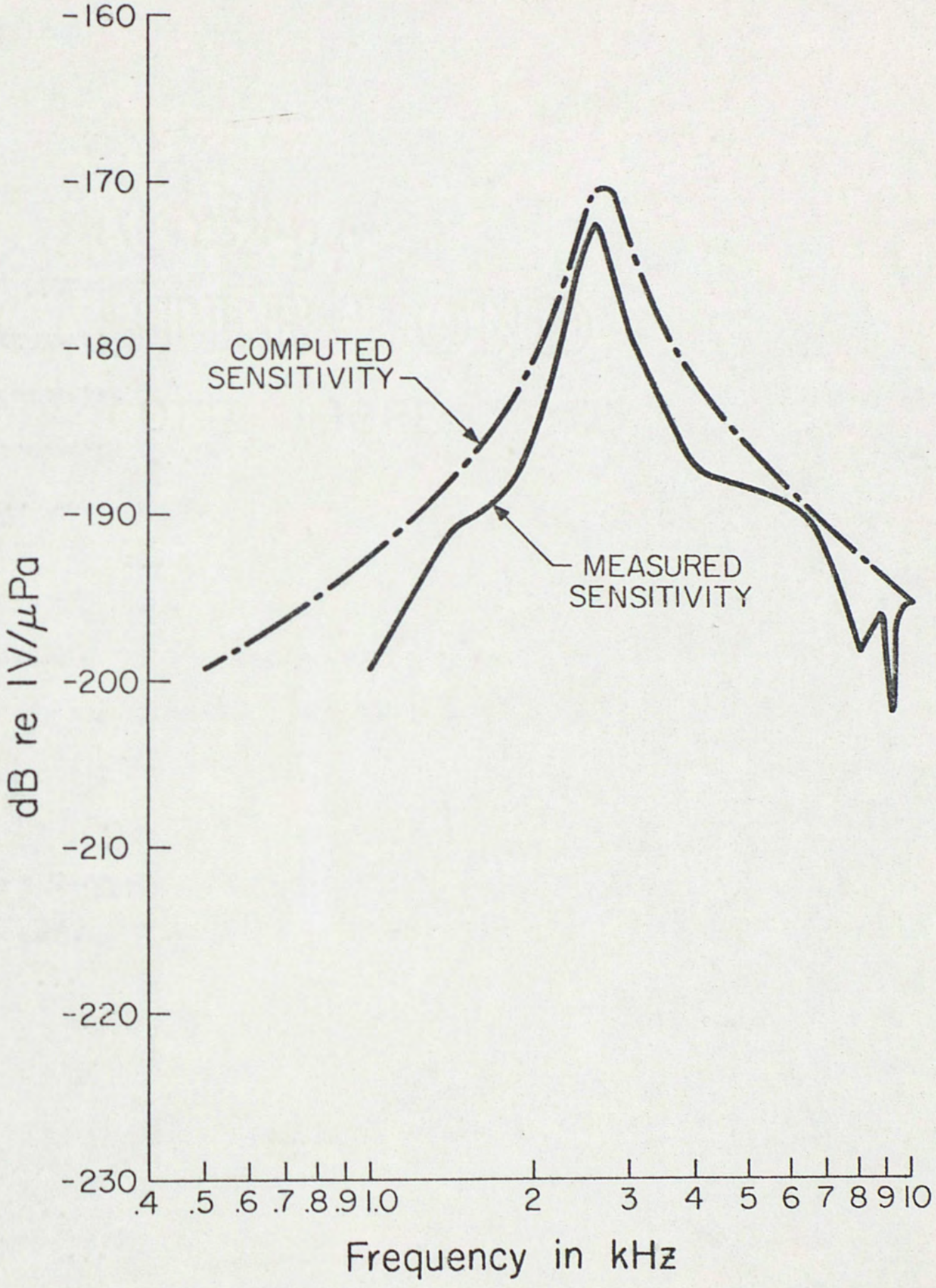

Fig. 37. Free field voltage sensitivity at 0.6 tesla (14.3 $\frac{kA}{m}$)

ratio of the receiving sensitivity to the transmitting current response shown in equation (104).

$$J = \text{reciprocity parameter} = \frac{M}{S} \tag{104}$$

M = receiving sensitivity

S = transmitting current response.

A necessary but not sufficient condition for reciprocity is that the transducer be linear, passive, and reversible [30]. The reciprocity parameter is discussed further by Bobber [30]. For the free-field condition the reciprocity parameter is given by Bobber [30] and shown in equation (105).

$$J = \frac{2d}{\rho f} \times 10^{-12} \tag{105}$$

where d is the measurement distance, ρ is the density of water, and f is the frequency. Thus via equations (104) and (105) and the computed transmitting current response of figure 35, the computed sensitivity of figure 37 is obtained. The agreement is fair over the frequency range considered. The "Q" of the transducer in the receiving mode is 7.

Transmitting Voltage Response for a Laminated Transducer

The effect of eliminating eddy currents upon the transmitting current response was seen in figure 34. In order to observe the effect of lamination and eliminating demagnetization upon the transmitting voltage response, the blocked impedance of figure 18 was substituted into figure 30. The rare earth iron rods were assumed to have been

quartered. The method of analysis using figure 18 was described at the end of Chapter III. The computed response at 0.4 tesla of the laminated transducer without demagnetization is shown in figure 38 compared with the computed response at 0.4 tesla of the unlaminated transducer with demagnetization. Before discussing figure 38, recall from the discussion at the end of Chapter III that the equivalent circuit of figure 18 is valid only up to about 2650 Hz; with this in mind, consider figure 38. The most important fact which can be drawn from figure 38 is that at resonance and below the laminated and unlaminated responses show very little difference. The reason for this similarity is due to the fact that in the laminated version the force generated by the rods is greater but at the same time the blocked mechanical impedance no longer decreases at the rate of the unlaminated transducer (see figure 12). Thus in the laminated transducer even though a greater force is generated by the rods a greater velocity (which is proportional to voltage) is required to overcome the larger blocked mechanical impedance. Therefore there are two opposing effects. The increased force would tend to produce a greater response if the impedance stayed constant, but the impedance increases in such a manner as to cancel the effect of the increased force. The close agreement between the two curves of figure 38 is probably fortuitous, but in general (at least at the lower frequencies) a large difference between laminated and unlaminated transmitting voltage responses is not expected. Notice that the peak response of the laminated transducer occurs 150-Hz higher than

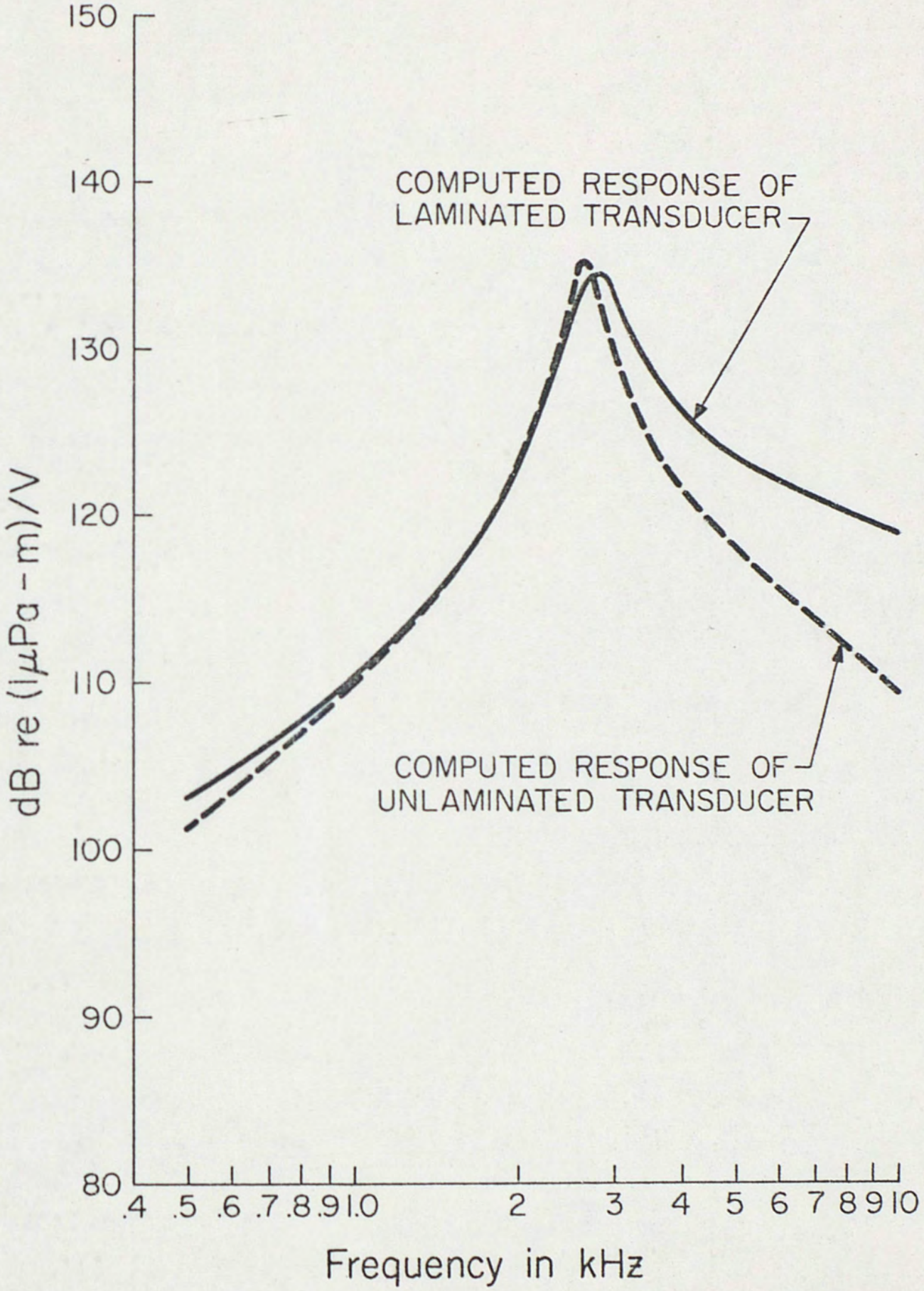

Fig. 38. Transmitting voltage responses of a laminated and an unlaminated transducer at 0.4 tesla

the peak of the unlaminated transducer at 2650 Hz.

The measured electroacoustic efficiency at resonance of the unlaminated transducer was 11%. This was obtained by a direct measurement of the input electric power and calculating the output acoustic power from the on-axis acoustic pressure and the directivity factor. From impedance measurements it was determined that about 50% of the input power was lost in eddy currents in the unlaminated version. The remaining 39% of the input power is dissipated in mechanical, viscous, and hysteresis losses.

The efficiency of the laminated version (quartered rods) can be obtained by using the equivalent circuit of figure 18 in the circuit of figure 30. The total input power was obtained by calculating the power dissipated in each resistance element. The electroacoustic efficiency at resonance calculated in this manner is 16%. The eddy currents dissipate 31.5% of the power. Mechanical and viscous losses in the fluid account for 49.8% of the energy dissipated. Alternating current ohmic losses account for 2.7% of the power consumed. Notice that in this case the electroacoustic efficiency has increased only 5%. The small increase in efficiency is due to the limiting effect of the large viscous loss in the contained fluid. Even if eddy currents were totally eliminated the electroacoustic efficiency would increase to only 23%. If the viscous loss is eliminated (by draining the fluid out), considerably different results are obtained. The electroacoustic efficiency of

the laminated (quartered rods) transducer at resonance (2650 Hz) is then 48.7%. Eddy currents consume 16.4% of the power and mechanical losses account for 33.5% of the losses. Alternating current ohmic losses in the power coils account for 1.4% of the power consumed.

Nonlinearity at Power Drive

In order to check the linearity of the rare earth iron transducer the sound pressure versus current was measured, this is shown in figure 39. Also shown in figure 39 is the linearity curve predicted from the transmitting current response (TCR) at 2.55 kHz. The measured curve departs from linearity by 2 dB at a .25-ampere (rms) drive. The acoustic waveform generated by the transducer shows considerable distortion at the high drive levels (.3 amperes and above). Before drawing any conclusions as to the cause of this nonlinearity and distortion consider figure 40. Shown in figure 40 are two linearity curves of the same transducer as in figure 39 except that the rare earth iron rods have been replaced by identically dimensioned ceramic (a well known linear material) rods. Notice that the transducer with the ceramic rods also shows a departure from linearity (about 4.5 dB at 200 volts). The ceramic version also shows increasing distortion with increasing drive field. It is believed that the nonlinearity shown in figures 39 and 40 is due to the flexing of the active piston under the large dynamic strain at resonance. Above resonance, where the dynamic strain and hence the piston flexing are small, the

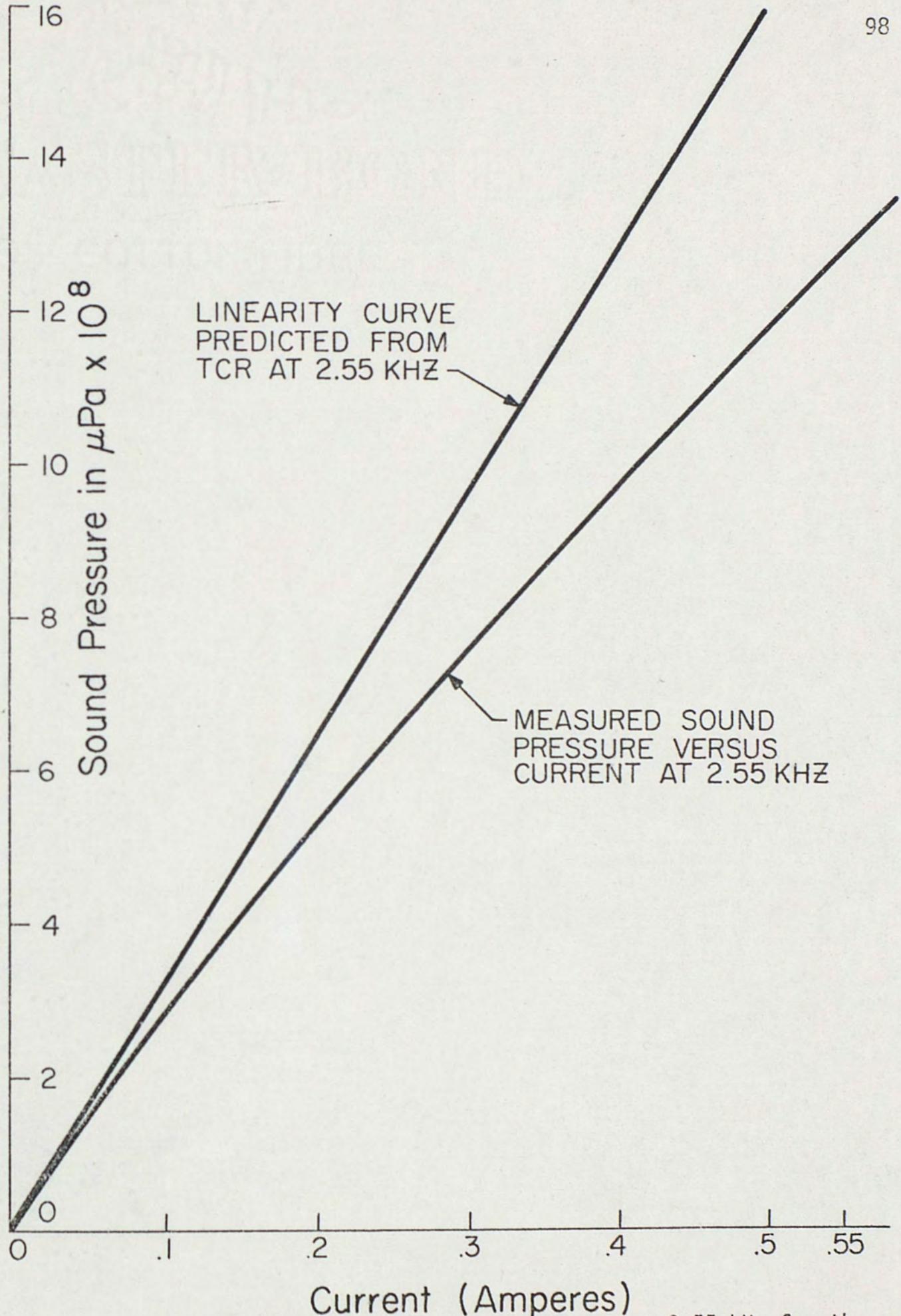

Fig. 39. Sound pressure versus current at 2.55 kHz for the rare earth iron transducer

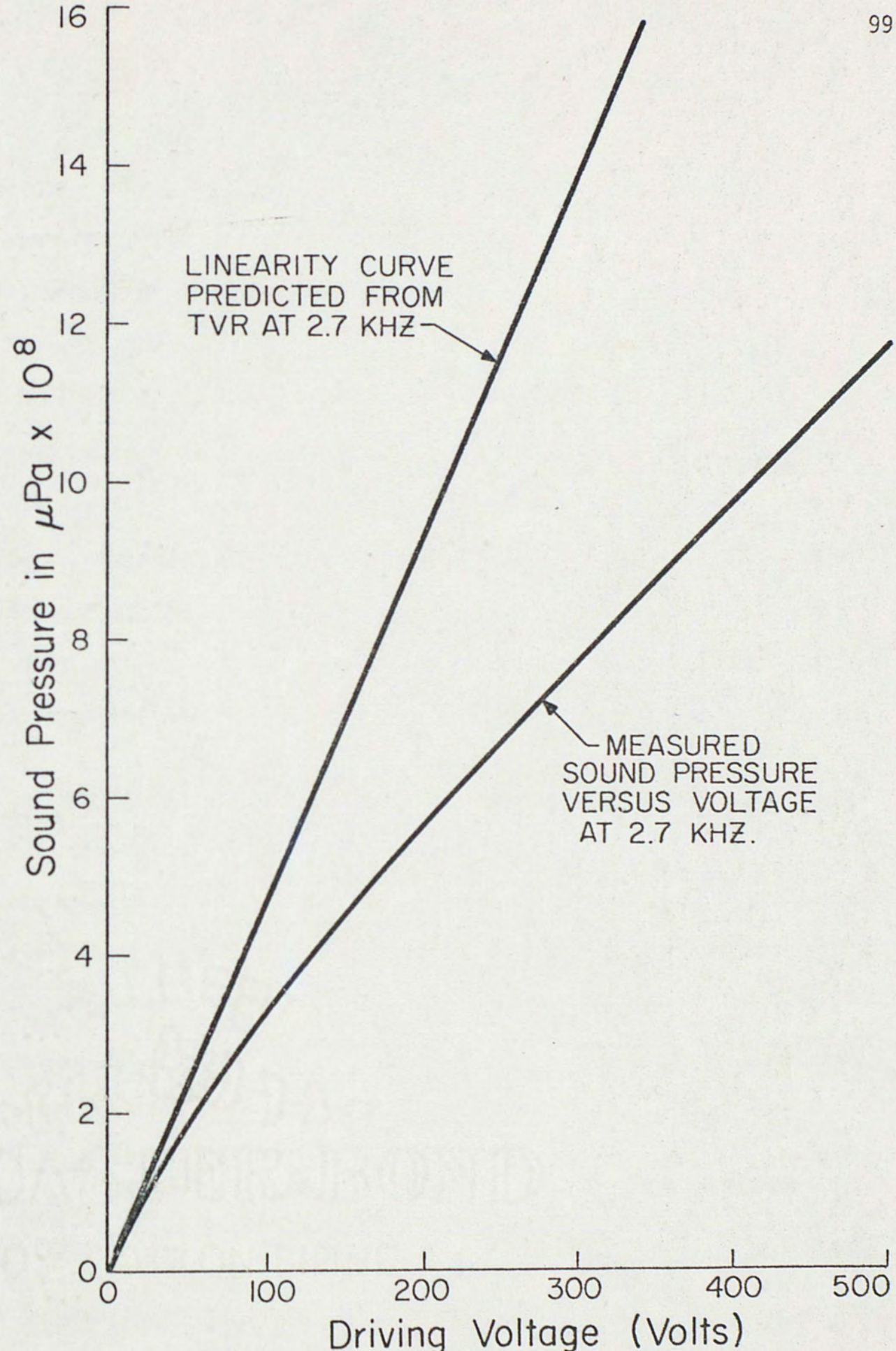

Fig. 40. Sound pressure versus voltage at 2.7 kHz for the ceramic transducer

distortion is negligible and the nonlinearity is greatly reduced. The piston flexing is due to the 35:1 area ratio between the rare earth iron rods and the active piston. If the area ratio were reduced to 10:1 or less the piston flexing could be greatly reduced. It should be noted that the transmitting current and voltage responses were measured with a drive level of approximately .1 ampere which is in the linear region of operation. The maximum acoustic power output by the rare earth iron transducer at resonance was 9 watts with a 400-volt drive, which corresponded to a sound pressure level of 184 dB ref 1 μPa at 1 meter. The equivalent circuit predicts that the laminated version (quartered rods) should output 40 watts at the same drive level and frequency assuming linear operation.

Comparison Between the Rare Earth and Ceramic Transducers

This section will compare the results of the rare earth iron transducer with the results of the same transducer where the rare earth iron rods have been replaced by ceramic rods. The three ceramic rods were each constructed of 20, .25-cm thick, 1.27-cm diameter, thickness-polarized lead-zirconate-titinate (PZT-4) disks. These disks were epoxied together to form three stacks 5.08-cm long and 1.27-cm in diameter. Thus the volume of ceramic and rare earth iron rods were nearly identical in each transducer.

The transmitting voltage response at 0.6 tesla versus frequency of the rare earth iron transducer is shown in figure 41. The

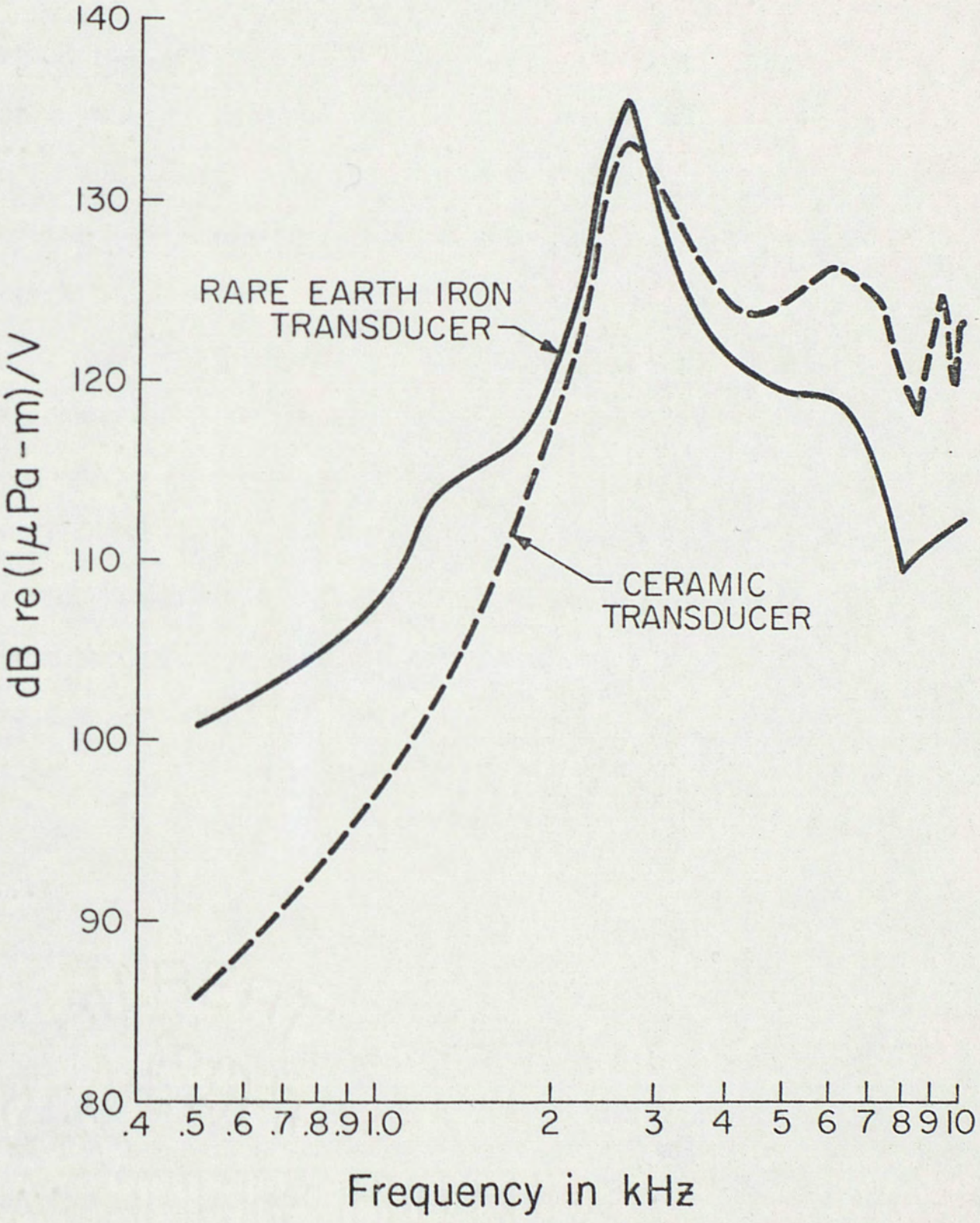

Fig. 41. Comparison of the transmitting voltage responses of the rare earth iron and ceramic transducers

response of the same transducer with the rare earth iron rods replaced by identical ceramic rods is also shown. This figure shows the advantage of the magnetostrictive rare earth iron transducer in terms of a greater sound pressure out per driving volt at the lower frequencies. The transmitting voltage response of the rare earth iron transducer is 15 dB above that of the ceramic transducer at 500 Hz and 2.5 dB above at 2.65 kHz (the resonance frequency). The Q of the rare earth iron transducer is 7 and of the ceramic transducer is 4.

The transmitting current response versus frequency for the rare earth iron at 0.6 tesla and ceramic transducers is shown in figure 42. The ceramic transducer produces a greater sound pressure per driving ampere. The difference between the two curves is due to the high impedance of the ceramic transducer and the low impedance of the rare earth iron transducer. If the rare earth iron transducer were laminated its response would be raised 4 dB at resonance bringing it within 1 dB of the ceramic version. The ceramic version shows an ω dependence far below resonance and the rare earth iron version an ω^2 dependence below resonance and an independence of ω above resonance. Here the Q of the rare earth iron transducer is 10 whereas the ceramic transducer has a Q of 5. The effective coupling coefficient of the rare earth iron transducer (that is, the coupling coefficient of the entire assembled transducer) at 0.6 tesla was measured to be .25 from the motional impedance loops [24]. The

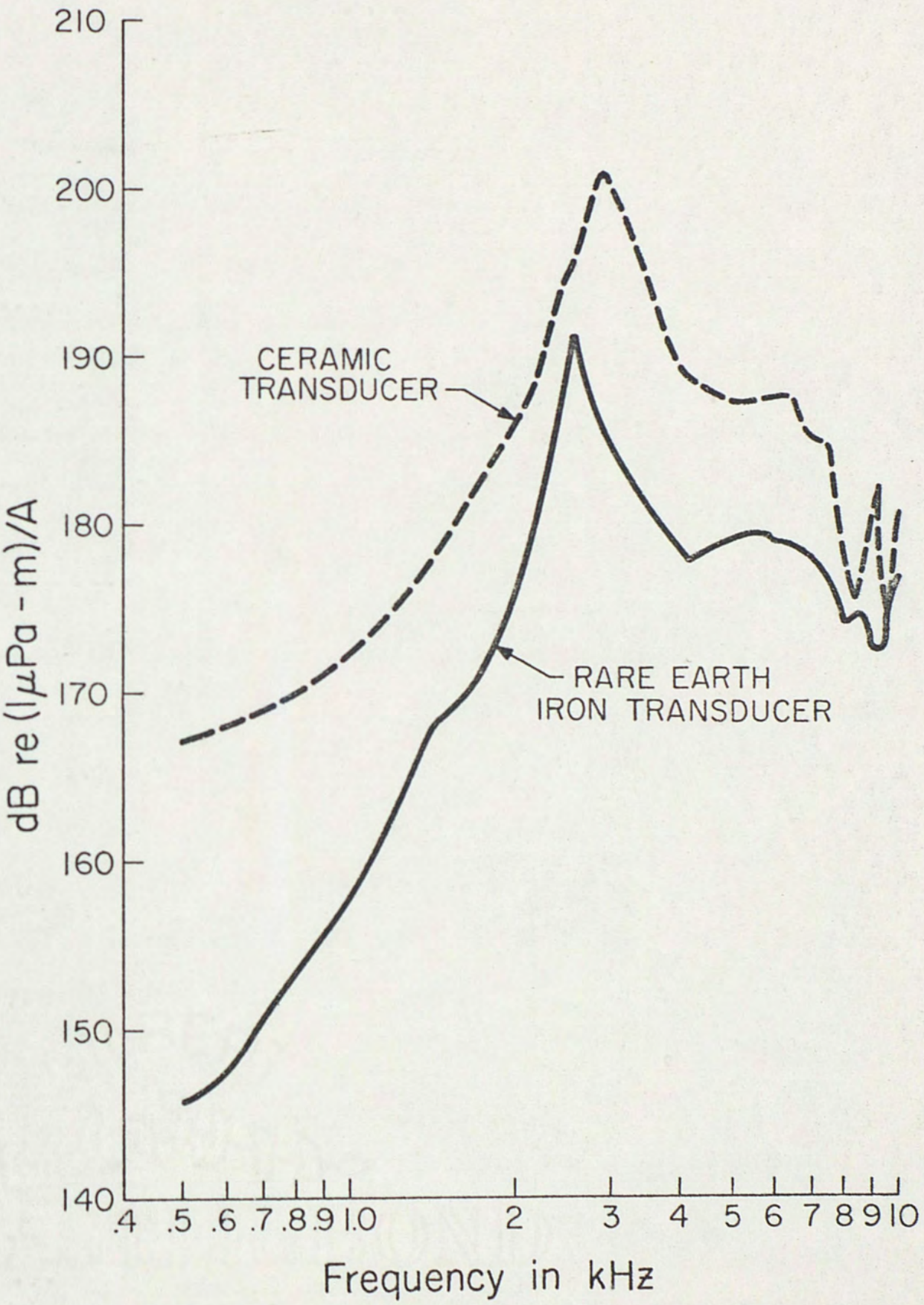

Fig. 42. Comparison of the transmitting current responses of the rare earth iron and ceramic transducers

reduction from the value of 0.6 for the alloy itself is primarily due to eddy currents and demagnetization. The effect of eddy current losses is to decrease both the effective coupling and the bandwidth (or increase the mechanical Q). For a laminated design an effective coupling between 0.5 and 0.6 is expected. The measured effective coupling for the ceramic version was 0.5. The measured efficiency of the ceramic version was 25%.

In figure 42 it can be seen that the peak response of the rare earth iron transducer occurs at 2.55 kHz and the ceramic version occurs at 2.9 kHz or 14% higher. Since the inverse of the elastic compliance coefficient ($1/s_{33}^{B}$) in the rare earth iron alloy is approximately 50% lower than in the ceramic, one would expect the rare earth iron transducer to resonate at a frequency lower than it actually does. This does not occur because the bias stress increases $1/s_{33}^{B}$ in the rare earth iron rods by 55% and the stiffness of the fluid behind the piston adds appreciably to the stiffness of the system thus leading to the observed 14% difference.

Figure 43 shows the free field voltage sensitivity of the two versions. The rare earth iron version is at a 0.6 tesla bias flux density. Here the ceramic transducer is superior to the rare earth iron alloy transducer with eddy currents. If the rare earth iron transducer was well laminated, its sensitivity would be raised by 4 dB at 2600 Hz and would be equal to or above the ceramic from 5 kHz on. The peak sensitivity of the rare earth iron transducer is at 2600 Hz while the ceramic peaks at 2900 Hz. Notice that the

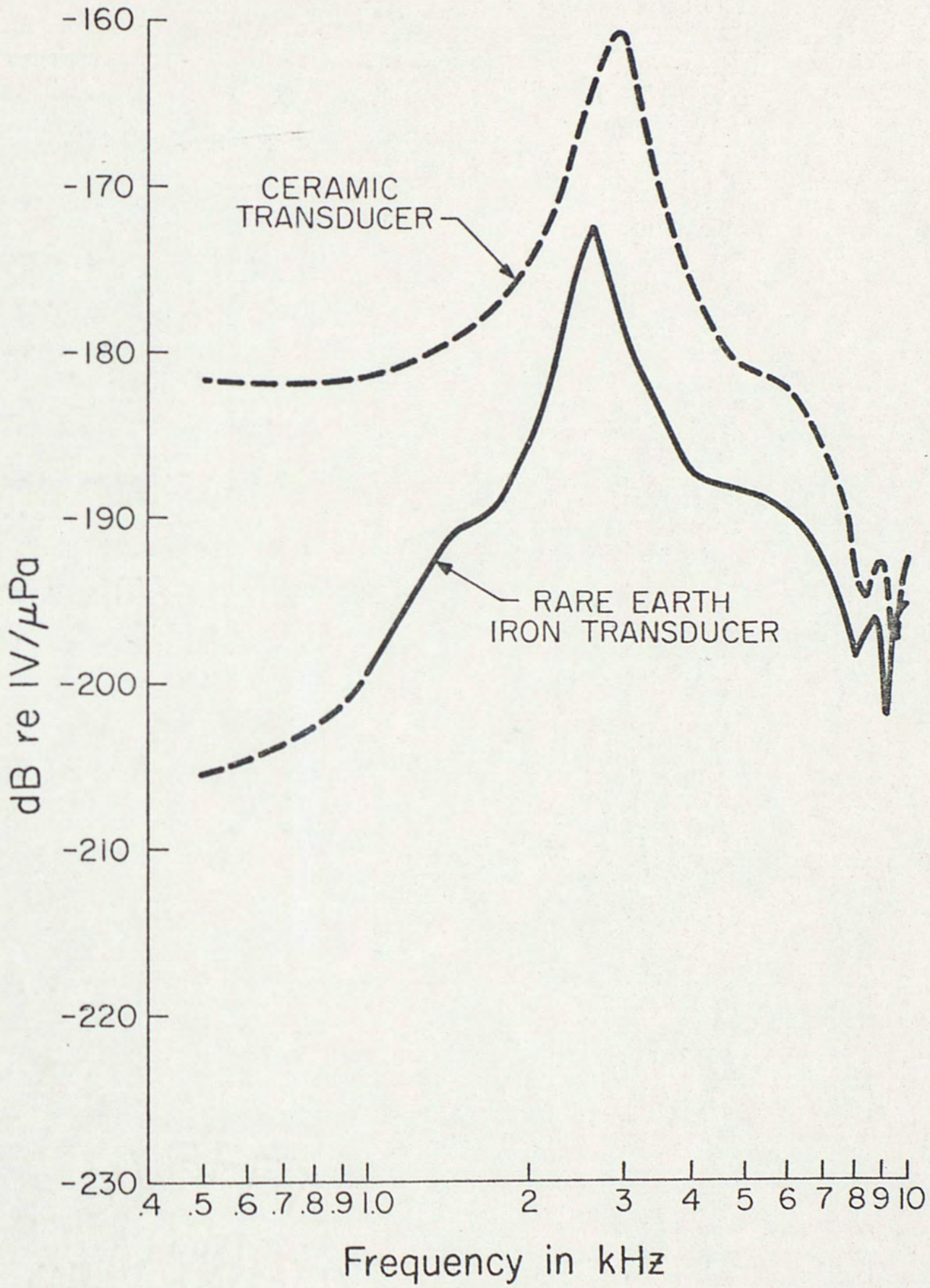

Fig. 43. Comparison of the free field voltage sensitivities of the rare earth iron and ceramic transducers

sensitivity of both versions is very high (a typical standard hydrophone has a sensitivity of -200 dB reference 1 V/μPa). The high sensitivity is due to the 35:1 area ratio between the piston and the ceramic rods. The large area ratio acts as a pressure multiplier thus increasing the sensitivity and the transmitting voltage and current responses. Notice that the large area ratio has the beneficial effect of increasing the sensitivity and responses but leads to the nonlinearity and distortion at power drive due to the piston flexing. The ceramic transducer is independent of ω far below resonance whereas the rare earth iron alloy transducer decreases as ω. The flat region of the sensitivity below resonance probably makes the ceramic transducer more desirable as a receiver at low frequencies.

CHAPTER V

CONCLUSIONS AND FUTURE STUDIES

The three major objectives of this paper, which were outlined in the introduction, have been met. The greatest problem in the present design is eddy current loss which accounts for about 50% of the input power. However, eddy currents can be greatly reduced by laminating the rare earth iron rods with a diamond saw or a spark cutter. Eddy currents are inherently lower in the rare earth iron material than in nickel because the rare earth iron alloy's incremental permeability is lower and resistivity higher.

Another problem area is in the requirement of large magnetic fields. The large magnetic fields can be produced by large current-turn densities but this leads to ohmic losses and requires blocking capacitors and chokes along with additional wiring. Permanent magnets can provide the requisite magnetic bias if some coupling coefficient is sacrificed and an aging effect, which would be absent with the use of direct current biasing circuitry, is accepted. In either case, saturation of the magnetic return path by the large dynamic and biasing fields could occur without proper design considerations.

Under advantages the lower inverse elastic stiffness constant (lower sound speed) in the rare earth iron material leads to smaller

resonators for a given frequency. This is offset somewhat by the tendency of the sound speed to increase with bias stress.

The low voltage (high current) requirement of the magnetostrictive rare earth iron material is of increasing importance as one goes to lower frequencies. At low frequencies piezoelectric ceramics (which have a capacitive reactance) require a very high voltage drive whereas to drive a magnetostrictive material one simply modulates a current source.

The larger electromechanical energy density of the rare earth iron material is a result of the larger strains available with the rare earth iron material. Of course, one pays the price of larger losses due to the large magnetic fields required.

The rare earth iron material appears very promising for use in an ultra-low-frequency projector for use in a closed tank calibration system where the low voltage and large displacement of the rare earth iron material is advantageous over a ceramic material. A flextensional transducer is also possible where one can take advantage of the larger displacement. A bender bar transducer would use a positive magnetostrictive ($Tb_{.27}Dy_{.73}Fe_{1.95}$) and a negative magnetostrictive ($Sm_{.7}Ho_{.3}Fe_2$) material. Here one also takes advantage of the large strains available.

Finally, for many reasons ceramics are not threatened by competition from rare earth iron alloys, but a complementary role is quite possible. At present application in low-frequency high-power projectors appears most promising.

LIST OF REFERENCES

[1] R. W. Timme, "Magnetomechanical Characteristics of a Terbium-Holmium-Iron Alloy," J. Acoust. Soc. Am., 59, pp. 459-464 (1976).

[2] A. E. Clark and H. S. Belson, "Magnetostriction of TbFe and TbCo Compounds," AIP Conf. Proc., 5, pp. 1498-1500 (1972).

[3] N. C. Koon, A. I. Schindler, and F. L. Carter, "Giant Magnetostriction in Cubic Rare Earth-Iron Compounds of the Type RFe_2," Phys. Lett., A38A, pp. 413-414 (1971).

[4] A. E. Clark, H. S. Belson, and N. Tamagawa, "Magneto-Crystalline Anisotropy in Cubic Rare Earth-Fe_2 Compounds," AIP Conf. Proc., 10, pp. 749-753 (1973).

[5] C. M. Williams and N. C. Koon, "Anisotropy Energy Measurements on Single Crystal $Tb_{0.15}Ho_{0.85}Fe_2$," AIP Conf. Proc., 18, pp. 1247-1248 (1973).

[6] A. E. Clark, "Magnetic and Magnetoelastic Properties of Highly Magnetostrictive Rare Earth-Iron Laves Phase Compounds," AIP Conf. Proc., 18, pp. 1015-1018 (1974).

[7] N. C. Koon, A. I. Schindler, C. M. Williams, and F. L. Carter, "Magnetostrictive Properties of $Ho_xTb_{1-x}Fe_2$ Intermetallic Compounds," J. Appl. Phys., 45, pp. 5389-5391 (1974).

[8] R. W. Timme and N. C. Koon, "Magnetostrictive Properties of Terbium-Holmium-Iron Compounds," J. Acoust. Soc. Am., 58S, p. S74 (1975).

[9] H. T. Savage, A. E. Clark, and J. M. Powers, "Magnetomechanical Coupling and ΔE Effect in Highly Magnetostrictive Rare Earth Compounds," Intermag. Conf., London, England, 1975.

[10] A. E. Clark and H. T. Savage, "Giant Magnetically Induced Changes in the Elastic Moduli in $Tb_{0.3}Dy_{0.7}Fe_2$," IEEE Trans. Sonics Ultrason., SU 22, pp. 50-52 (1975).

[11] H. T. Savage and W. A. Ferranco, "Magnetomechanical Coupling, ΔE Effect, and Magnetization in Rare Earth Iron Alloys," to be published in J. Underwater Acoust. (USN) Jan 1977.

[12] N. C. Koon and C. M. Williams, "Single Crystal Magnetostriction and Anisotropy of $Ho_xTb_yDy_{1-x-y}Fe_2$ Intermetallic Compounds," to be published in J. Underwater Acoust. (USN) Jan 1977.

[13] R. R. Smith and J. C. Logan, "Design of a Transducer Using Rare Earth Magnetostrictive Materials," to be published in J. Underwater Acoust. (USN) Jan 1977.

[14] O. L. Akervold, D. L. Hutchins, R. G. Johnson, and B. G. Koepke, "Rare Earth Magnetostrictive Transducer and Material Development Studies," to be published in J. Underwater Acoust. (USN) Jan 1977.

[15] J. L. Butler and S. J. Ciosek, "Development of Two Rare Earth Transducers," to be published in J. Underwater Acoust. (USN) Jan 1977.

[16] Technical Committee on Transducers and Resonators of the IEEE Group on Sonics and Ultrasonics, IEEE Standard on Magnetostrictive Materials: Piezomagnetic Nomenclature, The Institute of Electrical and Electronics Engineers, New York, 1971.

[17] G. V. Blessing and A. E. Clark, "Elastic Properties of $Tb_{.3}Dy_{.7}Fe_2$ Measured Ultrasonically," J. Acoust. Soc. Am., 60S, p. S53 (1976).

[18] R. W. Timme, "Device Oriented Material Measurements on Rare Earth Iron Alloys," to be published in J. Underwater Acoust. (USN) Jan 1977.

[19] Dr. K. A. Gschneidner, Jr., Ames Laboratory-ERDA and Department of Materials Science and Engineering, Iowa State University, Ames, Iowa, 50011.

[20] Dr. A. E. Clark, Naval Surface Weapons Center, White Oak Laboratory, Silver Springs, Maryland, 20910.

[21] R. W. Timme, Ph.D. Thesis, Ultrasonic Attenuation in KCℓ (unpublished), Rice Univ., Sept. 1970.

[22] R. M. Bozorth, Ferromagnetism (D. Van Nostrand Co., Inc., Toronto, 1951), Chaps. 17 and 19.

[23] F. W. J. Oliver, "Bessel Functions of Integer Order," in Handbook of Mathematical Functions, M. Abramowitz and I. A. Stegun, eds. (Dover Publications, Inc., New York, 1972), p. 430.

[24] National Defense Research Committee, The Design and Construction of Magnetostriction Transducers, Summary Technical Report of Division 6, NDRC Vol. 13 (1946), Washington, D.C., chaps. 2, 3, and 4.

[25] S. Hanish, R. V. Baier, B. J. King, and P. H. Rogers, Electroacoustic Modeling of Magnetostrictive Shells and Rings: Part 1 - Mathematical Modeling, Naval Res. Lab. Report No. 7767, 1974, p. 39.

[26] E. E. Mott and R. C. Miner, "The Ring Armature Telephone Receiver," Bell System Tech. J., 30, pp. 110-140 (Jan.1951).

[27] F. V. Hunt, Electroacoustics (Harvard University Press, New York, 1954), chap. 3.

[28] H. W. Katz, ed., Solid State Magnetic and Dielectric Devices (John Wiley and Sons, Inc., New York, 1959), pp. 112-114.

[29] L. L. Beranek, Acoustics (McGraw-Hill Book Company, Inc., New York, 1954), chap. 5.

[30] R. J. Bobber, Underwater Electroacoustic Measurements (U. S. Govt. Printing Office, Washington, D.C., 1970), chaps. 2 and 3.